TRANSIT NEW ZEALAND

RRU BULLETIN 84

BRIDGE DESIGN AND RESEARCH SEMINAR 1990

VOLUME 2: SEISMIC DESIGN OF BRIDGE ABUTMENTS AND RETAINING WALLS
(Summary Volume)

J.H. Wood and D.G. Elms

TRANSIT NEW ZEALAND

RRU

Wellington New Zealand

Road Research Unit Bulletin 84 Volume 2
ISSN 0549-0030

SEISMIC DESIGN OF BRIDGE ABUTMENTS AND RETAINING WALLS

J.H. Wood,

M.E., Ph.D., M.I.P.E.N.Z.
Director, Phillips & Wood Ltd,
Consulting Engineers, Lower Hutt,
New Zealand

and

D.G. Elms,

M.S.E., Ph.D., F.I.P.E.N.Z.
Professor of Civil Engineering
University of Canterbury, New Zealand

PRESENTED AT THE

BRIDGE DESIGN AND RESEARCH SEMINAR

CHRISTCHURCH 1990

Road Research Unit
TRANSIT NEW ZEALAND
Wellington New Zealand
1990

Road Research Unit Bulletin 84 Volume 2
ISSN 0549-0030

SEISMIC DESIGN OF BRIDGE ABUTMENTS AND RETAINING WALLS

J.H. Wood,

M.E., Ph.D., M.I.P.E.N.Z.
Director, Phillips & Wood Ltd,
Consulting Engineers, Lower Hutt,
New Zealand

and

D.G. Elms,

M.S.E., Ph.D., F.I.P.E.N.Z.
Professor of Civil Engineering
University of Canterbury, New Zealand

PRESENTED AT THE

BRIDGE DESIGN AND RESEARCH SEMINAR

CHRISTCHURCH 1990

Road Research Unit
TRANSIT NEW ZEALAND
Wellington New Zealand
1990

FOREWORD

Bulletin 84 comprises five volumes that were specially prepared for a seminar on Bridge Design and Research organised by Transit New Zealand's Road Research Unit in conjunction with the University of Canterbury. The Seminar was held from 15 to 17 November 1990, at the Christchurch College of Education.

The five volumes are:

Volume 1 : Strength and Ductility of Concrete Substructures of Bridges. (Summary Volume)

R. Park and T. Paulay

Volume 2 : Seismic Design of Bridge Abutments and Retaining Walls (Summary Volume)

J.H. Wood

Volume 3 : Seismic Design of Base Isolated Bridges Incorporating Mechanical Energy Dissipators (Summary Volume)

H.E. Chapman and D.K. Kirkcaldie

Volume 4 : Road Engineering in Soft Rock Materials. (Summary Volume)

D.N. Jennings, P. Black, S.A.L. Read and A. Olsen

Volume 5 : Summary Papers and Other Technical Papers

21 Titles 26 Authors

The material presented in the five volumes serves the following purposes:

(a) Summary Volumes and Summary Papers review research on highway structures undertaken in the six years 1985 to 1990 by the Road Research Unit's Structures Committee.

(b) Other Technical Papers disseminate information on a variety of topics in the field of highway engineering.

The Unit wishes to express its appreciation to researchers, their parent organisations and to all those who prepared material presented in the volumes of this Bulletin.

ABSTRACT

This report reviews and summarises the findings from a series of research projects related to the seismic design of soil retaining walls.

The behaviour of retaining walls under earthquake loading has been studied by both experimental and theoretical investigations. A significant effort has been devoted to both free standing walls and walls that are rigidly connected to a more major structure such as a bridge abutment.

Free standing walls, ranging from rigid or walls with low flexibility, to walls that can respond by outward sliding on soil failure planes, have been investigated. Analysis and design procedures for special forms of construction, including reinforced earth and tied-back walls, have been developed. The research has shown the validity of using the limiting equilibrium approach for many types of free standing walls. Provided outward movements can be tolerated under severe ground shaking, this method enables the wall to be designed for accelerations lower than the peak ground acceleration. Results of the studies show that the outward movements are not particularly large under inertia loads corresponding to about one-half of usual design level peak ground accelerations. This finding should result in a significant reduction in the costs of many high walls. For smaller walls, a static design for gravity and superimposed loads alone may provide sufficient strength to resist earthquakes. However, the main benefit from the research has been the increase in knowledge of the behaviour of free standing walls. This will lead to improved design and a reduction in damage from future earthquakes.

One method of simplifying bridge abutment structures is to build them monolithic with the superstructure rather than to separate them with sliding bearings, expansion joints, seismic gaps and restrainers. Abutment studies have been mainly directed towards the prediction and measurement of pressures that develop on these types of abutments as they displace under inertia forces imposed by the superstructure. The research results have increased the reliability of methods for predicting the soil stiffening effect of abutments and have shown how this influences the dynamic response of the bridge during earthquakes. With the publication of the recent research findings and the design recommendations in this report, there is likely to be an increasing use of monolithic abutments resulting in a reduction of bridge construction costs.

ACKNOWLEDGEMENTS

This report is largely a summary of the research carried out by the staff and a number of masters and doctoral students at the Civil Engineering Department of the University of Canterbury, Christchurch, New Zealand, and by staff at the Central Laboratories of Works and Development Services Corporation Ltd., Lower Hutt, New Zealand. In particular, the work carried out by G.H. Aitken, J.B. Berrill, G.J. Fairless, P.N. Jacobsen, C.S. Lai, R.B. Nagel, N. Sharma, and Y.H. Tso at the University of Canterbury, and A. Bracegirdle, M.B. Matthewson, R.B. Stevenson, S.J. Thurston, K.K. Yap, E.H. Yeo and P.M.F. Yong at Works and Development Services Corporation Ltd is gratefully acknowledged.

Professor R. Richards, Department of Civil engineering, State University of New York, Buffalo worked in collaboration with the University of Canterbury on several projects making a very significant contribution.

Part of the work reported on monolithic bridge abutment walls was carried out as an United States - New Zealand cooperative research project. Work on the project in U.S.A was carried out by The Earth Technology Corporation, Long Beach, California under the direction of G.R. Martin, C.B. Crouse and B. Hushman. The major contribution that this group has made in the area of bridge abutment walls is also gratefully acknowledged.

The authors gratefully acknowledge the generous financial assistance received from the Road Research Unit, University of Canterbury, Works and Development Services Corporation Ltd., and the United States National Science Foundation.

TABLE OF CONTENTS

PAGE

1

INTRODUCTION

During the past 15 years, a wide range of research projects related to the earthquake performance of soil retaining structures and bridge abutments have been carried out by New Zealand researchers and their overseas colleagues. Guidance and support for this work has been provided by the Structures Committee of the Road Research Unit (RRU) of Transit New Zealand.

The results of the studies have had a major influence on new standards and procedures currently being used for the seismic design of walls and abutments both within New Zealand and overseas. The purpose of this report is to provide a summary of the projects carried out by New Zealand researchers together with the main results. The findings of the research have also been summarised in design recommendations to encourage a wider application of the results.

The work in New Zealand has in the main been directed at studies on the following three categories of walls:

(i) Free standing walls.

(ii) Monolithic bridge abutments.

(iii) Reinforced earth walls.

The work on free standing walls was initially directed at walls that were assumed to be rigid or sufficiently stiff so that the wall deflections and movements did not significantly change the earthquake induced pressures. This work was extended to consider both walls that have significant deflections within the wall structure, and walls that may be displaced by the formation of failure surfaces in the foundation and backfill soil. In both these cases, the earthquake pressures were found to reduce significantly from the rigid wall pressures.

The work on bridge abutments has mainly been concerned with investigating the pressures on abutments walls where there is strong interaction between the abutment and bridge or where the abutment wall is cast monolithically with the bridge superstructure (Figure 1.1). For these cases, the wall is displaced by the inertia forces from the superstructure and maximum earthquake pressures can be considered to be a superposition of free wall pressures and pressures generated by movements of the wall relative to the backfill.

The emphasis of the reinforced earth wall studies has been on developing a limiting equilibrium theory to provide better estimates of the critical horizontal earthquake acceleration to initiate failure or permanent outward displacement. It was intended that this theory be used in conjunction with the Newmark (1965) sliding block method to provide a design approach based on allowable outward movement of the wall rather than requiring the wall to remain elastic (or undisplaced) under design level earthquake loads. A design procedure based on this approach was considered to be more satisfactory than the currently used empirical design methods that rely on arbitrary factors applied to experimental results from elastically responding model walls.

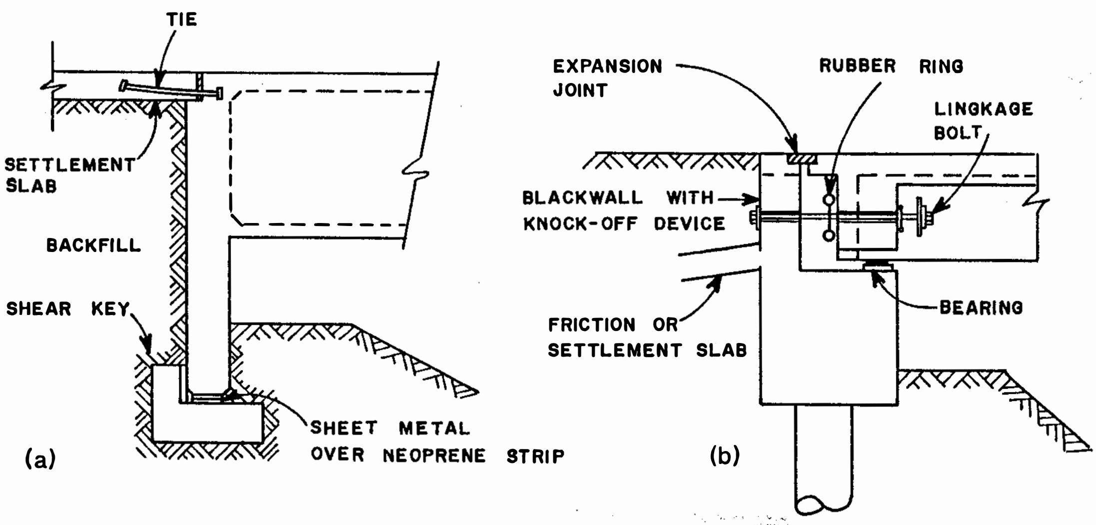

FIG. 1.1 BRIDGE ABUTMENT TYPES
(a) Monolithic (b) Bearing Type

Both theoretical and experimental studies have been carried out in the main research areas investigated. In this way, the major findings, conclusions and recommended design procedures have been thoroughly examined and verified. Ideally, full scale test studies should also be carried out but little work of this nature has been undertaken because of the practical difficulties and large costs involved in simulating earthquake effects on full scale walls.

The following section of this introduction gives a summary of reported wall failures during past earthquakes. The overall performance of some types of walls in recent severe earthquakes has not been particularly good, with damage having been sustained by bridge abutments and quay walls in particular. Because of these failures, and the general lack of understanding about earthquake pressures and wall response in earthquakes, the RRU Structures Committee initiated a major research effort relating to improving seismic design procedures for walls and bridge abutments.

The final sections of the introduction outline the basic assumptions and philosophy adopted in the New Zealand approach to seismic design of walls.

Chapter 2 summarises the research work undertaken. Rather than a sequential review, the approach used here has been to collate the results by wall type and subject matter. The projects in each area are identified by reference to the authors of the research reports that are listed in the References section at the end of the report.

Chapter 3 presents an overall summary of the results by making design recommendations for each of the types of walls studied.

Concluding comments and recommendations for future research are given in Chapter 4.

1.1 Earthquake Damage

Summaries of reported earthquake damage to retaining wall structures are given by Seed and Whitman (1970) and Nazarian and Hadjian (1979). Most of the damaged structures have been either quay walls or bridge abutments.

There have been many reports of sliding and rotational failures of quay walls in Japanese earthquakes. Reports of damage of this type are given by Amano, et al (1956), Matuo and Ohara (1960), and Hayashi and Katayama (1970). The greatest damage has occurred when the backfill has been saturated and failures have probably resulted from a combination of increased lateral soil pressure, hydrodynamic effects reducing the water pressure on the front face and liquefaction in the foundation or backfill soil (Seed and Whitman, 1970).

Movements and damage suffered by a large number of sheetpile bulkhead walls was reported by Kitajima and Uwabe (1979).

Damage to bridges, induced by large displacements or failures of the abutments and approaches, has been reported in a number of recent major earthquakes. Examples of this type of damage that occurred in the 1971 San Fernando earthquake, California, are illustrated in Figures 1.2, 1.3, 1.4 and 1.5. Damage to bridge abutments and approaches has been reported in the 1960 Chile (Duke and Leeds, 1960), 1964 Alaska (Ross et al, 1969, Scott, 1973), 1964 Niigata (Kawasumi, 1964), 1968 Inangahua (Evans, 1971), 1970 Madang (Ellison, 1971), 1971 San Fernando (Wood and Jennings, 1971 and Fung et al, 1971), 1972 Managua (Meehan et al, 1973), 1974 Lima (EERI, 1975) earthquakes. In many cases the abutment damage has been related to settlement and failure of approach fills and pounding of the bridge superstructure against the abutment. However, there have been a number of cases where there has been evidence of increased lateral pressures.

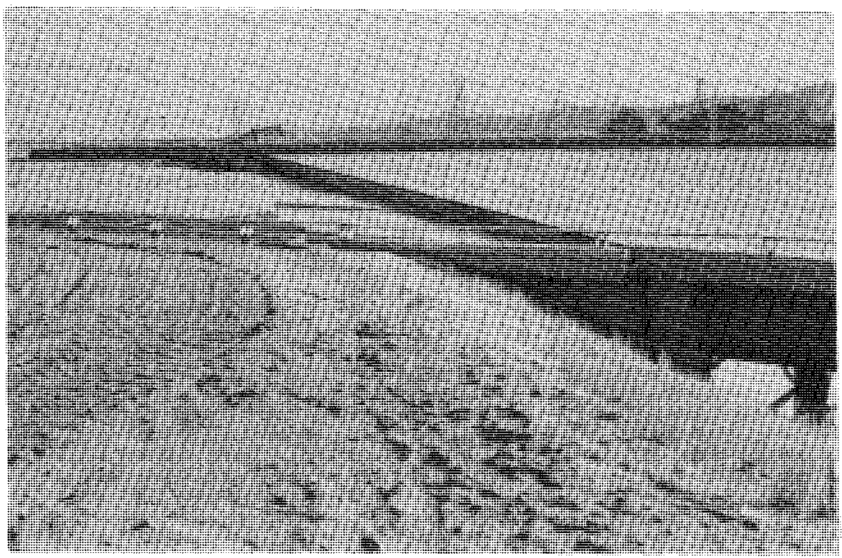

FIG. 1.2 SETTLEMENT OF APPROACH FILL AND SEPARATION OF APPROACH SLAB.
San Fernando Earthquake, 1971

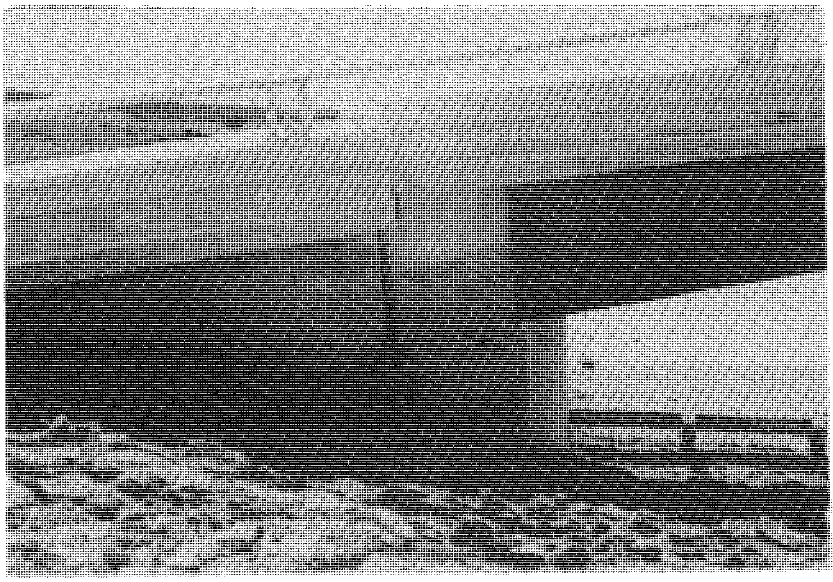

FIG. 1.3 FAILURE OF ABUTMENT WALL.
San Fernando Earthquake, 1971

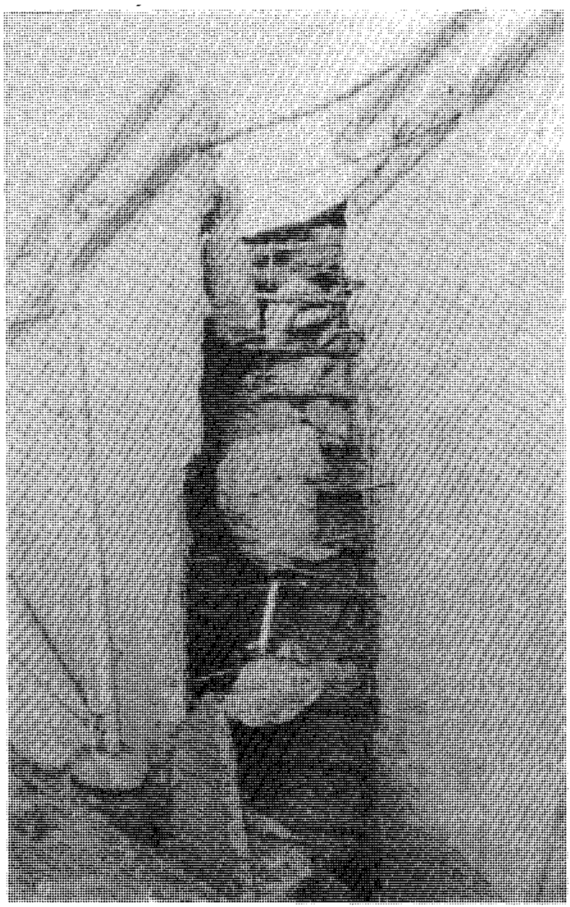

FIG. 1.4 FAILURE OF ABUTMENT WING WALL RESULTING FROM ABUTMENT PILE FOUNDATION FAILURE.
San Fernando Earthquake, 1971

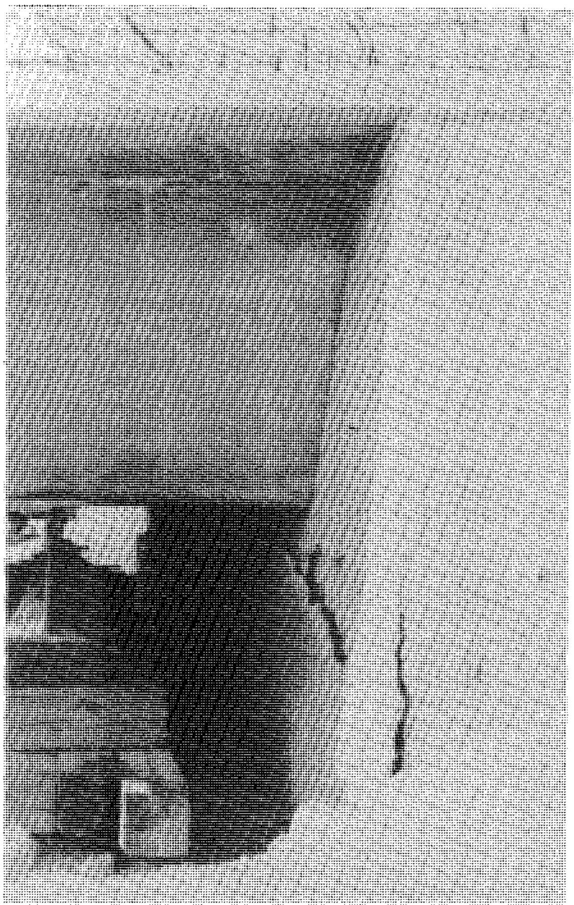

FIG. 1.5 FAILURE OF ABUTMENT WALL.
San Fernando Earthquake, 1971

Evans (1971) inspected 39 bridges within 50 km of the 1968, M 7.0, Inangahua earthquake and reported that 23 abutments showed measurable movements and that 15 had been damaged. Outward movement of the abutments had often been restrained by the superstructure, resulting in high pressures and damage near mid height of the abutment.

The performance of the abutment structure may have a significant influence on the distribution of loads on the main load resisting elements of the bridge, and abutment failures may initiate or aggravate failures in the spans, piers and bridge foundations. Abutment damage may also restrict the movement of emergency service traffic that is often of vital importance in the aftermath following an earthquake. (Figure 1.2)

In addition to the bridge abutments, a number of other types of retaining structures were extensively damaged by increased soil pressures from ground shaking and soil slide failures during the 1971 San Fernando earthquake. Structures damaged included underground reservoirs (Jennings, 1971), underground culverts (Hradilek, 1972), and open rectangular flood control channels (Lew et al, 1971, Wood, 1973, Clough and Fragaszy, 1977).

A study of reports of damage in past earthquakes would suggest that perhaps, with the exception of bridge abutments and quay walls, retaining wall damage has not been very extensive and has been limited to rather isolated cases of unusual wall structures. However, damage to walls is often considered to be of minor significance in relation to other more catastrophic structural failures and much of the damage to walls has probably been inadequately investigated and reported. A further factor is that well proportioned free standing walls often fail by outward sliding or rotation without damage to the structural components of the wall. In these cases, the walls may have been subjected to forces considerably greater than the design forces but because the failures are within the foundation soils there may be little or no visible damage. Provided the permanent outward movements can be tolerated there may be no need for repair.

1.2 Wall Deformation

It is usual to simplify the complex problem of interaction of earthquake elastic waves with wall structures by assuming that the earthquake ground motions are equivalent to dynamic inertia forces acting in the backfill mass. Dynamic pressures on the wall can be calculated by analysing the wall and backfill modelled as an elastic continuum or failure wedge subjected to gravity and horizontal body forces.

The pressures that develop on a wall during earthquake loading are very sensitive to the elastic flexibility of the structural components of the wall and the ability of the wall to move outward as a result of either permanent deformations in the foundation soils or inelastic behaviour of the structure. It is therefore important that analysis methods and seismic design procedures take into account wall deformations, or at least make gross recognition of the reduction in pressures from the rigid wall case.

The behaviour of wall structures during earthquakes can be broadly classified into three categories related to the maximum strain condition that develops in the soil near the wall. The soil may remain essentially elastic, respond in a significantly nonlinear manner or become fully plastic. The rigidity of the wall and its foundations will have a strong influence on the type of soil condition that develops.

Many low walls are of cantilever type construction. In this type of wall, lateral pressures from vertical gravity and earthquake forces will generally produce sufficient displacement within the wall structure to induce nonlinear behaviour or a fully plastic stress state in the retained soil. In more rigid free-standing walls, such as gravity (eg. reinforced earth and crib block walls) and counterfort walls, a fully plastic stress state may develop as the result of permanent outward movement from sliding or rotational deformations in the foundation. In cases where significant nonlinear soil behaviour or a fully plastic stress state occurs in the soil during earthquake loading, the well known Mononobe-Okabe (MO) method (Mononobe and Matsuo, 1929) can be used to compute earthquake pressures and forces.

Retaining structures that are either not free standing or have rigid foundations (piles or footings on rock) may not displace sufficiently, even under severe earthquake loading, for a fully plastic stress state to develop in the soil backfill. Particular examples of these types of walls include: bridge abutments that may be rigidly attached to the bridge superstructure or founded on piles, basement walls that are an integral part of a building on a firm foundation, and closed culvert or tank structures embedded in the ground. For many of these types of walls, the assumptions of the MO method are not satisfied, and design earthquake pressures and forces are likely to be significantly higher than predicted by this method.

In some types of wall structures, the soil behaviour may remain essentially elastic under combined earthquake and gravity loads, and theory of elasticity or elastic finite element solutions may be applied to provide earthquake design pressures (Wood, 1973). More generally, there will be sufficient deformation for nonlinear soil effects to be important or for wall pressures to be significantly lower than for a fully rigid wall. These intermediate cases are more difficult to analyse than the limiting cases described above. Approximations derived from the theory of elasticity solutions may often be satisfactory for wall design purposes, or alternatively, upper and lower bounds from the limiting cases of fully plastic stress conditions and rigid wall behaviour may provide sufficient information for less important structures.

1.3 Soil-Structure Interaction

Basement walls in buildings and abutment walls that are monolithic or rigidly connected to bridge superstructures, are often subjected to displacements relative to the soil mass because of the dynamic displacement response of the building or bridge during an earthquake. These types of walls may be subjected to a complex interaction of dynamic soil pressures arising from both the displacement response of the structure and earthquake elastic waves (or inertia loads) in the soil. (Figure 1.6)

The dynamic displacement of basement walls in tall buildings is likely to be dominated by the movements of the building but often basement structures are very rigid and wall displacements small. Where the backfill is a firm soil, small movements of the wall in a direction towards the retained soil can result in significant increases in pressures that need to be combined with the soil inertia force effect.

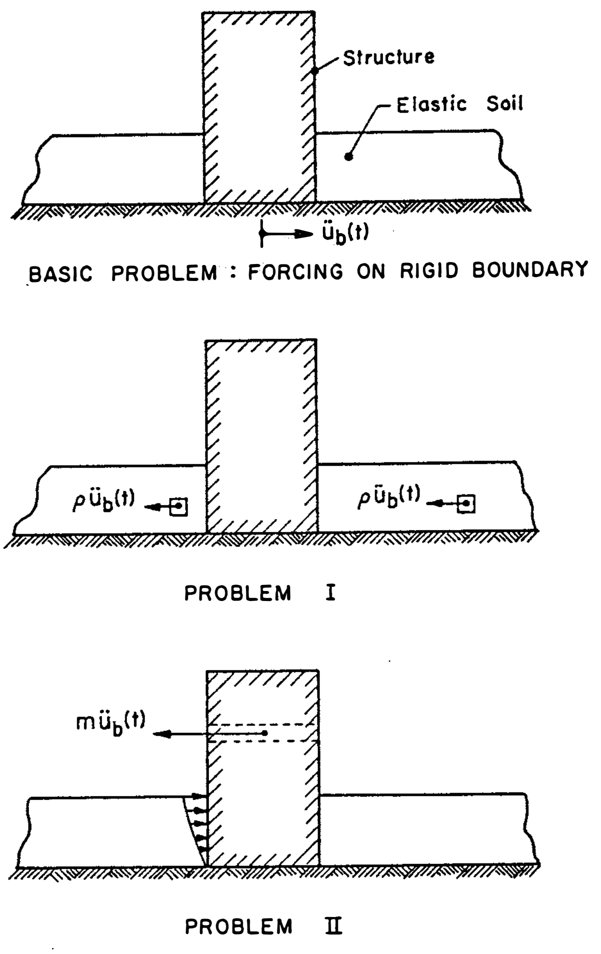

FIG. 1.6 COMPONENTS OF EARTHQUAKE PRESSURE
I Pressures From Soil Inertia Loads
II Pressures From Structure Response

In bridges that have monolithic abutments it is possible that the response of the bridge may be strongly influenced by the stiffness of the soil backfill at the abutment. The distribution of earthquake loads on the lateral load resisting elements of a bridge is dependent on the relative stiffness of the substructure components and their foundations. For earthquake loading along the direction of the bridge, monolithic abutments are frequently stiffer than the piers and thus attract a high proportion of the load. The pressures and total forces on the wall, are cyclic in nature with the wall being alternately forced against and pulled away from the soil during the vibration cycles of the bridge. Pressures developed by these movements may exceed the pressures from the soil inertia effects.

If a bridge is effectively isolated from the abutments by sliding bearings it may be possible to consider the abutment to behave as a free standing wall. However, some types of bearings transmit relatively large horizontal loads into the abutments, thus adding the complexity of soil-structure interaction similar to the monolithic case.

1.4 Plasticity Theory and Failure Modes

The MO method is based on simplified plasticity theory and is essentially an extension of the well known Coulomb sliding wedge method for estimating static pressures. The basic assumption is that the wall displacements are sufficiently large to produce a fully plastic stress state in the soil by either outward movement (active state), or by movement towards the backfill (passive state). The forces on the wall are calculated by considering the equilibrium of a failure wedge that is bounded by the backface of the wall, the backfill surface and a straight line failure plane (Figure 1.7)

In seismic design of retaining walls it is important that possible failure modes be investigated and capacity design principles used. For walls that are relatively rigid, the initial earthquake accelerations may induce pressures, corresponding to elastic soil behaviour, that are significantly greater than the MO pressures. If the wall has insufficient strength to resist these elastic pressures, then yielding and outward movement of the wall may occur with a fully plastic stress condition developing in the soil. With progressive yielding and the onset of a plastic stress condition, the pressures on the wall will decrease to the MO values. The outward yielding may result from either permanent displacements in the soil foundation or from yielding in the structural wall elements. The failure mode will depend on the wall configuration and the relative capacities available in each of the potential failure mechanisms.

Although it is common procedure to design bridge piers and building frames for inelastic behaviour under earthquake loads, it may be undesirable to design retaining wall structural components for yielding. In a wall structure, owing to the presence of lateral gravity pressures, yielding will tend to occur only in a direction away from the retained soil. In major earthquakes this may result in large permanent deflections and cracking with loss of serviceability.

If structural damage is to be avoided, it is necessary to design for either the maximum peak earthquake-induced pressures consistent with the type of soil behaviour expected, or to detail the wall to displace outwards, where this is possible, by movement on failure surfaces in the soil (sliding or tilting). Where soil failure modes are possible, the Newmark sliding block analogy (Richards and Elms, 1979) may be used to determine the approximate magnitude of the outward movement. This movement is a function of the ratio of the critical acceleration to initiate failure and the design peak ground acceleration. Theoretical studies and model tests on shaking tables have shown that for free standing walls, it is often possible to design for significantly less than the expected peak ground acceleration without exceeding acceptable limits for outward movement.

1.5 Resonance Effects

The fundamental period of vibration of most wall and backfill geometries is usually less than 0.5 s and it is therefore usual to design free standing walls for earthquake peak ground accelerations (or lower than peak values if outward movement occurs). However, typical earthquake response spectra are very steep at low periods (Figure 1.8) and any flexibility may lead to ground motion amplification, particularly close to the top of the wall.

Although amplifications have been noted in model studies (Fairless 1989, and Wood and Yong, 1987), the results of these investigations have probably been affected by the presence of rigid boundaries that reflect and contain the vibrational energy within the model wall/soil system. In full scale wall structures, there are seldom boundary effects and the damping will be higher because of energy losses by elastic wave radiation. Also, where soil failures develop, it is likely that the soil damping may be higher than commonly assumed. Thus, it is difficult to draw firm conclusions on whether resonance effects should be considered or whether it is satisfactory to design to peak ground acceleration levels.

It is usual to neglect resonance effects in design of most wall structures but this is not a conservative assumption and special studies may be required for high and important wall structures.

1.6 Simplifications for Design

Although mathematical modelling techniques, such as the finite element method, are available to investigate the interaction of soils and wall structures under seismic loading, many of the required input parameters will not be well enough defined to enable precise estimates of the wall response and earth pressures to be computed.

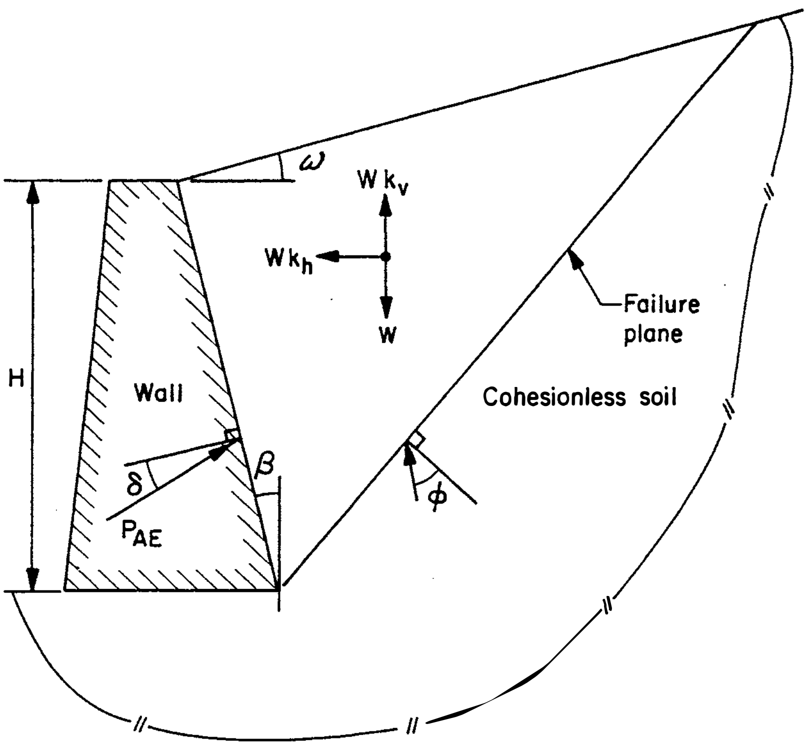

FIG. 1.7 FORCE ON WALL FROM LIMITING EQUILIBRIUM

Only for major structures will soils investigation information be sufficiently detailed to provide a good prediction of the soil behaviour under dynamic loading. The character of the earthquake motion is often only know in terms of generalised response spectra, and it is difficult to develop detailed information on the spatial variation in the ground displacements and how the ground shaking is modified by the foundation soils and by interaction with the wall. Thus, unless the wall is of unusual importance, it is acceptable for design purposes to use dynamic pressures calculated on the basis of simplified wall geometries and to use ground accelerations defined by response spectra that assume ground accelerations to be uniform within the extent of the surrounding soil mass. However, as mentioned previously, it is important that the simplified methods take into account the influence of wall deformations on the wall response. It is also necessary for the method to include inertia loads on the wall structure as well as the backfill and to consider any soil-structure interaction effects that may occur when the wall is part of a more major structure.

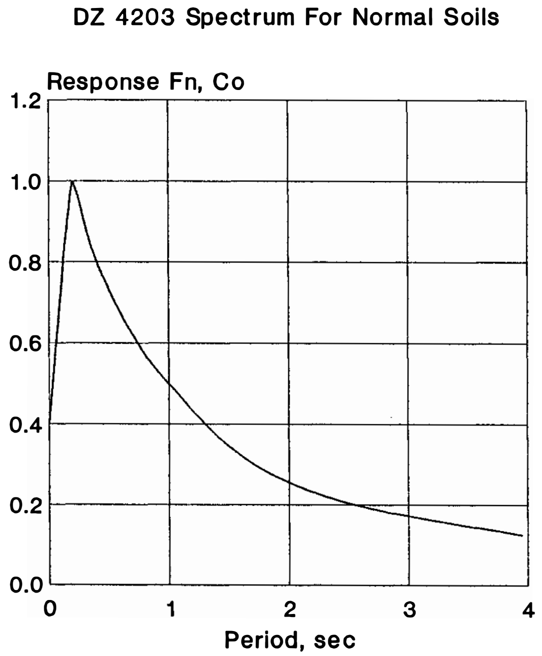

FIG. 1.8 ELASTIC RESPONSE SPECTRUM

WOOD AND ELMS

2

REVIEW OF WALL AND ABUTMENT RESEARCH

The seismic performance of a wide range of different types of walls and abutments has been considered in the research projects completed in New Zealand. It is convenient to review the work undertaken by considering the following topic areas:

(i) Rigid abutments and walls.

(ii) Deformable walls.

(iii) Walls translating by soil failure.

(iv) Walls rotating by base failure.

(v) Force/displacement relationships for walls displaced against the backfill.

(vi) Monolithic bridge abutments.

(vii) Reinforced earth walls.

(viii) Tied-back walls.

In the following sections of this Chapter, the work carried out in each of the eight topic areas is summarised and the main findings and results are presented. Where relevant to the New Zealand research, some of the findings from overseas work are also discussed.

2.1 Rigid Abutments and Walls

The analytical studies in this topic area (Wood, 1973) were motivated by the lack of established design procedures for estimating earthquake forces on rigid walls and walls where the MO assumption of a fully plastic stress state in the soil was inappropriate.

Results from the theoretical studies were used in the design guidelines for bridge abutments recommended by the New Zealand National Society for Earthquake Engineering (NZNSEE), (Matthewson et al, 1980). These design guidelines departed quite significantly from other design recommendations in that an attempt was made to relate the earthquake pressures to wall flexibility. Recommended rigid wall design forces were several times higher than those given by the MO theory.

Experimental work was carried out at a later stage when it was realized that there was still considerable confusion and uncertainty amongst practitioners about the validity of elastic theory to predict earthquake forces on rigid or almost rigid walls. The main objective of the testing programme was to provide an experimental verification of the proposed design forces.

The work on rigid walls was of particular relevance to bridge design because many abutment walls are stiffened by pile foundations or support from the bridge superstructure and do not satisfy the assumptions necessary for flexible wall behaviour.

2.1.1 Overseas Research

Results from quite a diverse range of experimental studies on the dynamic behaviour of model retaining walls have previously been published. Summaries of this work are given by Seed and Whitman (1970) and Yong (1985). Rather surprisingly, the reports on the behaviour of completely rigid walls are quite limited with many studies being directed to the more complex cases involving wall or foundation flexibility.

Probably the two most significant previous experimental studies related to rigid walls are described by Matuo and Ohara (1960) and Sherif et al (1982). Matuo and Ohara conducted tests on dry and water saturated sands in a box 400 mm deep by 1,000 mm long. Tests were conducted on a fixed end-wall (essentially rigid) and a movable end-wall that was permitted to rotate about its base. A harmonic forcing frequency of 3.3 Hz was used with the peak acceleration of the box varied between the range of about 0.1 g to 0.4 g. The theory of elasticity was used to derive approximate analytical pressure distributions for both the fixed and rotating walls. The experimental pressures for the rigid wall were significantly less than the theoretical values, but Matuo and Ohara attributed this difference to the influence of the side walls of the box and the elasticity of the pressure transducers. Both the measured and analytical pressure distributions showed a significant departure from the triangular shape that is commonly assumed in MO method.

In the Sherif et al (1982) experiments, the pressures on rigid walls were investigated using sand in a 1,000 mm high, 1,800 mm wide by 2,400 mm long box mounted on a shaking table. A sinusoidal input motion with a 3.5 Hz frequency and a maximum acceleration of up to 0.5 g was applied to the shaking table. The wall was capable of being displaced by rotation about the top or bottom and by pure translation. This enabled the effects of controlled deformations of the rigid wall to be investigated. Comparisons were made between the measured total dynamic force on the unyielding wall and the theoretical (theory of elasticity) solutions published by Matuo and Ohara (1961) and Wood (1973). Sherif et al concluded that the elastic theories overestimated the dynamic incremental force by a considerable margin. However, significant side and end wall effects would be introduced by the dimensions of the sand box used in their experiments and in view of the test results from the New Zealand research their conclusions are questionable.

One further shortcoming of previous model tests has been the lack of detailed attention to model scaling laws, resulting in the dynamic forcing inputs having frequencies considerably lower than the natural frequency of the model wall/soil system. Thus the possibility of dynamic amplification of the base motion has not been adequately considered.

2.1.2 Theoretical Study

A theory of elasticity solution for the pressures on a rigid wall statically loaded by a uniform horizontal body force in an elastic soil layer (Figure 2.1) was derived by Wood (1973). A dynamic solution for the related problem of horizontal dynamic forcing of the rigid boundaries was also given. The static solution gives a good approximation to the dynamic case providing the dynamic forcing frequencies are less than the natural frequencies of the retained soil layer.

The vertical end boundaries in Figure 2.1 were taken to represent rigid walls and the contact between the homogeneous linearly elastic soil and the wall was assumed to be smooth; that is, the vertical boundaries are assumed to be free of shear stresses. The lower horizontal boundary represents a rigid layer on which there are no displacements. A uniform static horizontal body force was assumed to act throughout the soil layer. For convenience, the magnitude of this body force was taken as $C(0)\gamma$; where $C(0)$ is the peak ground acceleration and γ the unit weight of the soil. Plane strain conditions were assumed so that the analytical model represented a long wall.

The normal stress, force and moment on the wall were evaluated for a range of L/H values between 0.5 and 10, and for Poisson's ratio, ν, between 0.2 and 0.5. Typical plots of the wall pressure distributions are shown in Figure 2.2. The wall forces and moments, found by integrating the normal pressure distribution on the wall and the moment of the pressure distribution about the base respectively, are shown in Figures 2.3 and 2.4.

A comparison between the analytical solution and the solution of the same problem using a standard finite element numerical method showed close agreement. The finite element

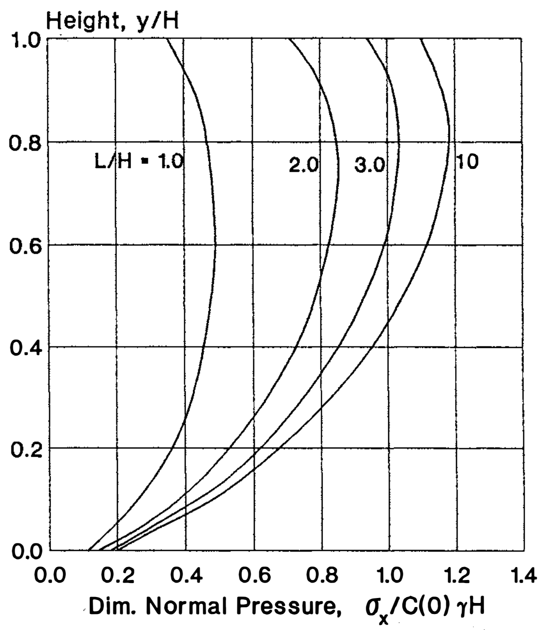

FIG. 2.2 SMOOTH RIGID WALL

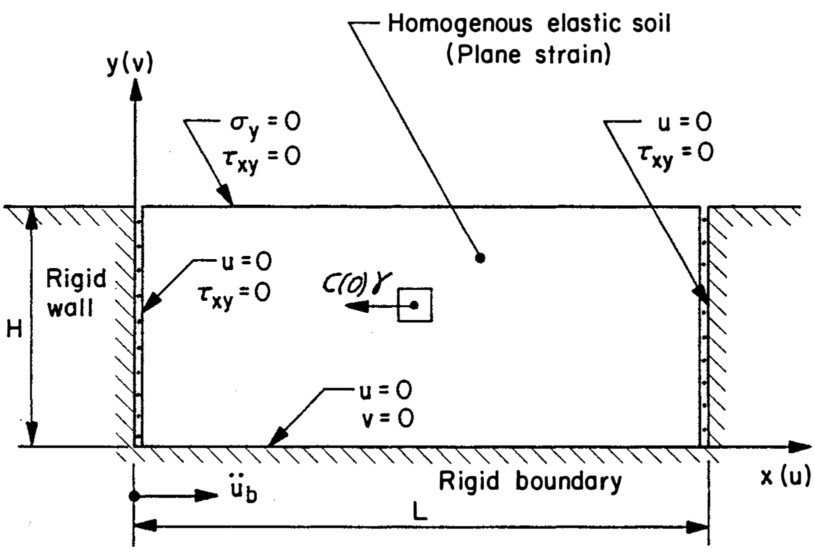

FIG. 2.1 RIGID WALL ANALYSIS

method was then used to compute solutions for the normal pressure on a rigid wall with fully bonded contact between the wall and soil. Pressure distributions for this case are compared with the analytical smooth wall solution in Figure 2.5. Apart from the stress singularity that occurs near the top of the wall for the bonded case, there is close agreement between the pressures for the two different boundary conditions.

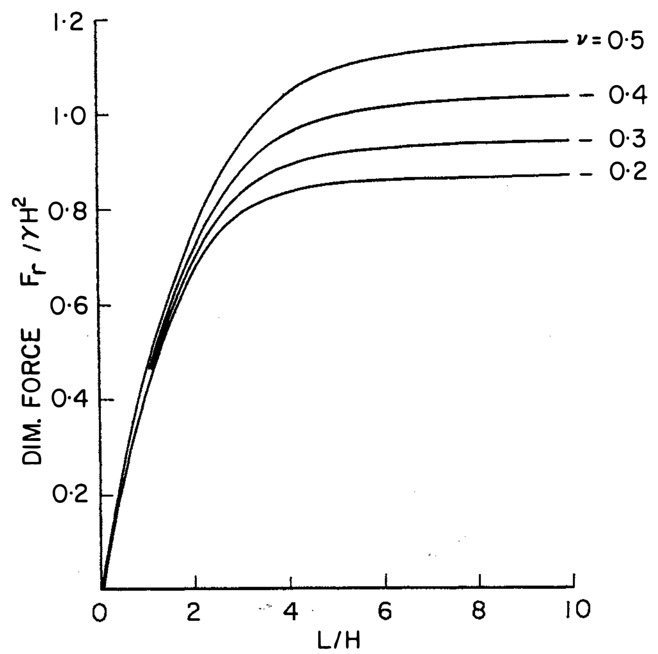

FIG. 2.3 FORCE ON RIGID WALL

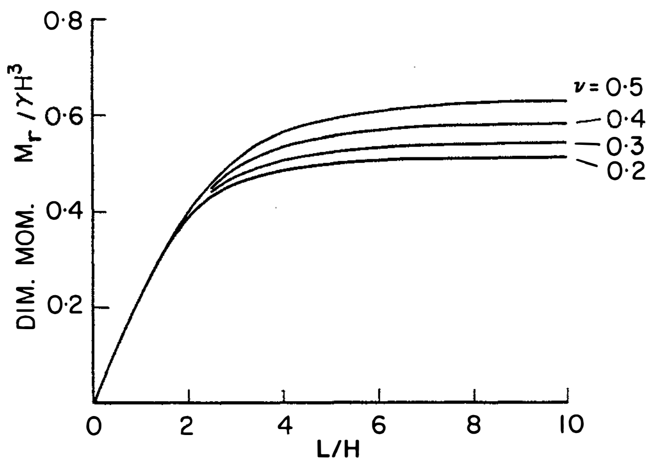

FIG. 2.4 MOMENT ON RIGID WALL

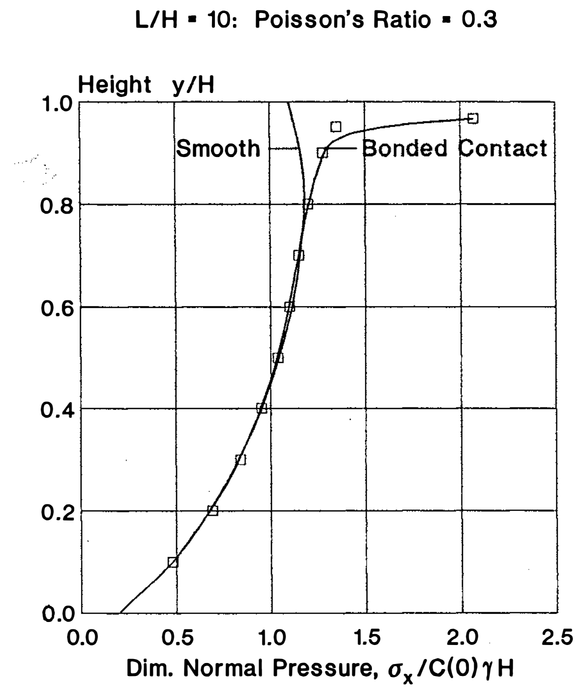

FIG. 2.5 NORMAL PRESSURE ON RIGID WALL

2.1.3 Model Wall Tests

Two series of model rigid wall tests were carried out and are described in reports by Yong (1985) and Thurston (1986 c). In the first series, a dry sand material was used as backfill. This work was extended in the second series by using moist sand and by carrying out a more detailed examination of the residual soil pressures that were found to develop as loose sand was compacted by vibrations of the shaking table used to test load the models.

The testing of the rigid walls was carried out using a sand box mounted on a 3.0 m long by 2.4 m wide shaking table driven in a single horizontal direction by a servo controlled electro-hydraulic actuator.

The model wall consisted of a 25 mm thick aluminium plate, 0.6 m high by 2.24 m wide, mounted at one end of the 2.15 m long sand box. The wall was supported horizontally by eight load cells arranged in two horizontal rows. This support method ensured that the flexural deformations of the wall were negligible producing essentially rigid wall behaviour.

Details of the model wall and instrumentation are shown in Figure 2.6. Pressures on the wall were measured with five pressure transducers located on the vertical centre-line of the wall. Four accelerometers were set up at various locations to record the motion of the table, wall and the sand mass.

The backfill soil was a relatively uniform sand having a D_{50} size of 0.25 mm. The sand was placed into the sand box by showering from a screw conveyor, which resulted in a very loose density state.

Wall pressures for the sand in a loose state were measured in a series of tests using a 4 Hz sinusoidal acceleration input with the table peak acceleration gradually increased from 0.05 g to 0.6 g. The total settlement of the sand during this initial series of tests was about 30 mm. Following the loose sand tests, the box was topped up with loosely placed sand and the complete sand volume compacted by 100 cycles of shaking at a peak acceleration of 0.6 g. A series of tests for the sand in this dense state were then carried using the same procedure as previously used for the loose sand. The tests were also repeated for the sand in a dense moist condition with an average moisture content of about 18%.

Measured densities for the very loose as placed state and the maximum density state were 14.6 kN/m^3 and 16.2 kN/m^3 respectively.

At the completion of the fixed frequency tests a further series of tests were performed sweeping the input frequency from 2 Hz to 65 Hz at a constant peak acceleration of 0.3 g. This test provided information on soil amplification and resonance effects.

The incremental dynamic force on the wall for the constant 4 Hz sinusoidal shaking of the backfill in loose, dense and moist conditions is plotted in Figure 2.7. The force increment is plotted in dimensionless form by dividing the measured dynamic force increment by the inertia unit force, $C(0)\gamma$, and H^2. For comparison, incremental dynamic forces from the theory of elasticity solution (Wood, 1973) and the MO method are also shown. There is good agreement between the experimental results and the elastic solution. As expected, the MO incremental force is considerably less than the experimental results.

A typical dynamic incremental pressure distribution for the dense backfill is compared in Figure 2.8 with the theory of elasticity solution and the NZNSEE recommendations (Matthewson et al, 1980). There is reasonable agreement between the measured and theoretical pressure distributions, but because of nonlinear behaviour of the sand in the relatively loose top layers close agreement was not expected. Over the range of accelerations tested, the experimental centre of pressure for the dense and moist backfill was at an almost constant height of about 0.58 H above the base of the wall. This is in close agreement with the theory of elasticity solution.

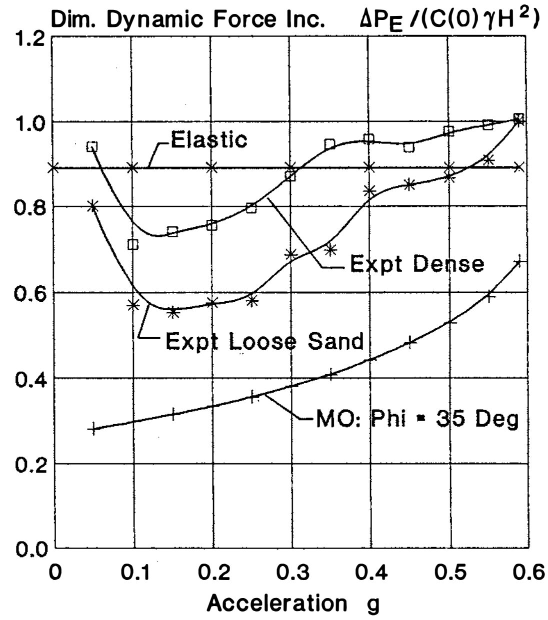

FIG. 2.7 RIGID WALL DYNAMIC FORCE INC.

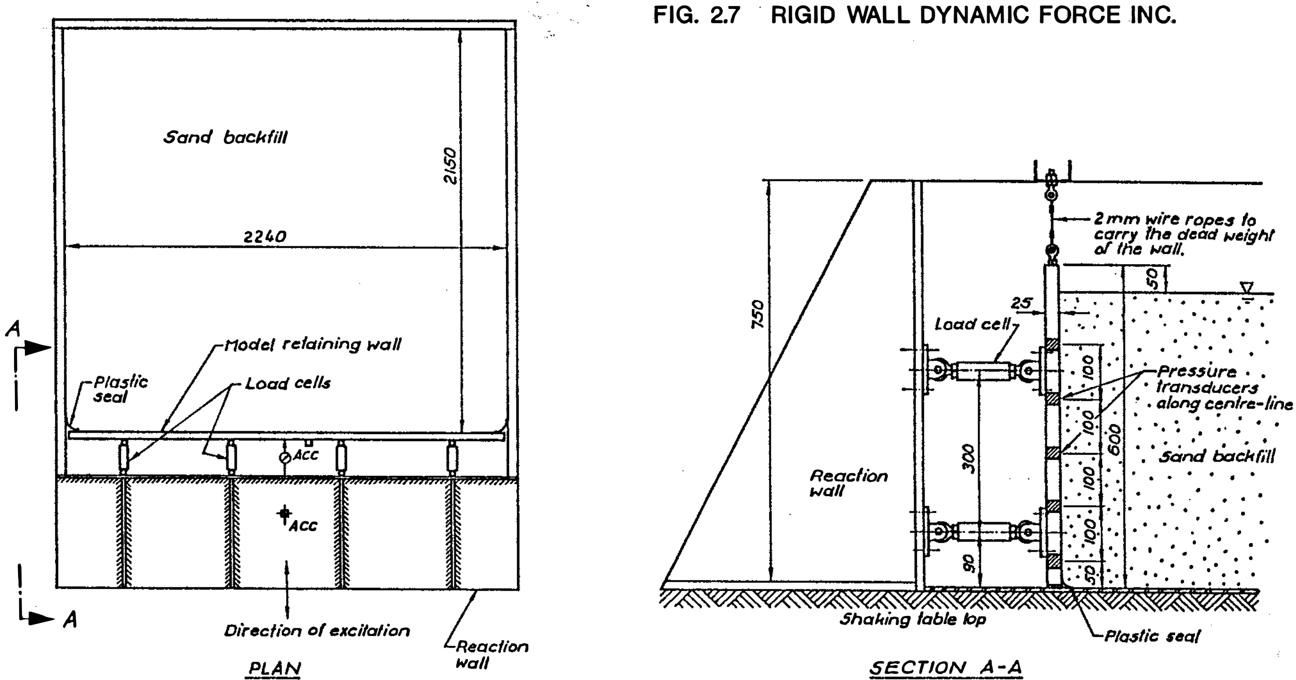

FIG. 2.6 RIGID WALL MODEL

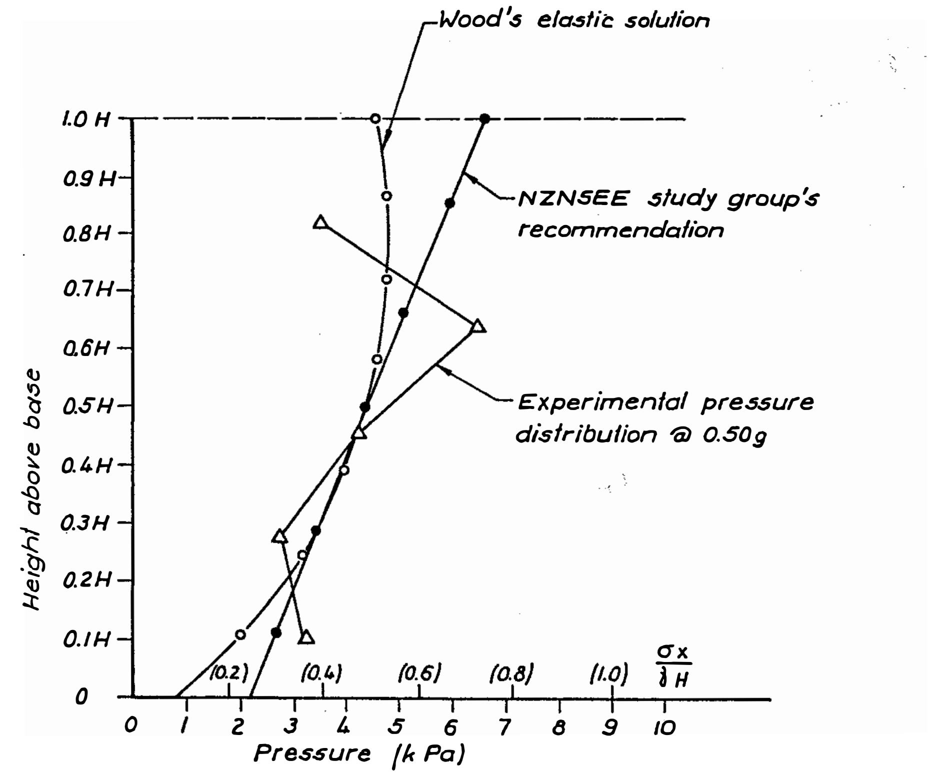

FIG. 2.8 DYNAMIC PRESSURE INCREMENT ON RIGID WALL

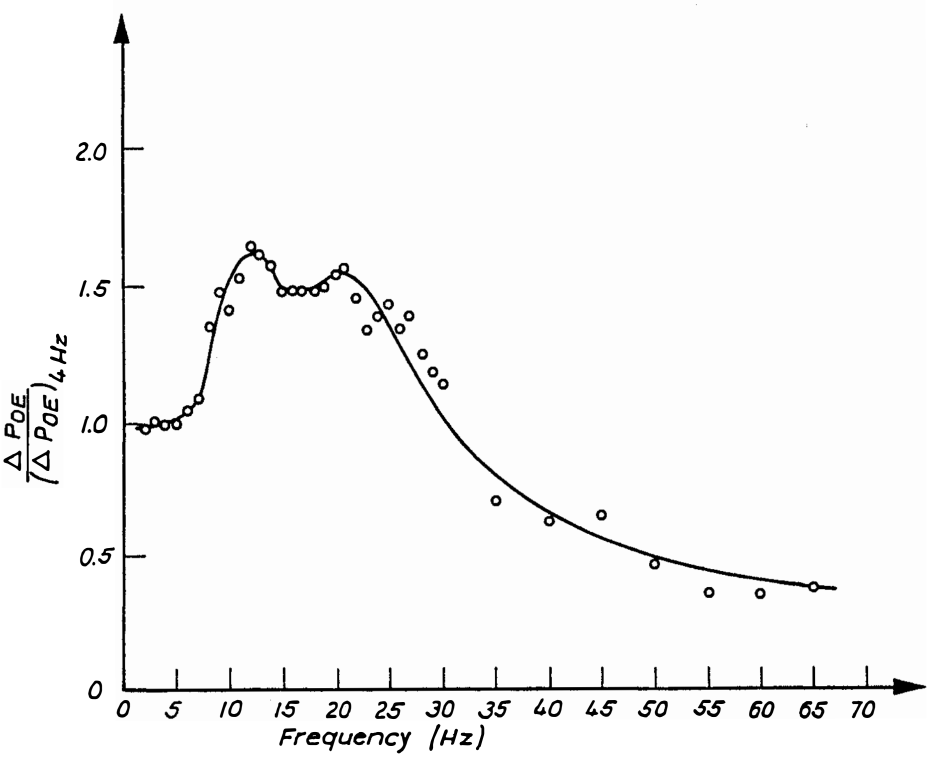

FIG. 2.9 DYNAMIC FORCE RATIO ON RIGID WALL

The dynamic force ratio on the wall measured during the frequency sweep carried out on the dense backfill is shown in Figure 2.9. The plotted force ratio is defined as the dynamic increment of wall force at a particular frequency divided by the dynamic increment measured at the 4 Hz frequency. A distinct resonance peak was observed between 10 Hz to 25 Hz. This frequency range is significantly less than the elastic theory prediction (Wood, 1973 and Yong, 1985) of about 50 Hz for the first natural frequency of the soil mass confined by rigid walls, but because of the low confining stresses, the equivalent elastic properties for the soil may have been lower than assumed. Fairless (1989) has suggested that scaling laws based on the theory of elasticity may not be appropriate for small sand models and that gravity-dominant scaling laws should be used (frequency scales as square root of model scale). The natural frequency of the model predicted by this scaling law is about 20 Hz, which is within the range of resonance observed in the testing.

The strong shaking generated in the tests produced a significant increase in the static soil pressures recorded before and after the completion of the tests. The increase of the static force at the completion of each acceleration level is shown in Figure 2.10. The increase was much larger in the loose backfill case than for the dense backfill. After the test series on the loose backfill, the static force on the wall was about 1.8 times the initial at-rest static force. For the dense case with peak accelerations lower than 0.3 g, increases in the static force were less than 2%. This increase in static pressure appears to be caused by the combined effect of backfill settlement and small elastic deformations of the wall. The dynamic pressures generated on the wall during the shaking cause small wall deflections and settlements and reorientation of the sand grains close to the wall. After each pressure pulse the wall does not completely return to its original position so that a residual pressure gradually develops as the number of cycles or acceleration level is increased. This effect may not be significant for full scale walls with less uniform soil.

2.2 Deformable Walls

There is a class of wall, termed here a deformable wall, that is intermediate between a rigid wall and a wall that displaces sufficiently for plasticity solutions to be applicable. Satisfactory solutions for this category can be obtained by theory of elasticity solutions or elastic finite element analyses.

2.2.1 Theoretical Study

Theoretical solutions for several deformable wall types have been presented by Wood (1973). Of particular interest was the solution for a wall deforming by rotation about its base (Figure 2.11). On the assumption of an elastic soil, the solution for a rotating wall can be obtained by superposition of the solutions for the rigid wall (Section 2.1.1) and the rotating wall forced against (or away from) the backfill. The forced wall solution is discussed in Section 2.5.2 below.

Considering moment equilibrium of the wall shown in Figure 2.11 gives:

$$M_r + M_f + \theta k_w H^2 = 0 \qquad (2\text{-}1)$$

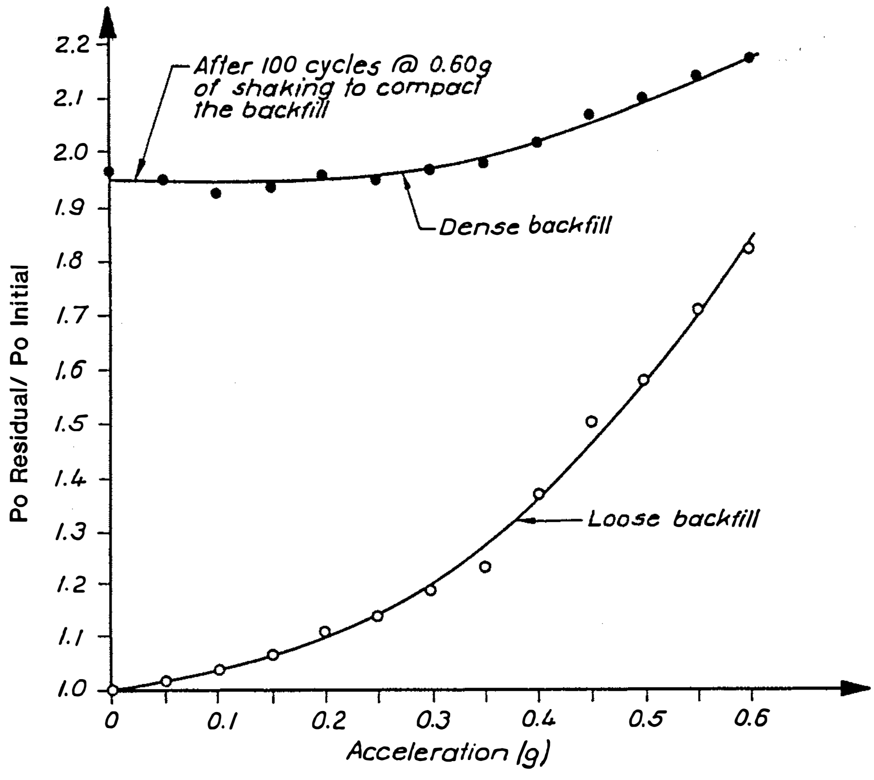

FIG. 2.10 INCREASE IN STATIC PRESSURES

Where:

M_r = The soil pressure moment on a rigid wall per unit length of wall.

M_f = The soil pressure moment on a forced wall per unit length of wall.

k_wH^2 = The rotational stiffness of the wall per unit length.

M_r, M_f and θ are taken as positive in the clockwise direction.

Expressions for M_r and M_f can be obtained from the wall moment solutions for rigid and forced walls shown in Figures 2.4 and 2.41. On the assumption of a large L/H ratio, the two moments can be approximated by:

$$M_r = 0.55\ C(0)\gamma H^3 \qquad (2\text{-}2)$$

$$M_f = 0.29\ E\theta H^2 \qquad (2\text{-}3)$$

Substituting these expressions into expression (2-1) and rearranging gives the wall rotation as:

$$\theta = \frac{-0.55}{(0.29 + k_w/E)} \cdot \frac{C(0)\gamma H}{E} \qquad (2\text{-}4)$$

Evaluating expression (2-4) for θ enables the total force and the pressure distribution on the wall to be calculated. The rigid wall force, F_r, can be obtained from Figure 2.3, and the forced wall force, F_f, can be obtained from Figure 2.40. The total earthquake force on the wall is then given by:

$$F_t = F_r + F_f$$

$$= 0.95\ C(0)\gamma H^2 + 0.4\ E\theta \qquad (2\text{-}5)$$

Figure 2.12 shows pressure distributions on the wall obtained by superposition of the rigid wall and forced wall solutions. The pressures plotted are only the component from the horizontal body force, representing the earthquake inertia load from the soil, and do not include the pressures from the static gravity forces. Pressures are plotted for a range of values of the dimensionless force parameter defined by:

$$P_r = \frac{E\theta}{C(0)\gamma H^2} \qquad (2\text{-}6)$$

It is informative to evaluate P_r for typical wall and soil properties. For example, if $E = 10$ MPa, $\theta = 0.002$ radians, $C(0) = 0.3$, $\gamma = 20$ kN/m^3, and $H = 5$ m, then expression 2-6 gives $P_r = 0.67$.

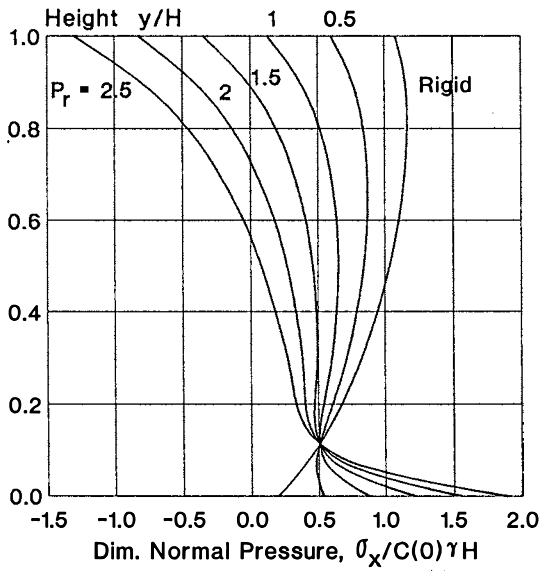

FIG 2.12 ROTATING WALL
EQ Pressure Increment

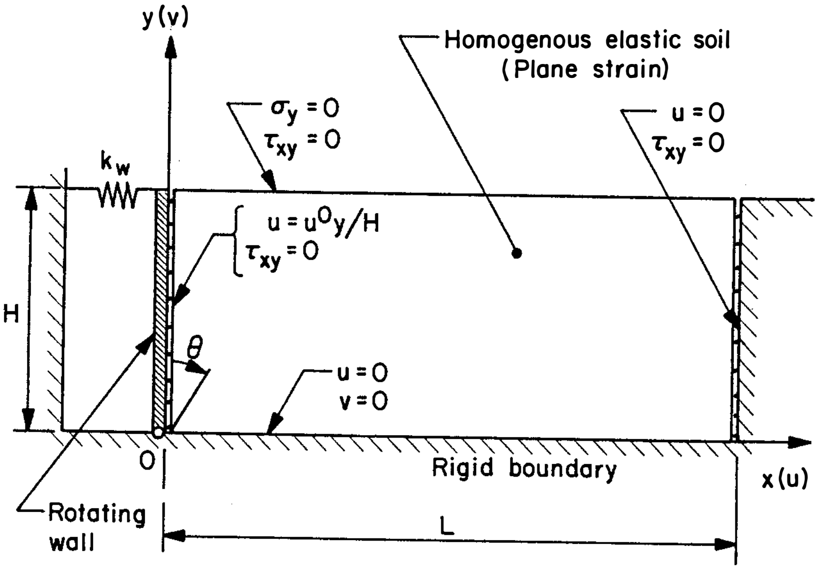

FIG. 2.11 WALL DEFORMING BY ROTATION ABOUT BASE

Figure 2.13 shows the combined earthquake and gravity stresses evaluated assuming the ratio of the at-rest pressure coefficient divided by the horizontal earthquake coefficient, $K_0/C(0) = 1.5$, (for example, $K_0 = 0.45$, $C(0) = 0.3$). For comparison with the plotted pressures, the MO pressure coefficient divided by the peak ground acceleration coefficient, $K_{AE}/C(0) = 1.9$, for a soil with $K_0 = 0.5$ (friction angle = 30°) and $C(0) = 0.3$. Figure 2.13 shows that at a P_r value of about 1.5, the pressure distribution is roughly triangular in shape and has a maximum value at the base that is approximately the same as the MO pressure distribution. It would appear reasonable to expect the theory of elasticity solution to give satisfactory pressures for P_r values of up to 1.0. At P_r values greater than about 1.5 the MO method should be used.

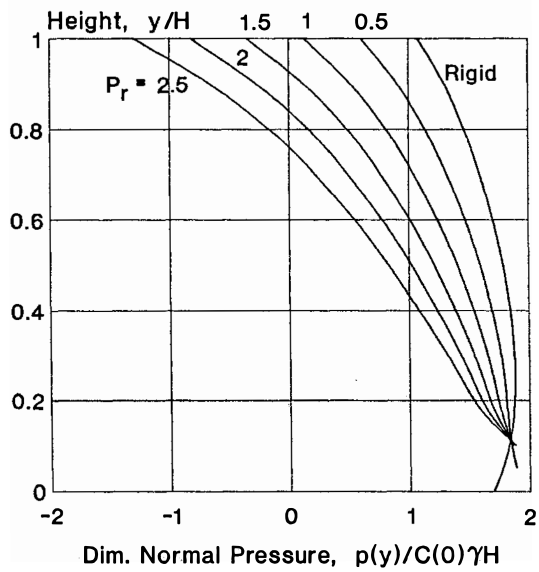

FIG. 2.13 ROTATING WALL
EQ + Gravity Pressures

2.2.2 Model Wall Tests

Yap (1987) and Stevenson (1988) carried out two similar series of tests on model deformable walls using a sand box on a shaking table to simulate earthquake dynamic loads. The flexibility was obtained by allowing the wall to pivot at its base, with rotational resistance provided by springs at approximately mid-height of the wall. In Yap's experiments, partly saturated dense sand was used and the walls were all relatively stiff. Stevenson used dry sand and varied the wall rotational stiffness over a greater range. The results were compared with Wood's theory of elasticity solution (Wood, 1973), the NZNSEE (Matthewson et al, 1980) design recommendations and the MO method.

The base of the wall was designed as a pin joint using loads cells with swivel joints to measure the reaction force (Figure 2.14). The wall stiffness was made adjustable by connecting the wall at mid-height through cantilever springs of variable length to load cells. Measuring the forces on the wall with load cells at two different heights enabled the centre of pressure to be determined as well as the total force on the wall. The height of the backfill behind the wall was 550 mm and the width of the wall 2,240 mm. The length of the sand backfill layer behind the wall was 2,150 mm.

The sand used was Firth's No 1 sand similar to that used by Yong (1985) for the rigid wall tests described in Section 2.1.3

A summary of the measured physical properties of the sand is given in Table 2.1

TABLE 2.1

Sand Properties - Firth's No 1 Sand

Property	Value
D_{10}	0.13 mm
D_{30}	0.19 mm
D_{50}	0.25 mm
D_{60}	0.30 mm
D_{60}/D_{10}	2.31
ϕ, loose (γ = 13.8 kN/m^3)	36°
ϕ, med dense (γ = 15.1 kN/m^3)	45°
ϕ, dense (γ = 15.7 kN/m^3)	51°

Displacement transducers were used to measure the wall deflections at six locations and an accelerometer was used to measure the table input motion.

For each wall stiffness set-up, the wall was dynamically shaken with a 4 Hz sinusoidal input at acceleration amplitudes increasing from 0.1 g to 0.6 g in increments of 0.1 g.

Prior to each set-up, the shaking table was run with a sinusoidal input motion of 0.6 g peak acceleration for several minutes to compact the sand into a relatively dense state.

The experimental results showed that the dynamic force on the wall increased in an approximately linear manner with the peak input acceleration up to an acceleration level of about 0.4 g. At higher accelerations there was a more rapid increase in the wall force that may have been related to general failure in the surface layers of the sand.

Figure 2.15 shows the dimensionless dynamic force increment defined by:

$$\Delta P_E' = \Delta P_E/(C(0)\gamma H^2),$$

plotted against the force ratio parameter defined by:

$$P_r = (E\theta)/(C(0)\gamma H^2),$$

for both the experimental results and the theory of elasticity solution. (P_r is effectively the ratio between the force

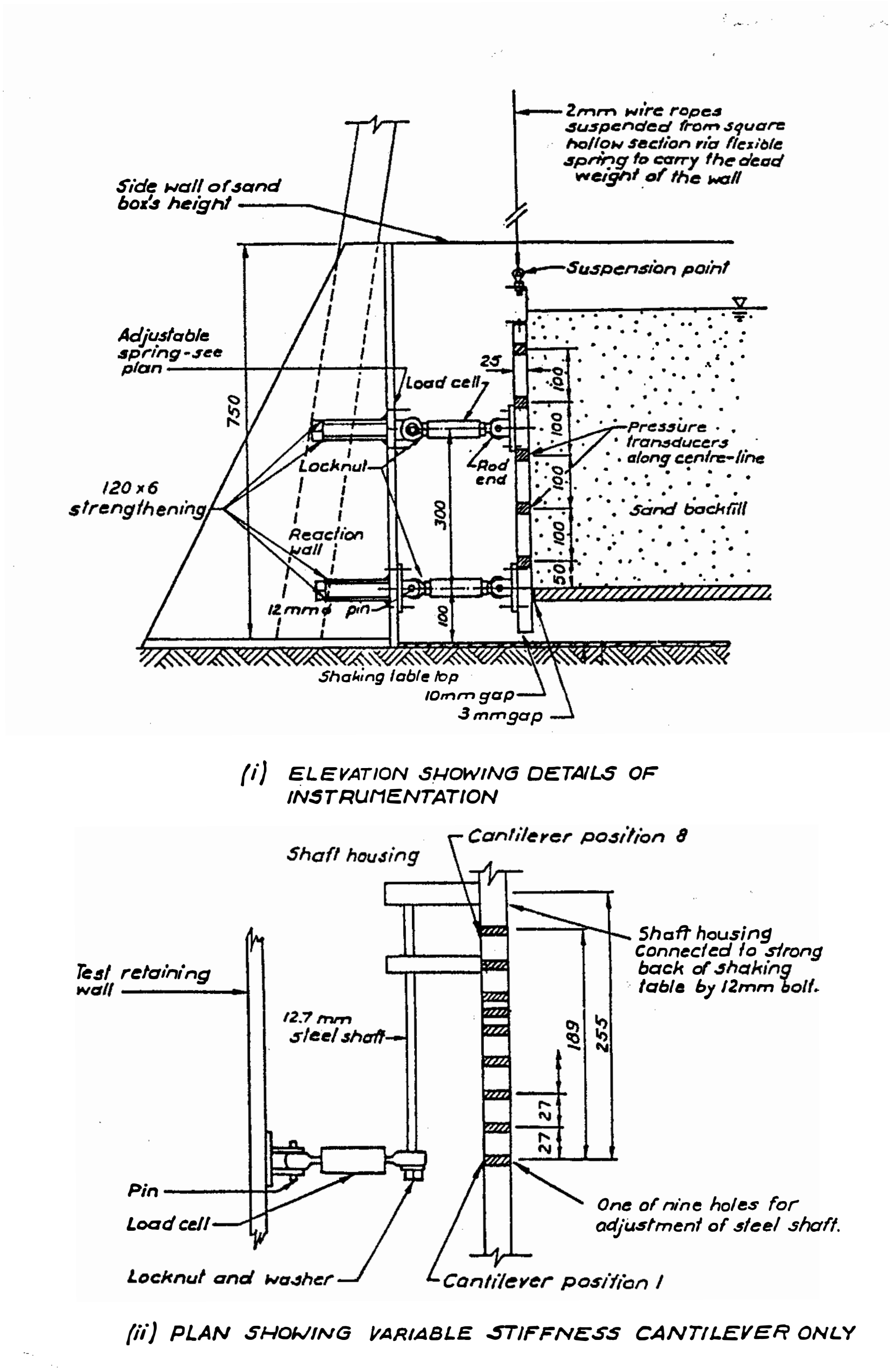

FIG. 2.14 ROTATING WALL MODEL
(Stevenson, 1988)

generated by wall movement and the inertia force). The experimental results were computed from the average of the forces recorded for the acceleration increments between 0.1 g to 0.4 g. The MO dimensionless force increment, $\Delta K_{AE}/C(0)$, for $\phi = 35°$ and wall friction $\delta = 2\phi/3$ is also shown and varies from 0.35 to 0.44 as the acceleration increases from 0.2 g to 0.4 g.

To compute the theory of elasticity solution, an average Young's modulus for the sand was estimated by carrying out static cyclic loading tests, rotating the wall against and away from the backfill. Several load cycles were carried out before and after the dynamic testing. A typical force displacement curve for the statically rotated wall is shown in Figure 2.16. The sand behaves in a nonlinear manner with a significant difference between the loading and unloading parts of the curve, making it difficult to define an equivalent modulus. An average Young's modulus of 4 MPa was assumed to be appropriate for the stiffer walls. This value was reduced to 3 MPa for the most flexible walls analysed. Modulus values for sand are often assumed to be about an order of magnitude higher than these values. But, the low values appear to be appropriate for the very low confining stresses and the relatively high shear strains in the backfill sand of the model walls.

Figure 2.15 shows that the theory of elasticity solution gives a good estimate of the wall dynamic force increment for values $P_r < 1.0$. At $P_r > 1.5$, the MO method gave forces in reasonable agreement with the measured forces for input accelerations greater than about 0.3 g. At lower accelerations the MO tended to underestimate the dynamic force increment to some extent.

Figure 2.17 compares the measured height of the centre of pressure, s, of the dynamic force increment with the elastic solution. The measured centres of pressure were taken

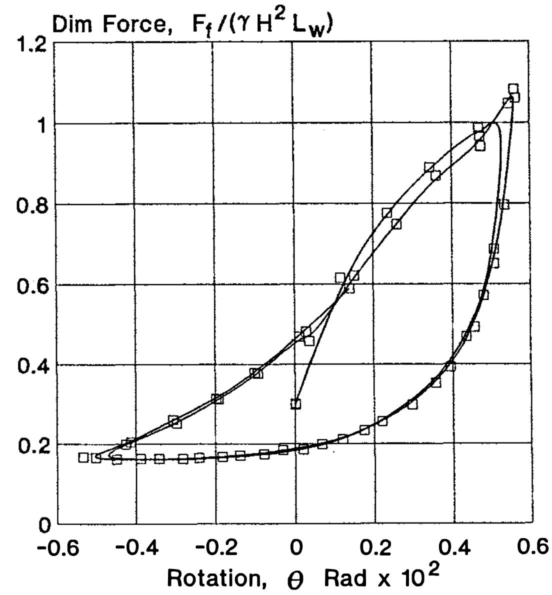

FIG. 2.16 ROTATING WALL TEST
Gravity + Rotational Force Component

as the average of the values for acceleration increments between 0.1 g to 0.4 g. Although both the measured and theoretical values decreased with increasing P_r, the measured centre of pressure tended to be lower than the theoretical value. At P_r values greater than 1.4, the measured value was lower than the H/3 value normally assumed for the MO pressure distribution.

The experimental work showed that for wall deformation resulting from base rotation, good estimates of the earthquake pressures and forces can be obtained by using the force ratio parameter P_r to interpolate between the upper and lower bounds given by the theory of elasticity and MO solutions.

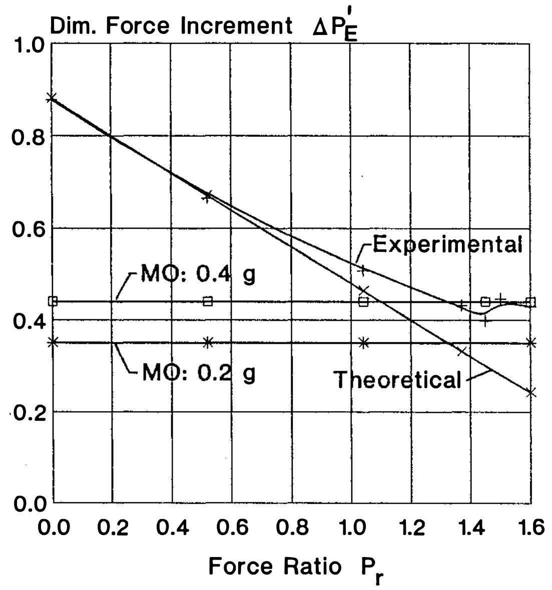

FIG 2.15 ROTATING WALL TEST
Comparison of Expt and Theor Force Inc

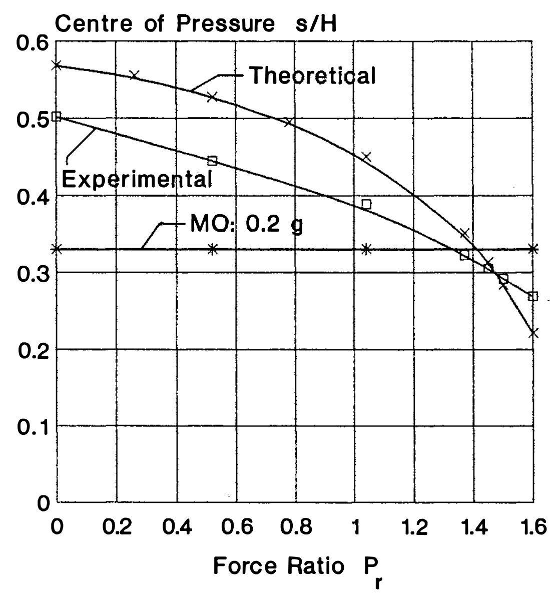

FIG 2.17 ROTATING WALL TEST
Comparison of Expt and Theor C o P

2.3 Walls Translating by Soil Failure

2.3.1 Theoretical Study

Richards and Elms (1979) (also see Elms and Richards, 1979) developed a wall design procedure that recognized that a wall does not necessarily fail when the ground acceleration reaches a value corresponding to a factor of safety of one on a sliding or rotational soil failure. If the critical acceleration (factor of safety equal to one) is exceeded, the wall will develop some relative permanent displacement to the underlying soil. Often wall structures are can tolerate significant permanent movement without damage. This approach is an extension of the Newmark (1965) sliding block method that was initially developed as a method for predicting the displacement of soil masses in slope failures on earth dams and embankments.

The forces acting on the wall in the Richards-Elms analysis are shown in Figure 2.18. The force acting on the back face of the wall is obtained from the MO method and is a function of the horizontal and vertical acceleration coefficients as well as the soil properties. The main resisting force is derived from the soil friction on the base of the wall (and passive resistance at the toe) that has a limiting value related to the wall weight and the soil friction angle. As the ground accelerations build up, the driving force against the wall may exceed the base resistance, resulting in relative movement between the wall and soil layer. The slip will stop as the acceleration peak reduces, resulting in a relatively small permanent movement. In a typical earthquake, there may be a number of peak accelerations that produce forces on the wall exceeding the critical sliding resistance causing intervals of sliding movement. Because of the high resistance to sliding when the inertia forces on the wall act against the backfill, the wall will generally only move in an outward direction. Each large acceleration peak therefore produces an accumulating movement in the outward direction.

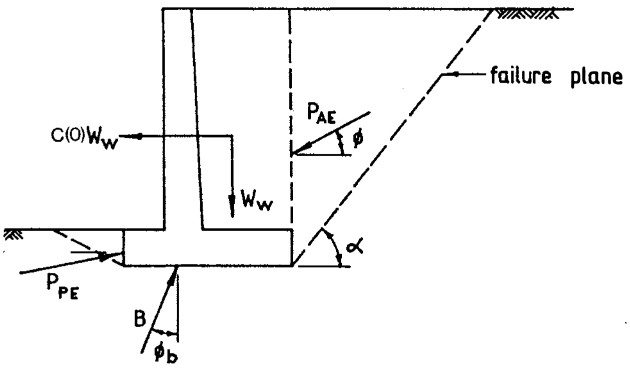

FIG. 2.18 TRANSLATING WALL ANALYSIS

The MO equations for the active pressure state are given in Figure 2.19 (Ministry of Works, 1973). A more general form includes the effect of vertical acceleration but for most walls this effect is small and can be neglected.

The MO method does not give detailed information on the shape of the increment of earthquake pressure and there are conflicting results from model tests carried out on shaking tables and other simplified plasticity methods (Athanasiou-Grivas, 1978; Prakash and Nadakumaran, 1979; Saran and Prakash, 1970). However, from the elastic solution for rotating walls outlined in Section 2.2.1 and other finite element studies by Wood (1973) it appears reasonable to conclude that providing the wall is sufficiently flexible for active conditions to develop, the increment of earthquake force will act at approximately H/3 above the base of the wall.

Richards and Elms (1979) investigated the influence of inertia loads from the wall mass on the factor of safety against sliding under earthquake loading and concluded that it was important to include these loads in the analysis. The importance of the wall mass will depend on the type of wall system. For gravity walls it is the wall mass that is providing most of the resistance to sliding and it is clearly necessary to consider the earthquake inertia loads on the total mass of the wall and sliding wedge. Many other wall types, including cantilever and counterfort walls, are analysed for stability by considering a virtual back plane passing through the wall heel and therefore can be analysed for sliding or overturning stability in a similar manner to gravity walls. For these walls, it is also necessary to include the inertia loads on the wall and the soil mass between the wall and the virtual back plane (Figure 2.18).

Critical acceleration levels for various wall assumptions can be obtained from the detailed analyses in Elms and Richards (1979). A simplified analysis method given by Whitman (1979) provides expressions for the critical acceleration that are suitable for most design applications. By considering equilibrium of the forces shown in Figure 2.18 on a wall with a vertical back face, horizontal backfill and zero back face friction angle, Whitman derived the following expression for the critical acceleration coefficient:

$$k_c = \frac{(FS-1)}{FS/\tan\phi_b + C_{AE}/K_A} \qquad (2\text{-}7)$$

Where:

FS = Factor of safety against sliding under static loads.

ϕ_b = Friction angle for wall base.

K_A = Active soil pressure coefficient (gravity loads).

C_{AE} = $\Delta K_{AE}/k_c$

ΔK_{AE} = MO coefficient of active earthquake pressure increment.

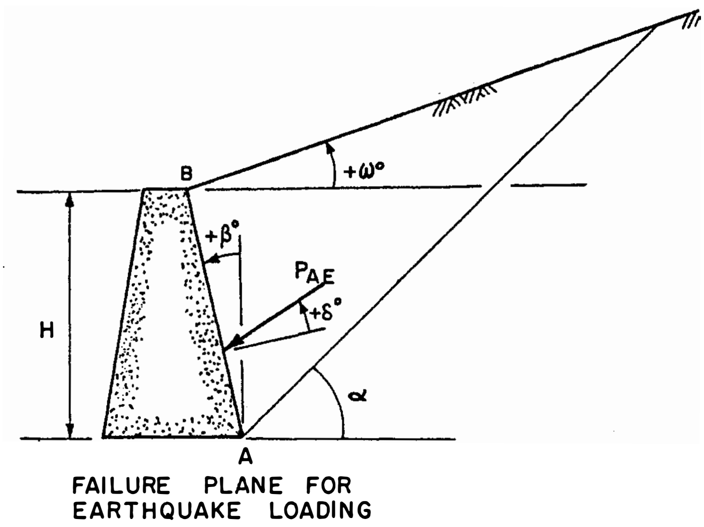

ACTIVE PRESSURE

$$P_{AE} = \tfrac{1}{2} K_{AE} \gamma H^2$$

$$K_{AE} = \frac{\cos^2(\phi-\beta-\theta)}{\cos\theta \cos^2\beta \cdot \cos(\delta+\beta+\theta)\left[1 + \sqrt{\frac{\sin(\phi+\delta)\ \sin(\phi-\omega-\theta)}{\cos(\delta+\beta+\theta)\ \cos(\beta-\omega)}}\right]^2}$$

$$\theta = \tan^{-1} C(0)$$

$$\cot(\alpha - \omega) = -\tan(\phi+\delta+\beta-\omega) + \sec(\phi+\delta+\beta-\omega)\sqrt{\frac{\cos(\beta+\delta+\theta)\ \sin(\phi+\delta)}{\cos(\beta-\omega)\ \sin(\phi-\theta-\omega)}}$$

FIG. 2.19 MONONOBE-OKABE EQUATIONS

Although ΔK_{AE} is a complex function of the earthquake acceleration coefficient and the soil properties, C_{AE} is reasonably constant and varies between 0.6 and 0.9 for soil friction angles between 30° and 35° and horizontal acceleration coefficients between 0.15 to 0.3. For design purposes, C_{AE}, can be taken as 0.75.

If the wall inertia force is neglected, expression (2-7) reduces to:

$$k_c = \frac{(FS-1)}{C_{AE}/K_A} \qquad (2\text{-}8)$$

Both expressions (2-7) and (2-8) are plotted in Figure 2.20 for soil friction angles of 30° and 35°. (Approximate values of C_{AE} were used to evaluate the expressions). Figure 2.20 shows that for a wall designed with a factor of safety of 1.5 against sliding, the critical acceleration coefficient, k_c, is approximately 0.11. If the inertia force on the wall mass is neglected, then the critical acceleration will be overestimated by a factor of about 2.

A number of studies have been carried out to find the displacement of a sliding block subjected to acceleration time histories from recorded ground motions. Newmark (1965) computed the maximum displacement

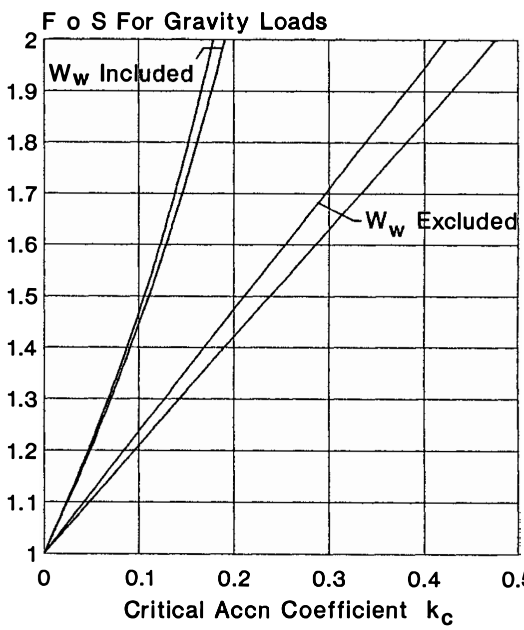

FIG. 2.20 SLIDING WALL

responses for four earthquake records, and plotted the results after scaling the earthquakes to a common maximum acceleration and velocity. Franklin and Chang (1977) repeated the analysis for a large number of both natural and synthetic records and added their results to the Newmark data. Their results were based on ground motions that had been normalised to a peak acceleration of 0.5 g and a peak velocity of 0.76 m/s. A probabilistic approach to the problem of computing displacements was used by Lin and Whitman (1986). Elms and Richards suggested that an expression that gave a good fit to the Franklin and Chang results for relatively low displacements was:

$$d = \frac{0.087\, V^2}{C(0) g} \cdot \left[\frac{C(0)}{k_c}\right]^4 \qquad (2\text{-}9)$$

Where:

C(0) = Peak ground acceleration coefficient

g = Acceleration of gravity

V = Peak ground velocity

Expression 2-9 applies for the case of unsymmetrical sliding where motion can only occur in one direction.

Other approximate expressions for the outward displacement have since been published by Matthewson et al (1980) and Nadim and Whitman (1985). These are compared with the Richards and Elms expression in Figure 2.21.

It is generally considered more desirable for outward movement to occur by a sliding failure rather than overturning. Elms and Richards (1979) investigated some of the wall parameters required to ensure a sliding type of failure but this work is specific to a trapezoidal wall shape.

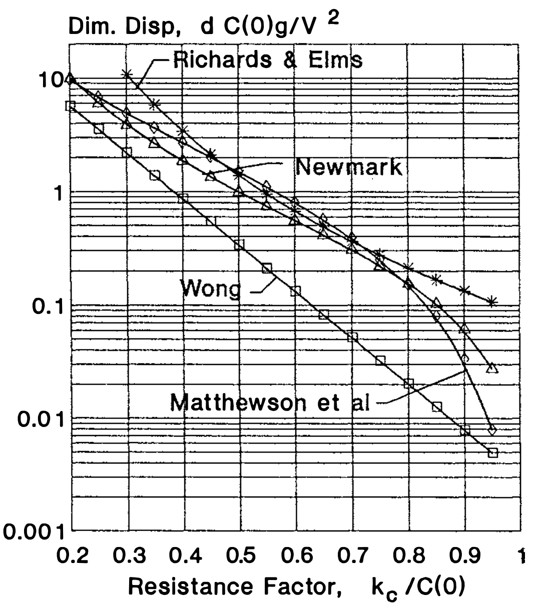

FIG 2.21 SLIDING BLOCK DISPLACEMENTS
Unsymmetrical Sliding

Parameter studies by Elms and Richards (1979) included consideration of the effect of vertical acceleration on the wall forces. More detailed work on vertical acceleration effects was subsequently carried out by Zarrabi-Kashani (1979) (see Whitman, 1979). Vertical accelerations affect both the sliding resistance and the dynamic pressure on the wall and simultaneous application of both vertical and horizontal accelerations results in a significant increase in the complexity of the analysis. Peak horizontal and vertical accelerations may not be well correlated in actual recorded ground motions and it therefore becomes necessary to carry out time history analyses to study the wall displacement response. Studies reported by Whitman (1979) show that in most cases the effect of vertical acceleration is probably small. The effect decreases with decreasing $k_c/C(0)$ ratios; that is with increasing displacement. With large $k_c/C(0)$ ratios the vertical acceleration can cause significant increases in displacement but in this case the displacement will be small and the difference may not be of practical significance for walls. A more detailed study of the effects of vertical accelerations and the shape of the response spectrum of the earthquake accelerogram on the displacement of a sliding block has recently been completed by Sharma (1990).

Richards and Elms (1979) suggested the following design procedure based on the sliding block approach:

- Select an acceptable outward displacement, d.
- Compute the critical acceleration coefficient k_c from expression (2-7) or Figure 2.20.
- Compute the total active thrust on the wall from the MO equations corresponding to the required k_c value.
- Find the weight of the wall required to develop sufficient base friction to resist the MO total force P_{AE} and the inertia force applied to the wall $k_c W_w$.
- Check that the wall will slide rather than overturn.

For the case of a smooth wall with a vertical back face and horizontal backfill, the required weight of wall to resist the earthquake forces corresponding to a critical acceleration coefficient k_c is given by:

$$W_w = \frac{P_{AE}}{\tan\phi_b - k_c} \qquad (2\text{-}10)$$

Alternatively, use can be made of the approximate expression:

$$W_w = \frac{0.5\, \gamma H^2 (K_A + k_c C_{AE})}{(\tan\phi_b - k_c)} \qquad (2\text{-}11)$$

By using the coefficient C_{AE}, (approximately 0.75 for typical friction angles and k_c values), expression (2-11) eliminates the need to evaluate P_{AE}.

Richards and Elms concluded that a gravity wall designed for any reasonable safety factor under static loads will experience permanent displacements in strong ground shaking. If the wall is designed to resist at the point of sliding failure, an earthquake force corresponding to about half the peak ground acceleration, the outward movement is unlikely to exceed about 100 mm. In many applications this might be an acceptable displacement.

2.3.2 Model Wall Tests

Lai (1979) (Lai and Berrill, 1979) carried out shaking table tests on model gravity retaining walls to check the validity of the Richards-Elms sliding block method for predicting the critical acceleration and the outward translation displacement of gravity type retaining walls. The tests were carried out using a 2.4 m long, 510 mm wide, glass-sided rectangular tank mounted on an electro-hydraulic shaking table.

Figures 2.22 and 2.23 show details of the 300 mm high model wall, that was backfilled to 250 mm above its base and rested on a depth of soil below the wall base of 100 mm. Since the wall weight was an important parameter in the theory, provision was made to add mass to the model base by bolting on steel plates. The low centre of gravity ensured translational rather than rotational failure.

Bending moment and vertical and horizontal shear forces on the rear face of the model wall were measured with strain gauges on the wall stem. Displacements of the top of the wall relative to the tank were measured with two displacement transducers and two accelerometers were used to record the tank and wall base accelerations.

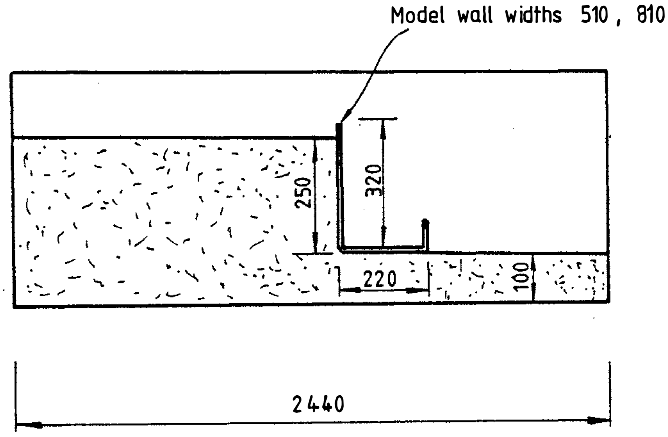

FIG. 2.22 TRANSLATING MODEL WALL
(Lai, 1979)

A fairly uniform fine to medium sand, with an angle of internal friction reported to be about 30° was used in the tests. This friction angle is lower than measured in some of the other model tests described in the following sections.

Tests were carried out using both a 5 Hz periodic excitation and scaled accelerograms recorded during the 1940 El Centro and 1966 Parkfield earthquakes. Several series of tests were carried out using different wall weights.

Figure 2.24 shows a comparison of theoretical predictions and measured displacements of the wall subjected to the El Centro accelerogram. Results for three different wall weights (that is the different critical accelerations) are shown. There was good similarity between the

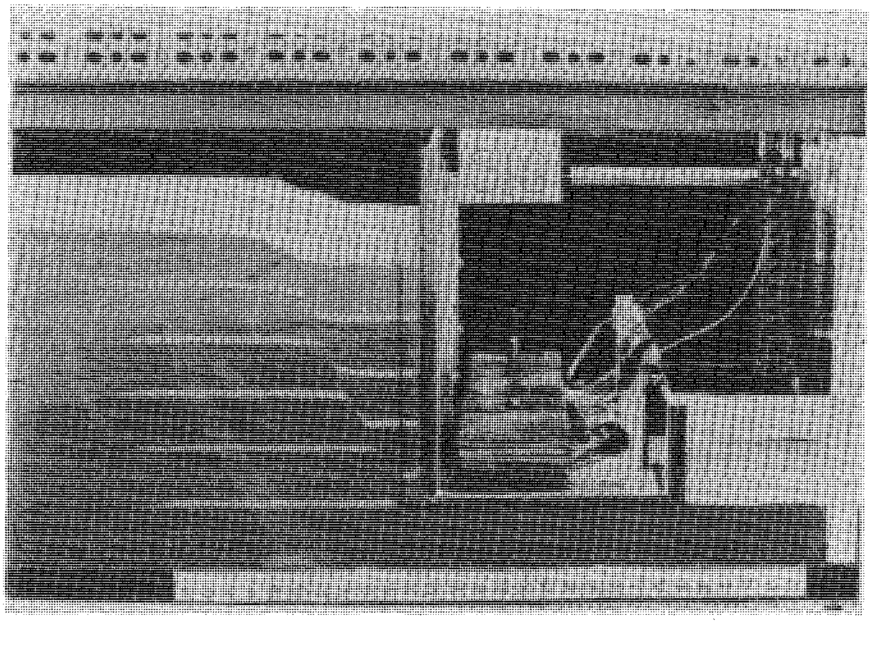

FIG. 2.23 FAILURE WEDGE BEHIND MODEL WALL.
(Lai, 1979)

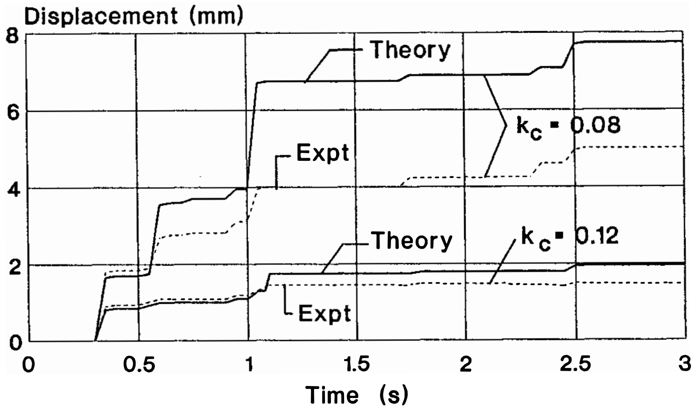

FIG 2.24 WALL DISPLACEMENTS (Lai, 1979)
Comparison of Theory and Experimental

measured and predicted results but the measured displacements were always less than predicted. It was thought that some of the differences were caused by a lowering of the backfill with increasing displacement and changes in the base friction caused by the shaking. It also appears that the base friction may have been greater than assumed in the analysis.

Lai's comparison between the theoretical critical accelerations to initiate sliding and measured values is shown in Figure 2.25. There was good agreement between the measured values and theoretical predictions using a base friction angle of about 25°.

The general conclusion from the work was that the sliding block theoretical model predicted the observed sliding behaviour of the model wall remarkably well.

Jacobsen (1980) made a detailed theoretical comparisons between the experimental results of Lai (1979) and Zarrabi's (1979) double block model. In Zarrabi's work, carried out at Massachusetts Institute of Technology, a wall sliding block and a soil failure wedge are included in the analysis to consider the vertical acceleration of the soil wedge as it moves downwards behind the outward displacing wall. Analytical results from the double block model were in closer agreement with Lai's experimental results than the simple single sliding block solution.

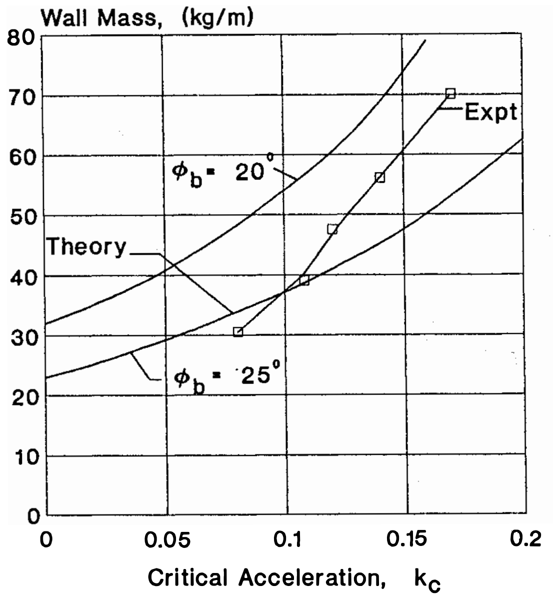

FIG. 2.25 WALL CRITICAL ACCELERATION (Lai, 1979)

Although Zarrabi's theoretical analysis method predicted that the inclination of the failure surface changed with time, this was not observed in the model testing, suggesting that a correction to the double block analytical approach may be necessary.

Jacobsen observed that the acceleration of the wall increased above the critical level required to initiate sliding until the wall acceleration exceeded the shaking table acceleration, then decreased until sliding stopped. This behaviour is predicted by the Zarrabi model but not the simple block model. By integrating the wall and shaking table accelerations it was found that the sliding stopped when the ground and wall velocities matched. This result is as predicted by the theory.

Jacobsen found that the displacement results were sensitive to the friction angle assumed for sliding contact on the wall base. He also found that the base friction appeared to be velocity dependent. In view of the difficulty in closely defining this parameter for practical design applications, it appeared that further refinement of the simple sliding block theory could hardly be justified.

A further series of tests was carried out by Aitken (1982) to examine sliding wall behaviour in more detail and in particular to study the detail of the response to a simple sinusoidal input motion. The sand box and backfill sand were the same as used by Lai. The wall geometry was also the same but the wall was stiffened and sandpaper was glued to the back face and base to produce rough contact conditions.

The electro-hydraulic system used by Lai was not capable of producing a smooth sinusoidal acceleration. In the Aitken experiments, a smooth acceleration was obtained by forcing the box with a spring driving mechanism attached to one end of the box. Details of the test set-up are show in Figure 2.26.

Releasing the spring mechanism set the box in damped sinusoidal motion. The amount of initial compression in the spring was varied to produce different acceleration levels. The stiffness of the spring was 254 kN/m, which resulted in a natural frequency of 2.62 Hz. Damping in the system was about 4% of critical.

Direct shear tests were carried out on the sand. Results showed that the friction angle was very sensitive to the density of the sand. Although the initial density of the sand used in the test was readily measured from the weight and volume, it was considered that the density in the failure wedge would change with outward movement of the wall. To overcome this difficulty, in-situ soil properties were measured by pulling the wall with a load cell and observing the failure force and the angle of the resulting static failure wedge. The wall was also pulled with no backfill behind the wall. These tests enabled estimates to be made of the backfill friction angle and the friction angles against both the backface and base of the wall.

Failure development was examined carefully in the tests by using time-lapse photography and single pulses rather than continuous shaking. Initially the acceleration to initiate sliding was very high with no clear failure surface developing but a zone of shear distortion growing from the base of the wall. The initial acceleration response of the wall shown in Figure 2.27 did not have a plateau and equilibrium analysis implied an angle of internal friction tending towards the maximum attainable by the sand in its densest possible state (far higher than placement density). On the application of subsequent pulses, a failure surface grew from the foot. Following full development of the failure surface (Figure 2.29), the wall failed with an acceleration plateau (Figure 2.28) corresponding to the sliding-block assumption and with a value close to that predicted by the maintainable (large shear displacement) angle of internal friction.

Figure 2.30 compares the measured critical accelerations required to initiate sliding with theoretical values from the MO analysis, assuming a base friction angle of 37° (as measured), and wall friction equal to the soil internal friction (rough wall). The limiting range of the soil friction angle (as determined by shear box tests) was estimated to be between 31° to 36°. The first and fourth values of plotted critical accelerations correspond to the test acceleration traces shown in Figures 2.27 and 2.28. Because there was no clear plateau for the critical acceleration in the first two tests, it is probably not valid to define the critical acceleration as a single parameter. As shown in Figure 2.27, the wall acceleration continues to increase significantly above the critical value at the initiation of relative movement. The results showed that the measured critical acceleration, following the full development of the failure plane, was within the range of the theoretical estimate.

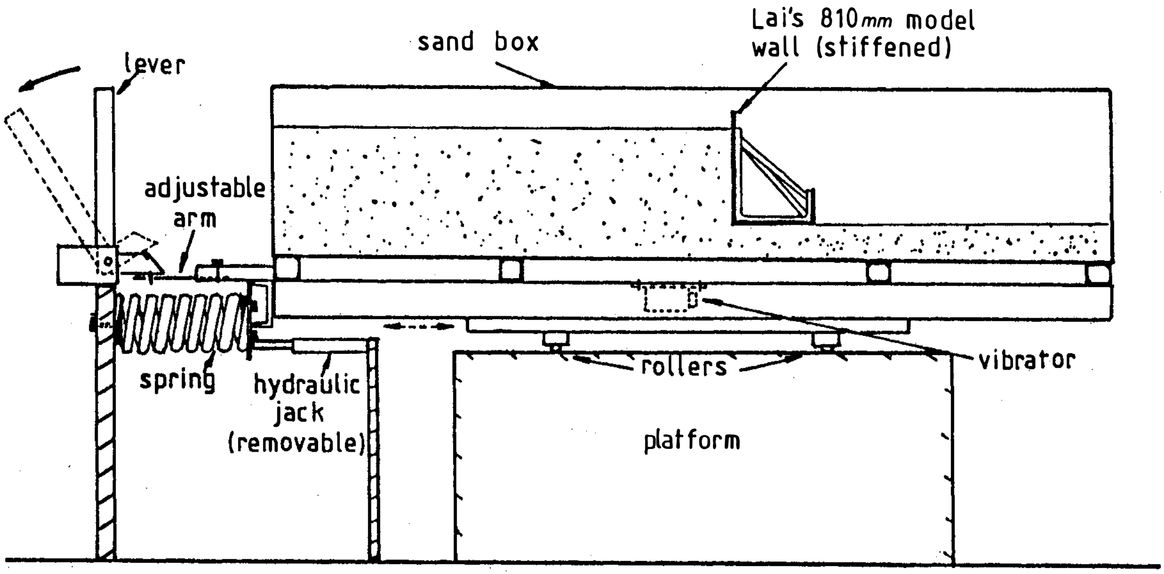

FIG. 2.26 MODEL WALL IN SPRING DRIVEN BOX
(Aitken, 1982)

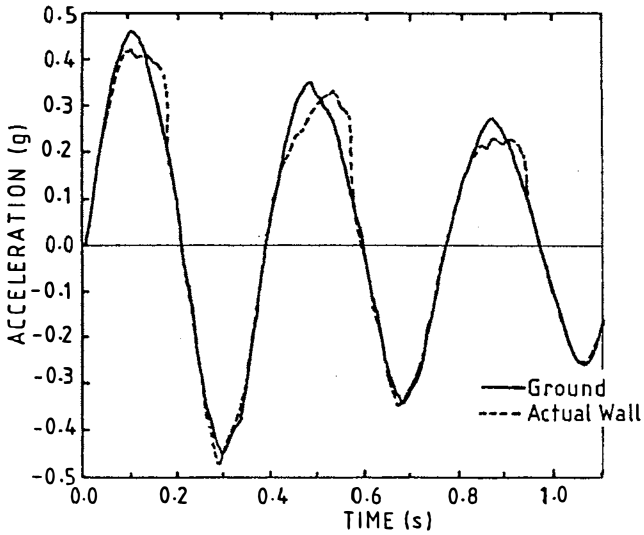

FIG. 2.27 INITIAL ACCELERATION RESPONSE (Aitken, 1982)

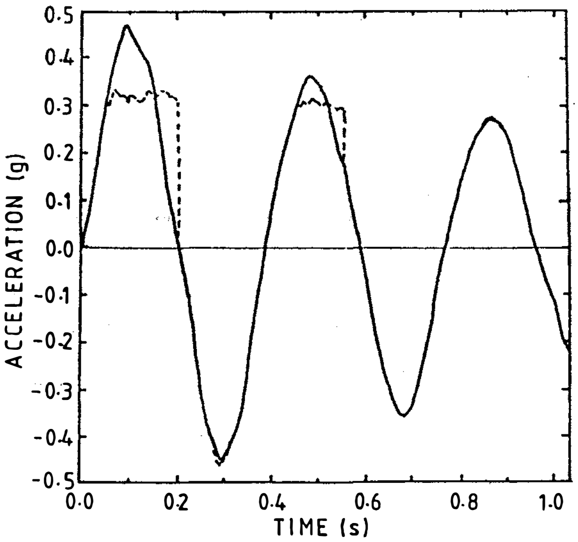

FIG. 2.28 FINAL ACCELERATION RESPONSE (Aitken, 1982)

It was concluded that the Richards-Elms approach gives a good prediction based on the maintainable angle of internal friction, but the estimated displacement will be less than the actual displacement because of the high accelerations required to initiate failure.

2.4 Walls Rotating by Base Failure

Although it is generally considered that wall failure by rotation of the base or foundation is less desirable than failure by outward sliding, there are some situations where it may not be possible for sliding to occur. A particular example is an U shaped flood control channel with symmetrical cantilever walls on either side of the waterway. Significant sliding is very unlikely because of the high passive resistance that can be developed to resist any out of balance in the earthquake pressures on either side. In this situation, failure may occur by the development of plastic hinging at the base of the cantilever stems. In free standing walls, there may be situations were sliding is prevented by other structures resulting in the possibility of a rotational failure in the soil foundation.

If the rotational displacement is sufficiently large, a fully plastic stress state may develop in the backfill soil and both the static and earthquake pressure forces can therefore be expected to be of similar magnitude to the translating wall case. The major difference between translational and rotational failure is that in the rotational case there is no well defined sliding on a failure plane in the soil. In the sliding case, the model wall experiments showed that the failure plane develops near the base of the wall and progresses along a plane to the soil surface. In the rotational case, a fully plastic stress state may not initially develop near the base leading to higher pressures than for the sliding wall case. It seems reasonable to expect the centre of pressure to be rather lower for the rotational case than the translational case.

2.4.1 Theoretical Study

Elms and Richards (1988) presented a theoretical analysis of a rotating wall using a simplified plasticity theory. The simplified slip field shown in Figure 2.31 was assumed in their analysis. For constant volume, the material at the top of the wall will move outward and downward parallel to the plane defining the failure zone. There is no sliding along the inclined "failure surface" which bounds the failure zone.

Like the MO method, the analysis does not give the location of the centre of pressure on the wall face and an assumption has to be made for this parameter to obtain a solution for the total force on the wall. However, the moment at the base of the wall was not particularly sensitive to the assumption made regarding the height of the centre of pressure.

Typical results for wall moment as a function of the assumed height of the centre of pressure, s, are shown in Figure 2.32. The soil friction parameter ϕ_c is not strictly the internal friction angle for the soil although in the limiting case for large wall rotations it approaches the soil friction.

For typical wall and soil parameters, inspection of the results shows that the wall moments are almost the same as the MO values obtained on the assumption that the height of the centre of pressure is at about H/3 above the base.

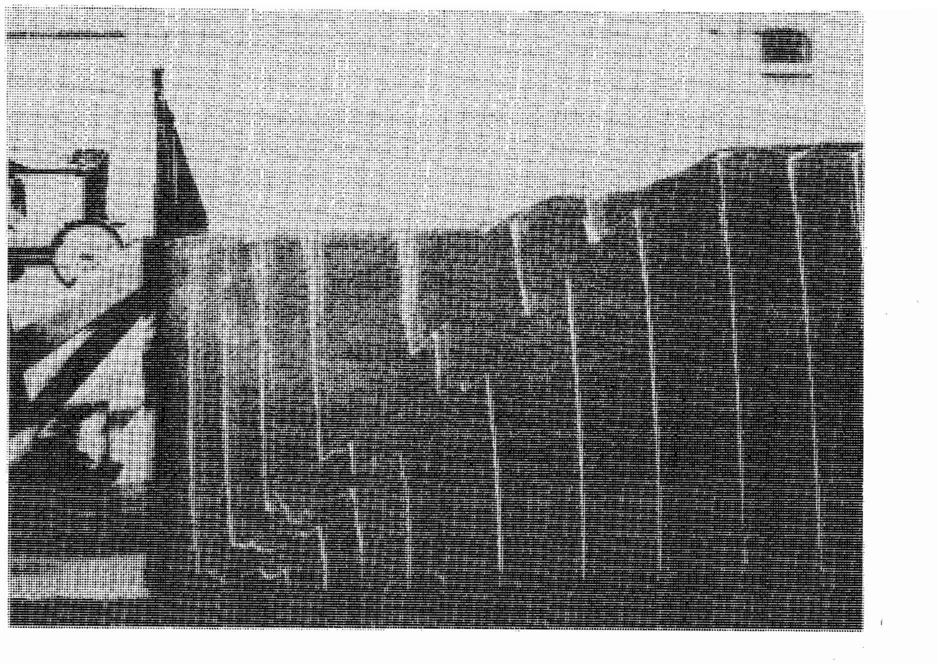

FIG. 2.29 FAILURE WEDGE BEHIND MODEL WALL.
(Aitken, 1982)

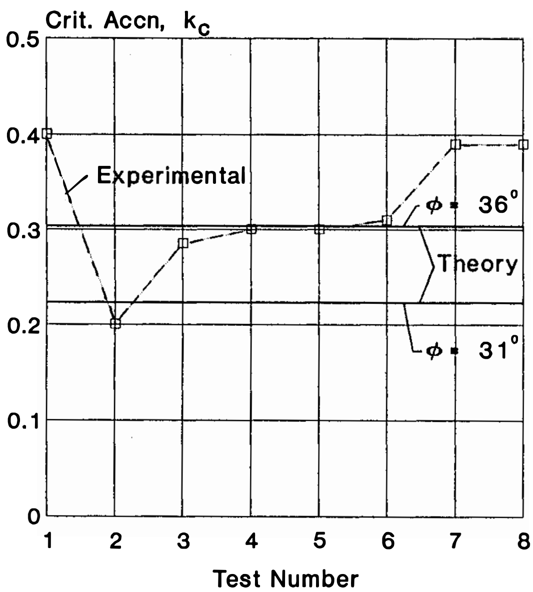

FIG. 2.30 WALL CRITICAL ACCELERATION
(Aitken, 1982)

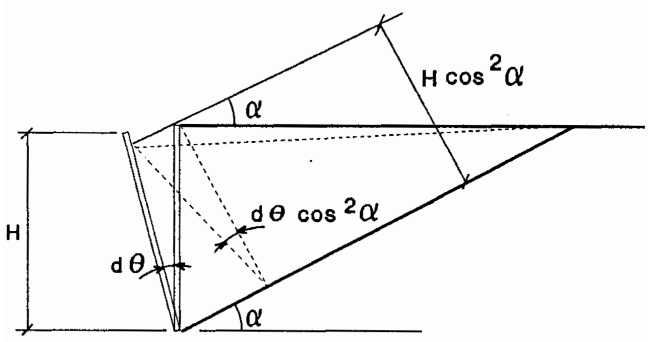

FIG. 2.31 LINEAR DISPLACEMENT FIELD

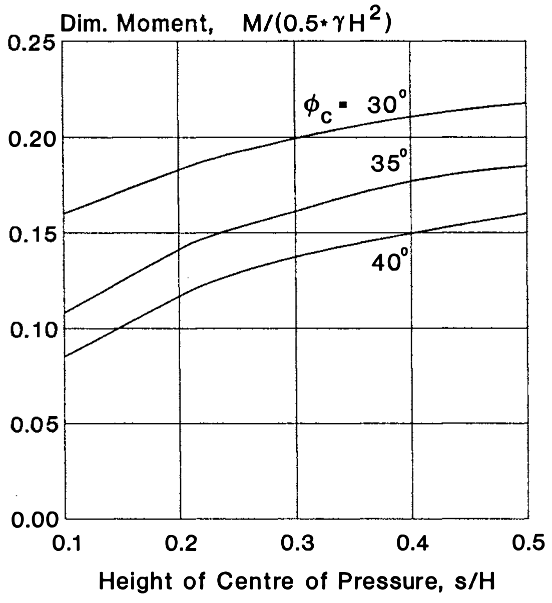

FIG. 2.32 MOMENT ON OVERTURNING WALL (Elms and Richards, 1988)

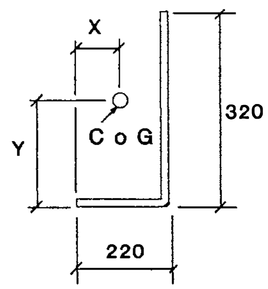

	WALL		
	A	B	C
Mass (kg)	13.1	26.3	26.3
M o I (kg m^2)		1.1	1.0
X (mm)	77	81	39
Y (mm)	113	160	160

FIG. 2.33 ROTATING WALL MODELS

2.4.2 Model Wall Tests

A preliminary study of model walls failing by rotation about their bases was carried out by Aitken (1982). He used a similar model wall and test set-up described above for the translating wall investigation. Rotational failure was induced by increasing the height of the centre of gravity of the wall and holding the base to prevent sliding. Two series of tests were carried out with the horizontal position of the centre of gravity varied with respect to the base of the wall. Details of the walls tested are shown in Figure 2.33.

Typical acceleration and displacement traces for the first series of tests (centre of gravity (C o G) near the heel of the wall) are shown in Figure 2.34. Because of the rocking response, the accelerations at the top of the wall exceeded the base acceleration at the peaks in the input motion. The displacement at the top of the wall showed an oscillatory motion with displacements both away and towards the backfill. A small amount of permanent displacement developed in the outward direction. No clear failure plane developed during the test. Overall, the response appeared to be similar to that expected from a wall system that remains reasonably elastic and apparently the forces on the base were not sufficient to produce a significant rotational failure in the foundation soil.

The conclusion from this preliminary work was that further investigation was required to study this case which appeared to be more complex than failure by simple translation.

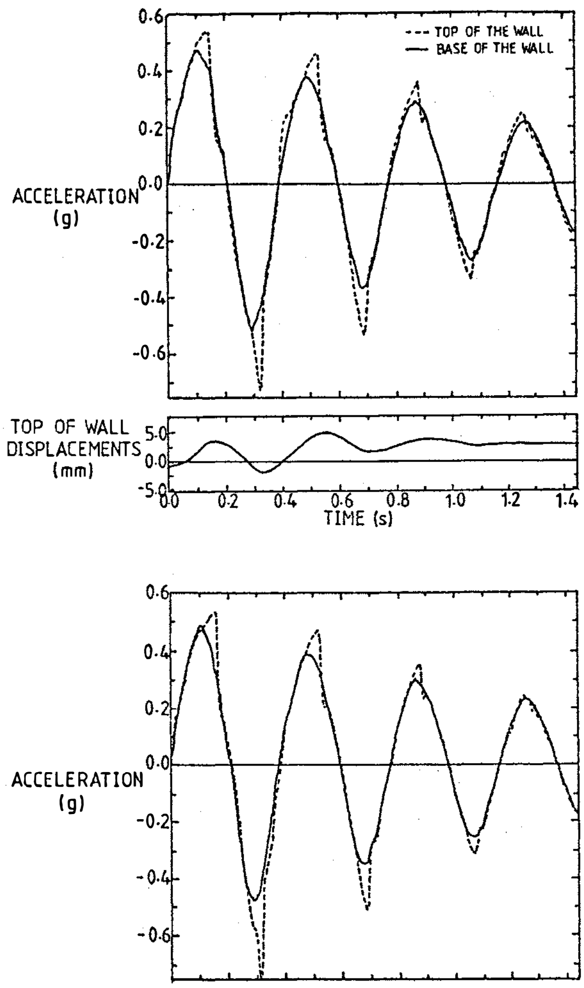

FIG. 2.34 ACCELERATION RESPONSE OF ROTATING WALL (Aitken, 1982)

2.5 Force/Displacement Relationships for Walls

The research in this area was motivated by the very limited information available on the soil stiffening effect and the pressures that develop as a wall is dynamically forced against a soil backfill. This information is required for the analysis of the earthquake response of bridges with monolithic abutments and buildings with basement walls.

2.5.1 Overseas Research

Liam Finn (1963) derived a theory of elasticity solution for a rigid plate displaced horizontally or rotated against an elastic quarter-space. This problem was also investigated by Tajimi (1970) for dynamic harmonic forcing of the plate. The assumptions and boundary conditions considered by Tajimi are shown in Figure 2.35. The vertical boundary at the base of the wall is assumed to be restrained against horizontal translation. Most wall and abutment structures effectively rest on an unrestrained soil layer and thus the boundary conditions of the analytical model are only an approximation for practical wall applications.

The dynamic solution was only obtained for the case of a smooth plate or wall. Liam Finn's static solution was more general, covering both cases of smooth and rough contact between the wall and soil. These static solutions are plotted in Figure 2.36 and 2.37 for the cases of uniform translation of the wall and rotation of the wall about its base. Solutions for the case of rotation about the top of the wall can be obtained by superposition of the results for translation and rotation about the base.

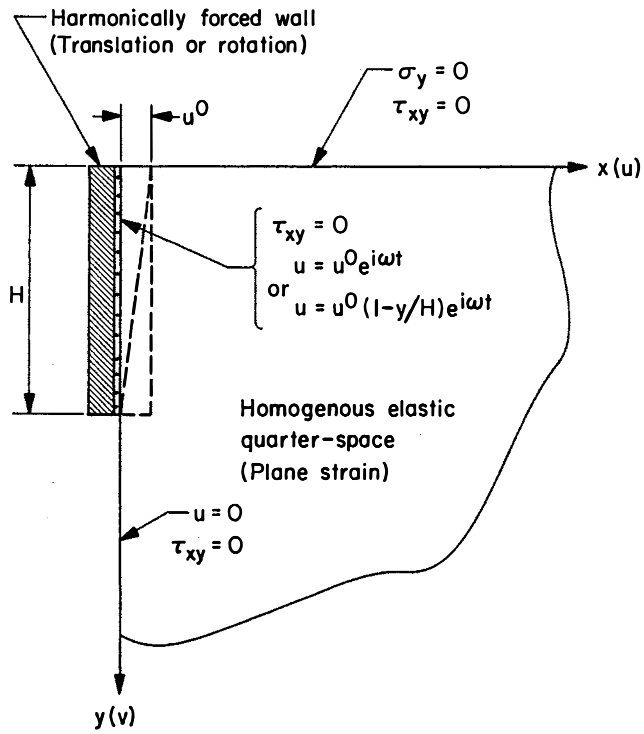

FIG. 2.35 TAJIMI'S ANALYSIS

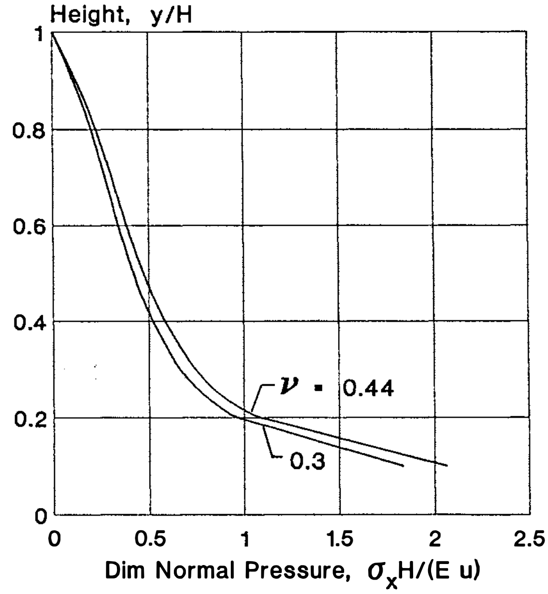

FIG. 2.36 TRANSLATION OF RIGID WALL
(Liam Finn, 1963)

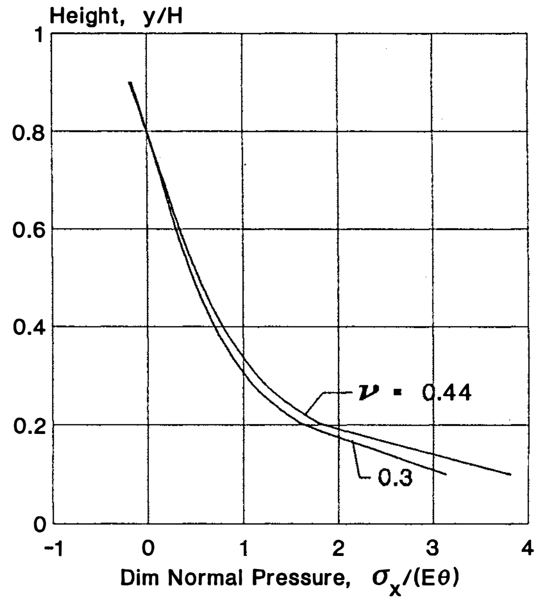

FIG. 2.37 ROTATION OF RIGID WALL
(Liam Finn, 1963)

2.5.2 Theoretical Study

Finite element solutions for walls translating and rotating against an elastic soil layer with the wall assumed to be founded on a rigid layer were computed by Wood (1973). Details of the model and boundary conditions are shown in Figure 2.38.

The solutions for normal pressure against both smooth and rough (bonded contact) rotating walls are shown in Figure 2.39. The pressures are plotted in dimensionless form by dividing by $E\theta$, where θ is the wall rotation angle, and do not include the gravity stresses from the weight of the soil layer. Although tension is indicated by the negative values at the base of the smooth wall, over the range of wall movements for which the solution is likely to be valid, the addition of gravity pressures will largely eliminate the tension zones. The wall pressures are dependent on the soil elastic constants (Poisson's ratio, ν and Young's modulus, E) and the magnitude of the rotation. In contrast, the rigid wall pressures were independent of Young's modulus.

Forces and moments on the statically forced smooth rotating wall, obtained by integration of the pressure distributions, are shown in Figures 2.40 and 2.41.

Normal pressures for the case of a smooth wall translated against an elastic backfill are shown in Figure 2.42. In this case, the horizontal displacement of the wall u^0 divided by the height H appears in the dimensionless normal stress expression instead of the wall rotation angle θ.

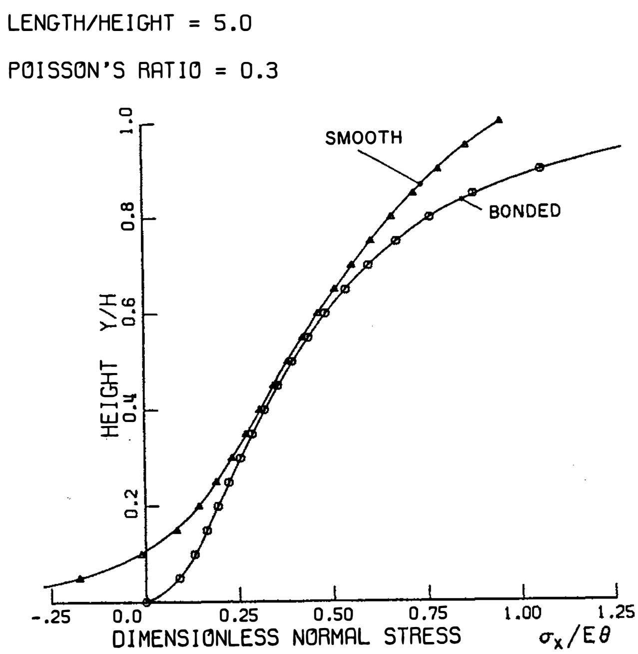

FIG. 2.39 PRESSURE INCREMENT ON ROTATING WALL
Rigid Base

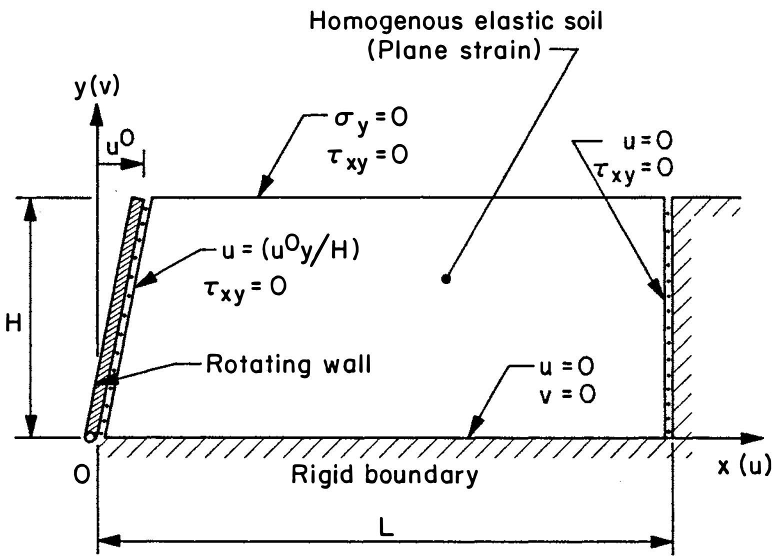

FIG. 2.38 FORCED WALL ANALYSIS
Rotation About Base

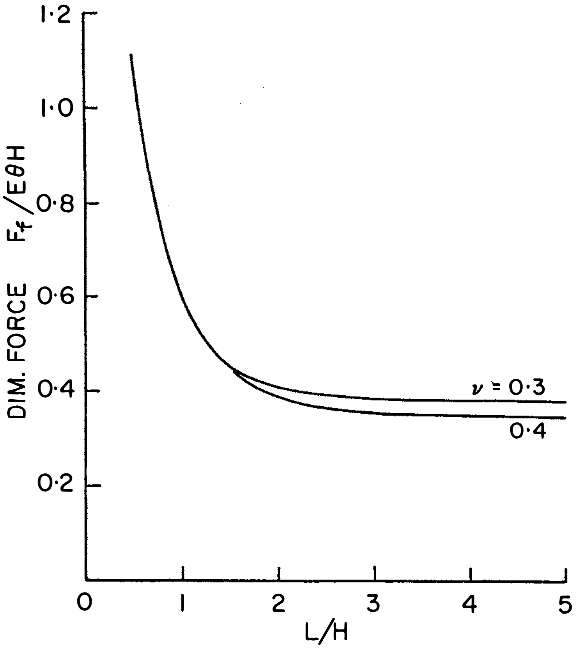

FIG. 2.40 FORCE ON FORCED ROTATING WALL

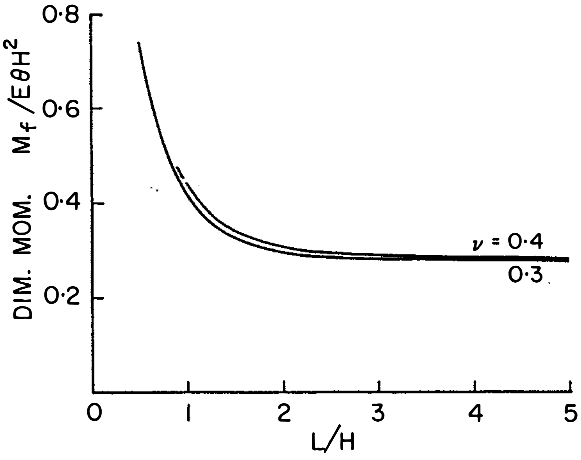

FIG. 2.41 MOMENT ON FORCED ROTATING WALL

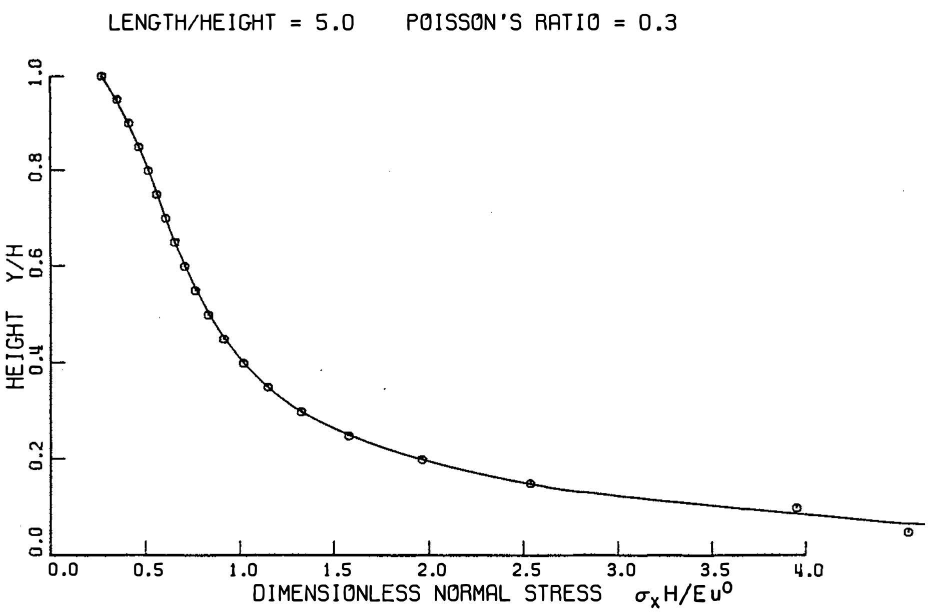

FIG. 2.42 PRESSURE INCREMENT ON TRANSLATING WALL

Finite element solutions for normal pressures on translating and rotating walls resting on a deep layer of soil were computed by Wood (1985). The boundary conditions assumed in the analyses are shown in Figure 2.43. For most wall applications, these conditions are probably more appropriate than the rigid base assumption or the boundary conditions that were used by Tajimi and Liam Finn (Figure 2.35). Normal stresses on the wall obtained from these analyses are shown in Figures 2.44 and 2.45.

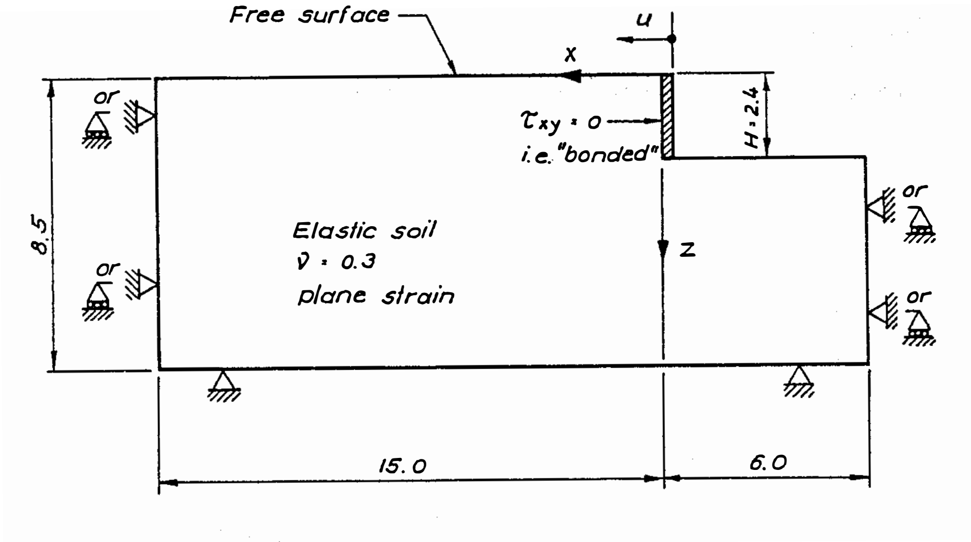

FIG. 2.43 FORCED WALL ON DEEP SOIL LAYER

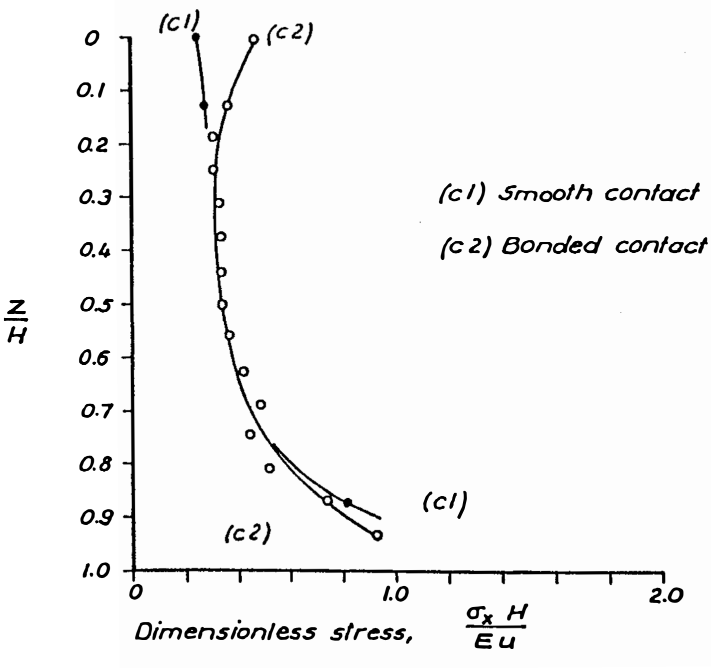

FIG. 2.44 PRESSURE INCREMENT ON TRANSLATING WALL
Deep Soil Layer

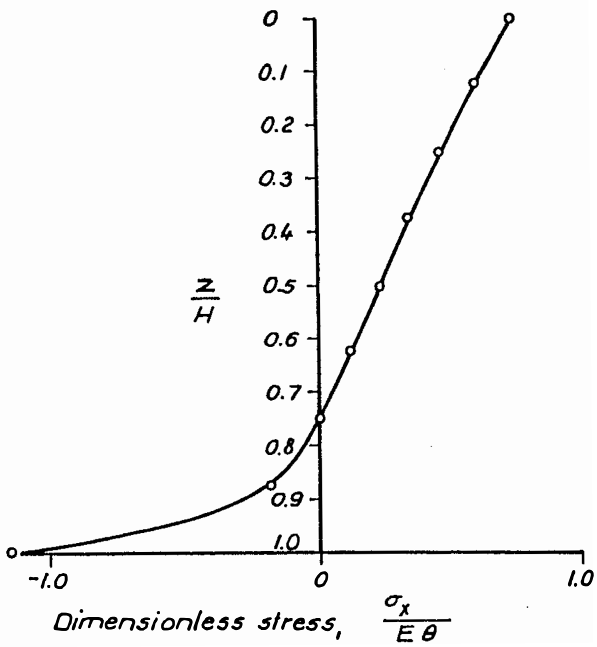

FIG. 2.45 PRESSURE INCREMENT ON ROTATING WALL
Deep Soil Layer

2.5.3 Experimental Project

To verify the theoretical solutions and to obtain data suitable for application in the design of monolithic bridge abutments, an experimental project to measure force/displacement relationships for walls displaced cyclically against the backfill soil, was carried out by Thurston (1986).

Two separate test series were undertaken. In the first series (Thurston, 1986 a, Thurston, 1987), a model rigid wall was translated horizontally with cyclic displacements against a sand backfill material. The wall was 1.0 m high and 2.41 m wide. It thus represented a prototype abutment at a scale ratio of between about 1:4 and 1:2. In the second series (Thurston, 1986 b), a similar rigid wall was cyclically forced against the sand backfill by rotating it about its base. In most practical situations, the abutment wall displacement is likely to have both translation and rotational components, but it was considered desirable to simplify the tests as far as possible and produce basic data that could be combined in an approximate way to cover a wide range of practical abutment configurations. A third stage of the project, which is currently in progress, involves finite element studies to compare theoretical predictions with the experimental results.

The project was part of an United States - New Zealand cooperative research programme on the seismic design of monolithic bridge abutments. The NZ laboratory studies were complementary to the small scale model centrifuge tests and prototype field studies carried out by the Earth Technology Corporation in California. These tests are described in Section 2.6.2.

(i) Translation Tests

The test set-up for the translation displacement case is shown in Figure 2.46. A heavy steel plate, representing the abutment wall, was connected to a large concrete block with 12 load cells. The block was supported on roller bearings that allowed the block to be translated horizontally by a servo controlled electro-hydraulic actuator. The concrete block was of sufficient mass and stiffness to prevent any significant rotation of the steel wall plate that therefore moved against the soil in a translation mode.

The force on the wall was measured with the actuator load cell as well as the 12 wall support load cells that were arranged in two horizontal lines along the wall. This load cell configuration gave the total force on the wall and the location of the centre of pressure. Pressures on the wall face were measured with ten 90 mm diameter strain gauged diaphragm type pressure transducers. Horizontal displacements of the wall were measured with the actuator displacement transducer and six displacement transducers mounted against the steel wall plate.

The wall backfill material was a well-graded coarse gravelly sand with 90% of the material between sizes of 0.3 mm to 4.75 mm. Initially the sand was compacted at a moisture content of about 5% using 200 mm lifts and a flat vibrating compacter of 60 kg weight. Because of bulking, the sand compacted in this way ended up in a very loose state. Following initial tests in this condition, further tests were carried out after the sand had been compacted by the same method but at a much higher moisture content and again after the sand had been compacted in a fully saturated condition using an immersion type concrete vibrator. In this way, tests were performed with the sand in very loose, loose and dense states. The sand in both the loose and dense states was allowed to dry out after compaction to give moisture contents of about 6% at the time of testing.

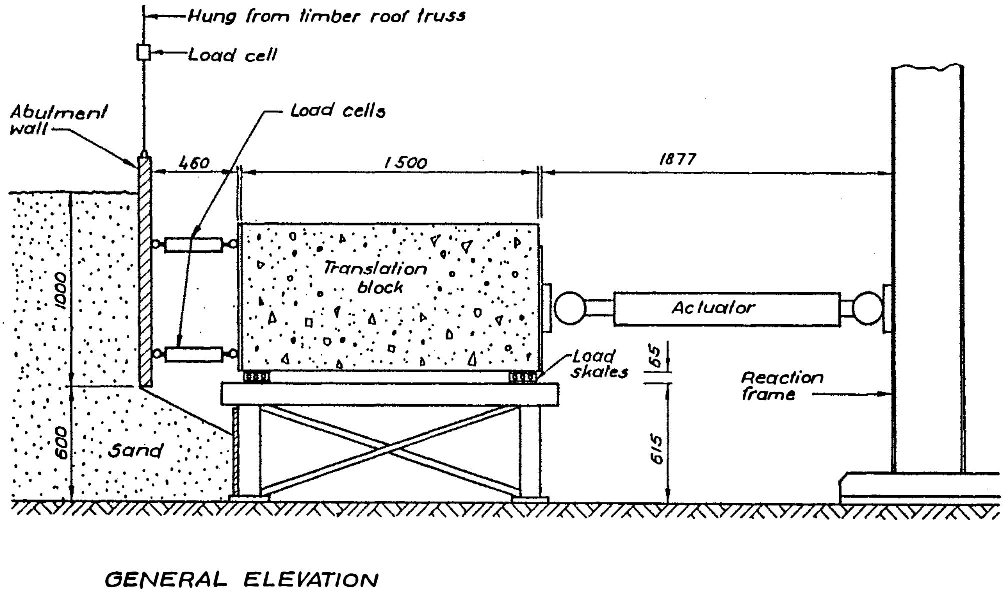

FIG. 2.46 MODEL WALL FOR TRANSLATION

The wall was translated with both slow cyclic and relatively high speed dynamic cyclic displacements. In the slow speed tests the wall was cyclically pushed against and pulled from the sand with the peak displacement amplitude, in a direction towards the sand, gradually increased from 0.25 mm to 20 mm. The dynamic tests were made following the slow cyclic runs using the servo controlled actuator to apply a 4 Hz sinusoidal displacement function. Amplitudes were gradually increased until the maximum displacement against the soil reached 4 mm. At the completion of the dynamic tests, a further static test was carried out in which the wall was pushed against the sand until a complete failure surface developed in the sand.

Scala penetrometer tests on the compacted sand gave average values of 50 mm and 10 mm per blow for the loose and dense states obtained by the compaction methods described above. (These values are in fact indicative of loose and dense sand).

Hysteresis loops from the static cyclic tests on dense sand are shown in Figure 2.47. Force/displacement "spine" curves developed from the hysteresis loops for the three test series on the different sand densities are shown in Figure 2.48. Also shown in this figure is a force displacement relationship developed from a nonlinear finite element study (Wood, 1985). Quite good agreement exists between the experimental and theoretical results but the agreement is sensitive to the initial tangent stiffness of the sand that was estimated from the results of Scala penetrometer and density measurements.

Soil pressures measured during the slow cyclic tests on the dense soil are shown in Figure 2.49. A comparison is given between the measured distributions for the loose backfill and finite element results in Figure 2.50. Again, providing reasonable assumptions are made regarding the soil initial tangent Young's modulus, reasonable agreement was obtained between the experimental and theoretical pressures.

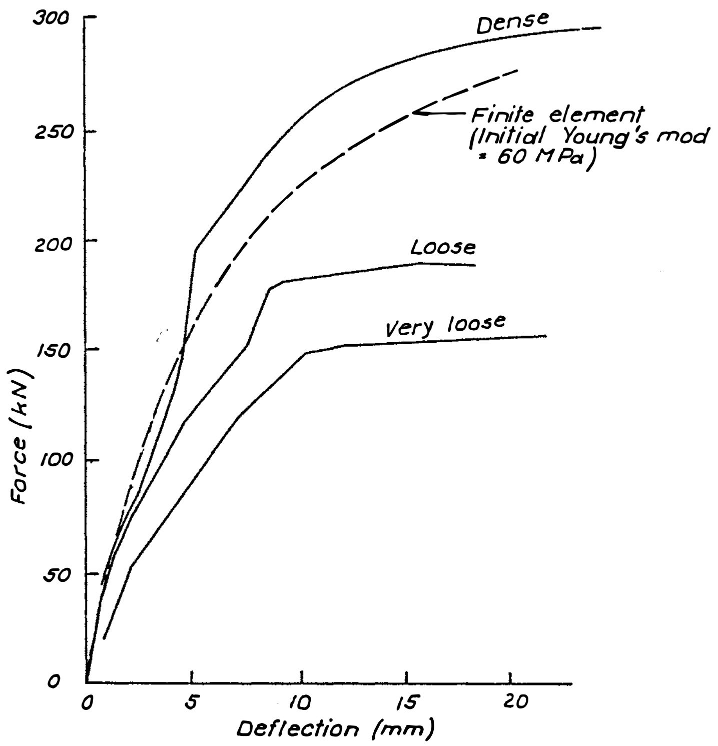

FIG. 2.48 FORCE "SPINE" CURVES FOR TRANSLATING WALL

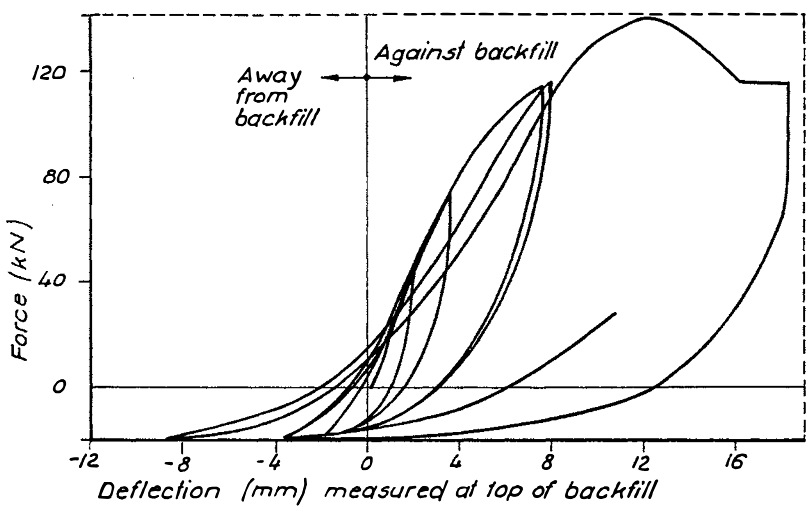

FIG. 2.47 FORCE ON MODEL TRANSLATING WALL
Dense Sand

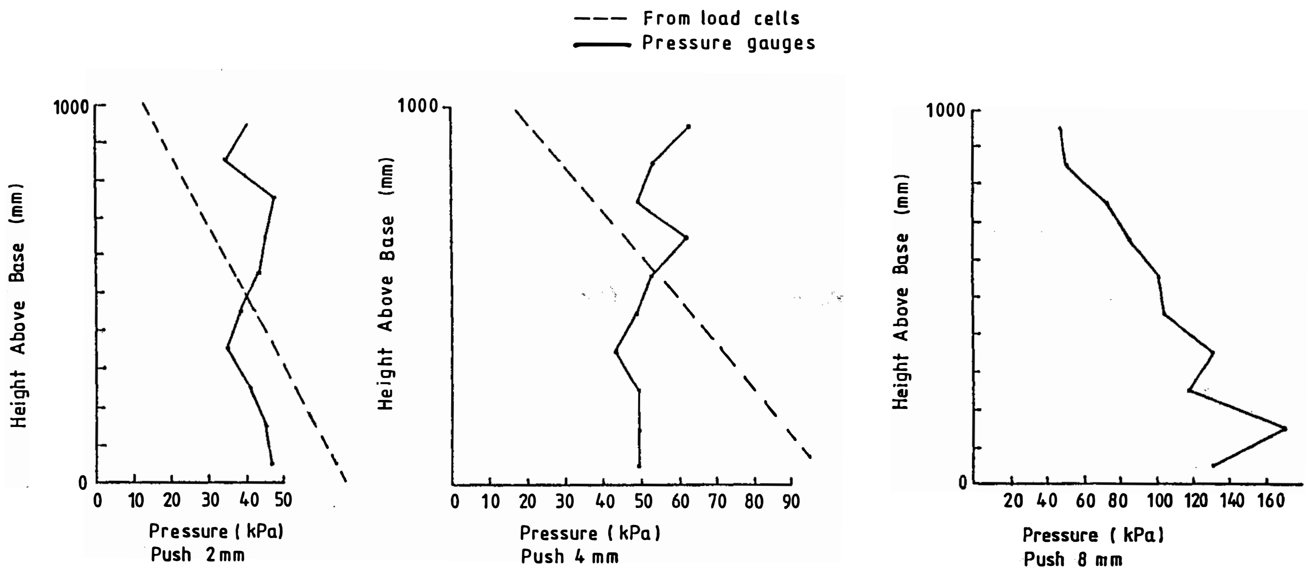

FIG. 2.49 PRESSURES ON MODEL TRANSLATING WALL

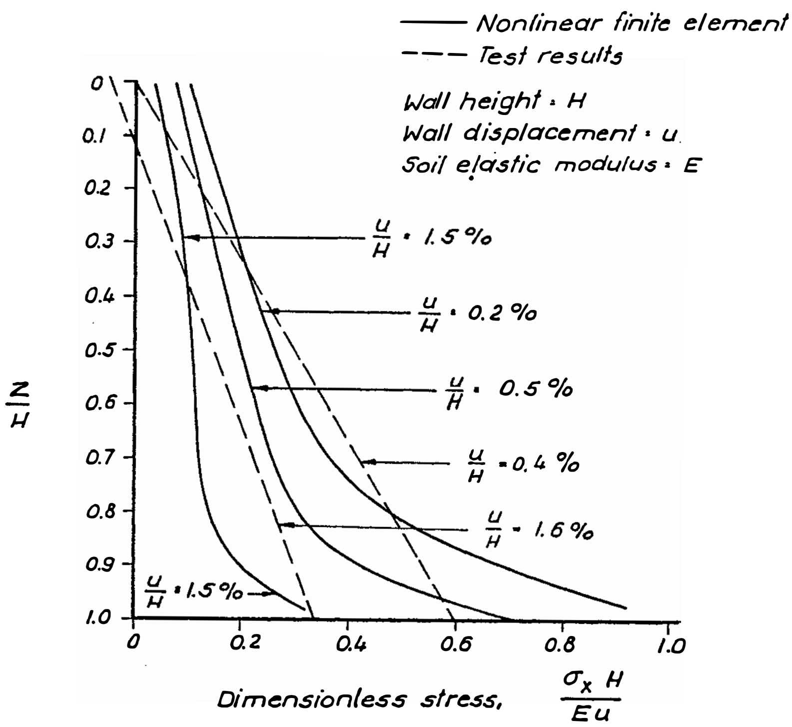

FIG. 2.50 COMPARISON OF TEST AND FE PRESSURES

(ii) Rotation Tests

The test set-up for the case of rotational displacement of the wall is shown in Figure 2.51. The instrumentation used was similar to that described for the translation tests. The sand used previously for the translation tests was compacted to loose-medium and dense states as described above. Slow cyclic and dynamic tests were carried out followed by a static load-to-failure test. Amplitudes in both the slow cyclic and dynamic tests were gradually increased to 8 mm. A 4 Hz sinusoidal displacement function was used in the dynamic tests.

Scala penetrometer tests on the compacted sand gave average values of 30 mm and 10 mm per blow for the two different compaction methods. The higher of these two values indicates sand of a loose-medium density whilst the lower value indicates a dense sand.

Hysteresis loops obtained from the slow cyclic tests on dense sand are shown in Figure 2.52. Pressure distributions obtained from both the pressure transducers and the wall load cells are shown in Figure 2.53. Reasonable agreement between both methods of measurement was found for the total force and centre of pressure.

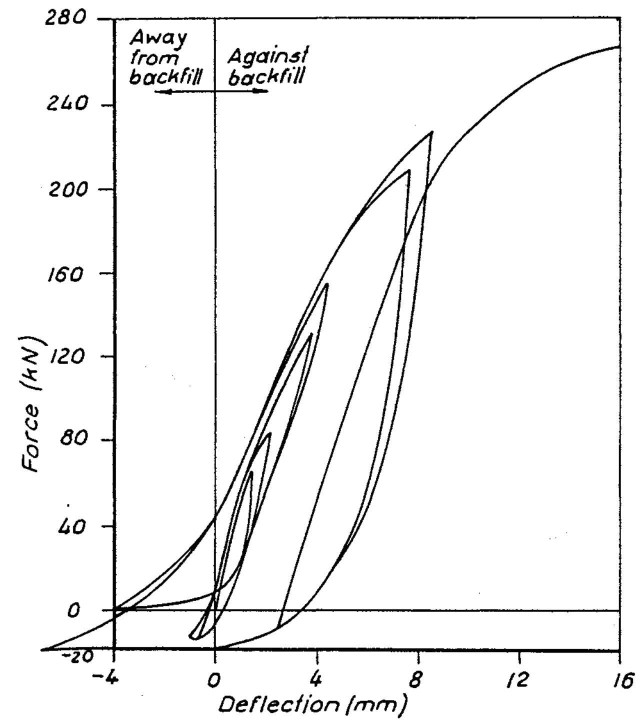

FIG. 2.52 FORCE ON MODEL ROTATING WALL
Dense Sand

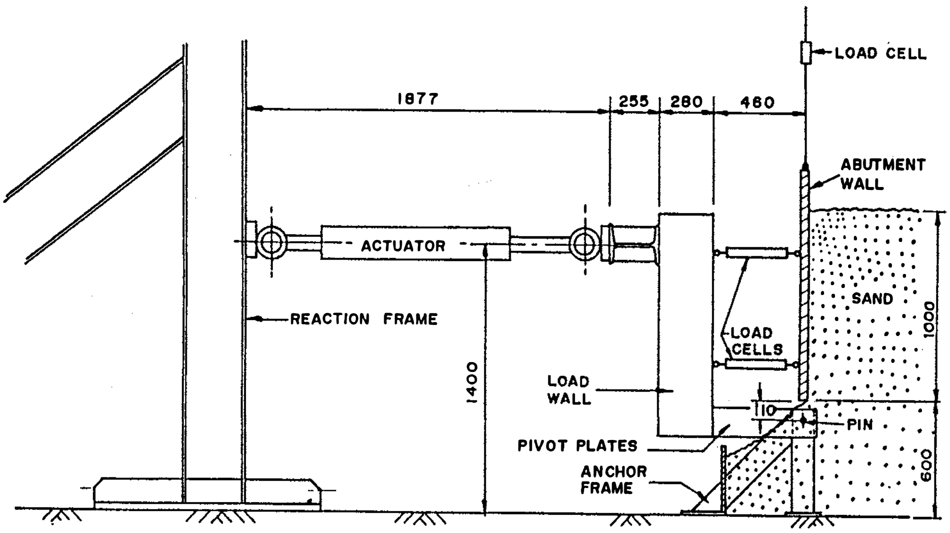

FIG. 2.51 MODEL WALL FOR ROTATION

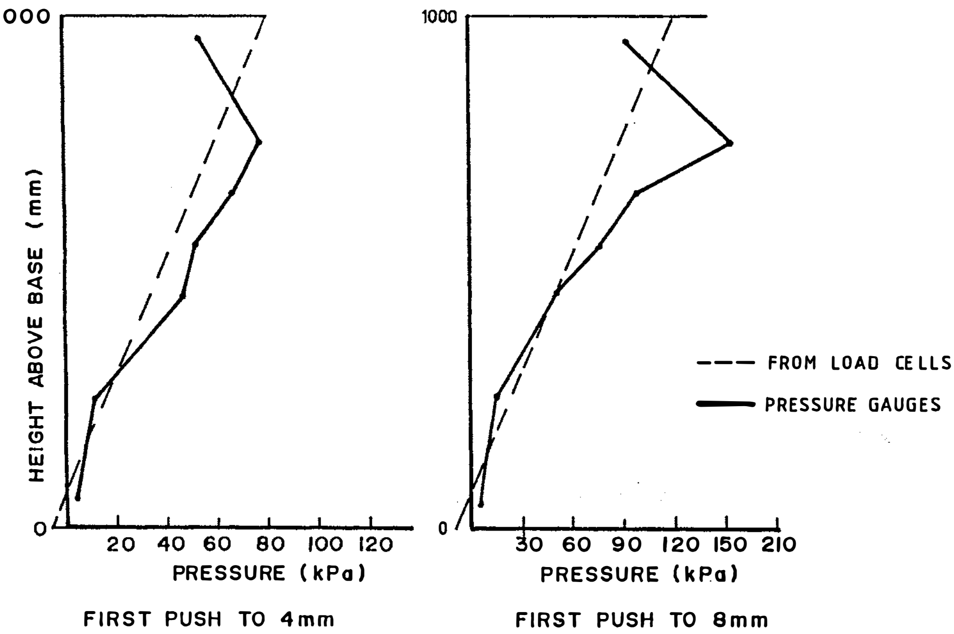

FIG. 2.53 PRESSURES ON MODEL ROTATING WALL

2.6 Monolithic Bridge Abutments

One method of simplifying abutment structures is to build them monolithic with the bridge superstructure rather than to separate them with sliding bearings, expansion joints, seismic gaps and restrainers. On some bridges, joints and bearings have resulted in considerable long-term maintenance problems and their elimination may result in a significant reduction in both capital and maintenance costs. However, the analysis of the earthquake response of a bridge with monolithic abutments is more complex than for a bridge with isolated abutments. In the latter case the bridge and abutment response can usually be analyzed independently.

A project on the seismic design of monolithic bridge abutments was carried out as an United States - New Zealand cooperative research project. A summary of this project, which formed an extension of the more basic force/displacement study described in Section 2.5, is presented in the following sections.

The project was directed by The Earth Technology Corporation, Long Beach, California with research funding from the US National Science Foundation, the RRU Structures Committee and the New Zealand Ministry of Works and Development. A detailed project outline was presented by Crouse et al (1985).

2.6.1 Theoretical Study

Typical monolithic bridge abutments may have sufficient flexibility to cause significant changes to the simple theoretical pressure distributions solutions for rigid walls forced against the backfill. To study this effect, Wood (1985) used the finite element method to compute pressures for horizontal displacements of a typical abutment wall. Details of the abutment wall and bridge structure modelled are shown in Figure 2.54. The finite element representation and the boundary conditions assumed are shown in Figure 2.55.

The soil was assumed to have a Young's modulus, E = 90 MPa, and Poisson's ratio, ν = 0.3 and the wall an E_c = 60 GPa and ν_c = 0.2, (wall concrete assumed to be uncracked and stiffened by reinforcement). The influence of the bridge superstructure stiffness was investigated by analysing the following two cases:

(a) The top four elements (representing the depth of the superstructure) assumed to be rigid and translated with a uniform horizontal displacement at their nodes.

(b) The top four nodes restrained by boundary springs representing the flexural stiffness of the superstructure. The ends of the springs remote from the wall were subjected to a uniform horizontal displacement.

Normal pressures on the wall for the two cases are compared in Figure 2.56 with the bonded contact rigid wall solution. The results show that the wall and superstructure flexibility can have a significant influence on the shape of the normal pressure distribution. Only the pressures from the wall movement are plotted and gravity stresses need to be added to give the total forces on the wall.

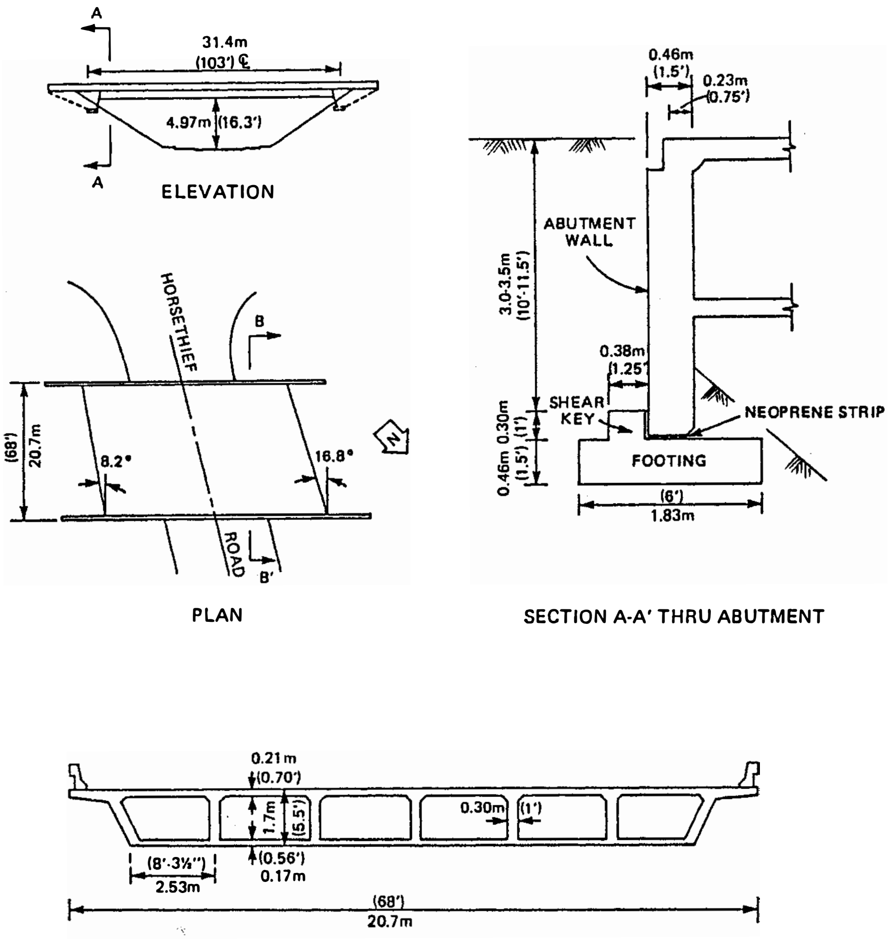

FIG. 2.54 HORSETHIEF ROAD UNDERCROSSING BRIDGE

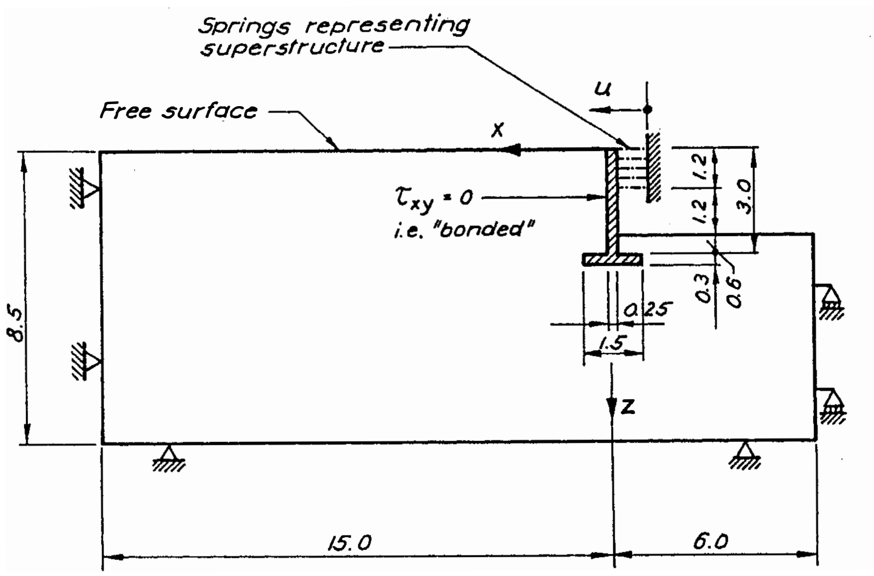

FIG. 2.55 FE ANALYSIS OF BRIDGE ABUTMENT WALL

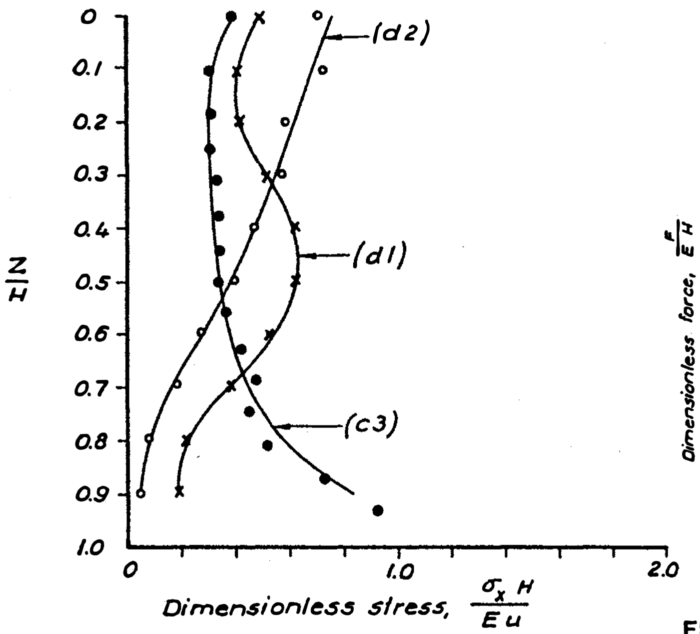

FIG. 2.56 PRESSURE ON BRIDGE ABUTMENT WALL
(c3) Rigid Wall; (d1) Flex Wall, Rigid Superstructure
(d2) Flex Wall, Flex Superstructure

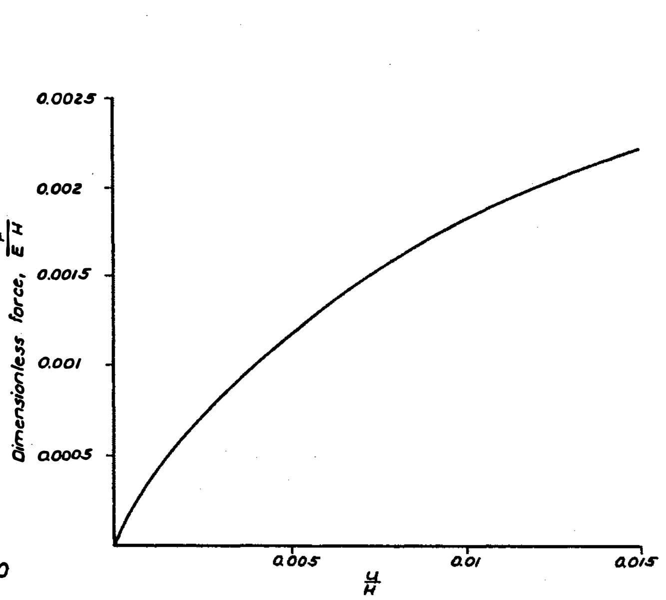

FIG. 2.57 FORCE ON ABUTMENT WALL FROM FE ANALYSIS

The effects of a nonlinear soil were also investigated for the case of the abutment wall with the flexible superstructure using nonlinear finite elements. Soil parameters were assumed that represented a dense granular backfill. The force displacement relationship for the wall translated into the nonlinear soil is shown in Figure 2.57. The force has been plotted in dimensionless form using a Young's modulus value selected so that the total force on the wall in the first displacement increment of the nonlinear analysis (u/H = 0.043%) was the same as the force on the wall translated with an equal displacement against an elastic soil. This gave a modulus value of 84 MPa. Normal stresses on the wall, for various displacement increments, are compared in Figure 2.58 with the solution obtained for the elastic soil case. The nonlinear soil produces a significant reduction in the normal stresses at the top of the wall and with increasing deformation, the pressure distribution becomes more uniform over the height.

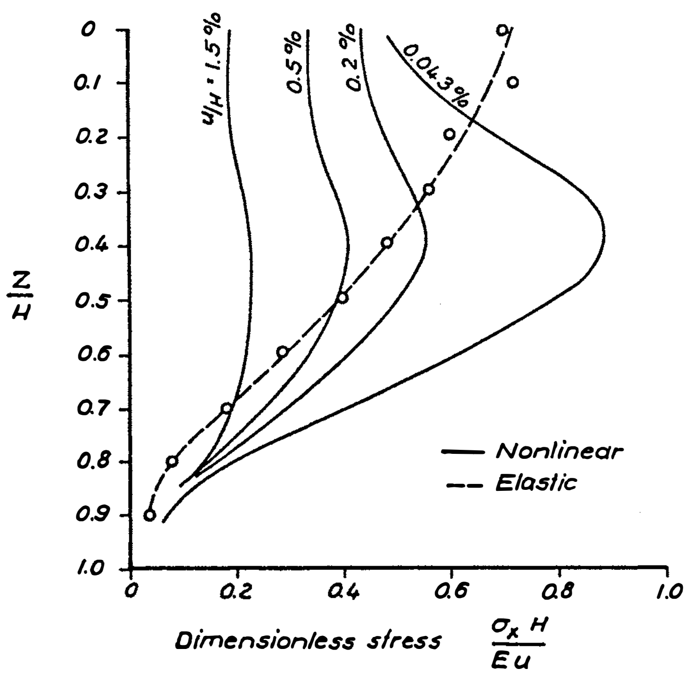

FIG. 2.58 PRESSURE ON ABUTMENT WALL, FE ANALYSIS

2.6.2 Experimental Project

(i) Field Tests

Ambient vibration, quick-release and forced vibration tests were conducted on the Horsethief Road Undercrossing bridge, located on Interstate Highway 15 near Corona, California (Crouse et al 1985). The bridge shown in Figures 2.54 and 2.59 is a prestressed-concrete box girder bridge with monolithic abutment walls at each end. Vertical support is provided by a rectangular footing beneath each abutment. The connection between the abutment wall and footing is effectively pinned with a thin neoprene strip separating the bottom of the wall from the footing. The shear key on top of the footing at the back of the wall is designed to resist lateral movements of the bridge. The footings rest on sandy soil with some coarse gravel content. The average shear wave velocity of the upper 3 m of soil beneath the footing was measured as 260 m/s. The backfill was similar material but with a lower shear wave velocity of 210 m/s.

The response of the bridge was measured with 30 accelerometers placed at various locations on the bridge deck, abutment walls and footings. Displacement transducers were used to measure any relative movements between the footings and abutment walls but no significant displacement was recorded.

Quick release tests were conducted by applying a 45 kN tension force in a steel wire rope attached at one end to the bridge deck and at the other end to a concrete approach slab. Quick release of the tension in the cable set the bridge into free vibration.

Most of the experimental work was centred on forced vibration testing using a large eccentric mass shaker. The shaker was bolted to the bridge deck midway between the two abutments at a point approximately 4.6 m from the longitudinal centre line (Figure 2.60). The two counter rotating weights of the shaker were adjusted to apply unidirectional harmonic shaking in the longitudinal and transverse directions. The excitation frequencies ranged between 2 Hz and 14 Hz and the peak applied loads varied between 9.0 kN and 445 kN, representing between 0.1% to 4% of the weight of the bridge. Because of the type of shaker used, the applied loads were relatively small at the lower frequencies.

The three dimensional finite element model of the bridge shown in Figure 2.61 was used to interpret the experimental data and to give a comparison between theoretical predictions and the test results. The box section superstructure and abutment walls were modelled with plate elements. This allowed the geometry of the bridge, including the abutment skews, to be accurately represented. The soil beneath the abutment footings was modelled by a set of three mutually perpendicular translational springs attached to each node at the bottom of the wall. The interaction between the abutment wall and backfill wall was modelled by lateral springs perpendicular to the wall face at each wall node. It was assumed that the frictional forces between the wall and soil were small and this effect was not modelled.

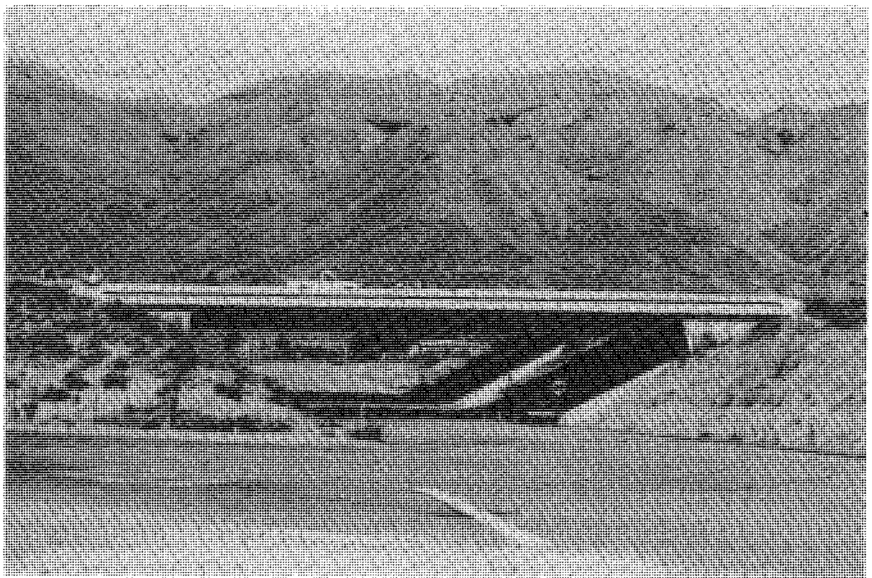

FIG. 2.59 HORSETHIEF CANYON UNDERCROSSING BRIDGE

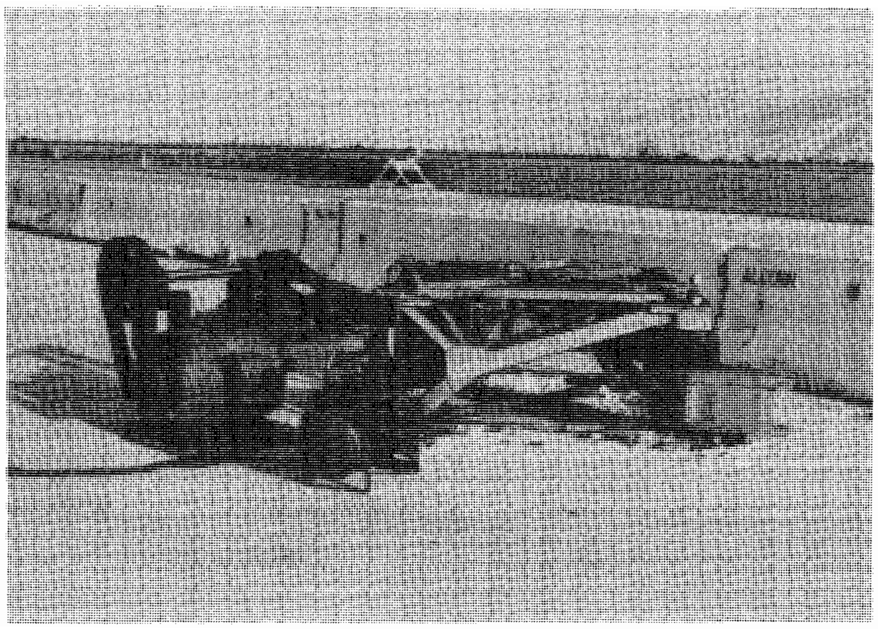

FIG. 2.60 ROTATING MASS SHAKING MACHINE ON DECK OF HORSETHIEF CANYON UNDERCROSSING BRIDGE

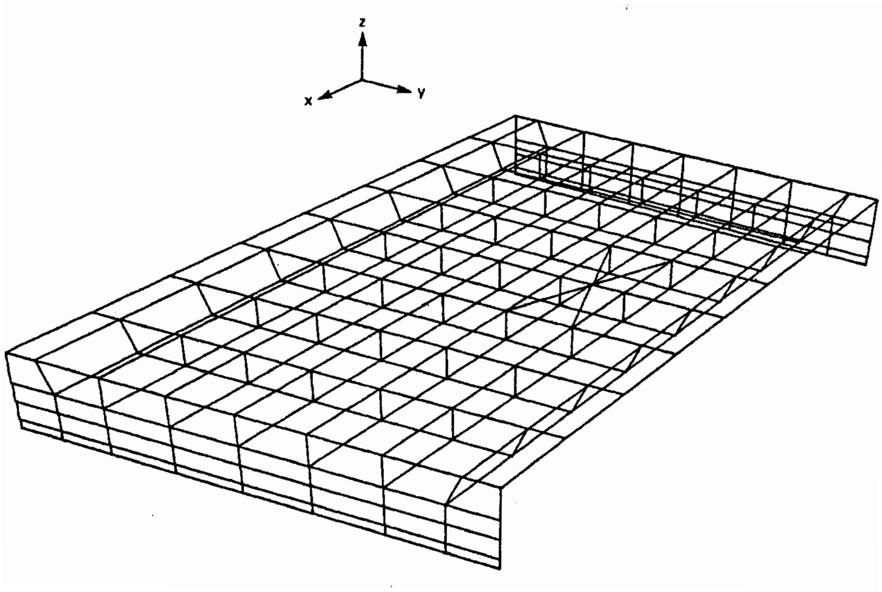

FIG. 2.61 FINITE ELEMENT MODEL OF BRIDGE

Young's modulus for concrete was taken as 34 GPa. The spring stiffness values were estimated by both applying Rayleigh's Principle to modal displacements calculated from the acceleration response, and using elastic theory (Wong and Luco, 1978 and Gazetas, 1983). In the elastic theory approach, the footings were assumed to be rigid rectangular foundations with a length to width ratio of 11 on the surface of an elastic half space. The elastic half space was assumed to have a shear wave velocity of 260 m/s and a Poisson's ratio of 1/3. Stiffness estimates for the wall springs were obtained from the finite element rigid wall translation solutions (Wood, 1973).

The calculated spring stiffnesses were adjusted to produce a good match between the measured and calculated natural frequencies of the bridge/foundation system. Values of the adjusted spring stiffness values and the values calculated by the two theoretical approaches are given in Table 2.2.

TABLE 2.2

Horsethief Canyon Undercrossing Bridge: Spring Stiffness Values

Method	Stiffness of Each Footing or Wall kN/mm			
	Footing Long	Footing Tran	Footing Vert	Wall Normal
Rayleigh		2,200	5,300	2,000
Elastic	3,900	2,300	4,400	2,200
Adjusted	3,900	2,500	5,300	2,800

Considering the walls and footings at both ends of the bridge, the total spring stiffness of the soil in the longitudinal direction is 13,400 kN/mm. This is a remarkably high stiffness value showing the ability of the monolithic abutment to resist horizontal loads at deformation levels that would not produce any appreciable nonlinear behaviour of the soil.

Normal mode shapes and natural frequencies computed for the finite element model are shown in Figure 2.62. A comparison of the measured and computed natural frequencies is given in Table 2.3.

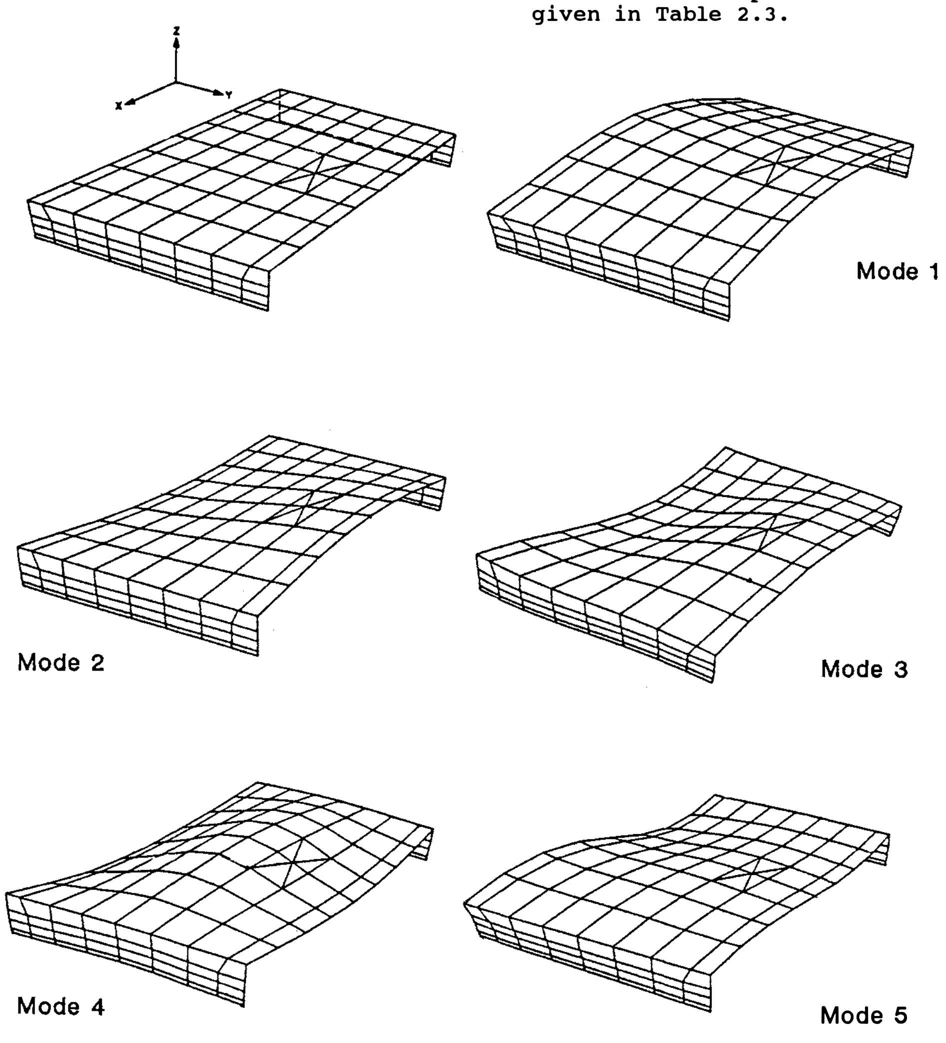

FIG. 2.62 MODE SHAPES FROM FE ANALYSIS

TABLE 2.3

Horsethief Canyon Undercrossing Bridge: Natural Frequencies and Measured Damping Values

Mode No	Description	Natural Freq. Hz			Damp %
		FE Model	Amb. Test	Forc Test	
1	Deck, Flexure	4.8	4.7	4.7	2.5
2	Deck, Torsion	6.5	6.7	6.4	3.5
3	Tran Rocking	9.3	9.7	8.2	15
4	Tran Flexure	10.7	11.2	10.6	2.0
5	Long Transln (2nd Long-Flex)	11.9	15.5	14+	

Because of the very high stiffness of the soil in the longitudinal direction, mode 5, which had the largest component of longitudinal motion, was not positively identified by the testing. It was thought to have a natural frequency of about 15 Hz. Generally there was good agreement between the observed and theoretical frequencies confirming that the assumptions made for the elastic properties of the soil and bridge were reasonable. Significant transverse rocking on the foundations was observed in the third mode at 9.7 Hz and this behaviour would account for the high damping recorded in this mode.

(ii) Model Studies

A scale model of the Horsethief Road Undercrossing bridge was tested using a centrifuge at California Institute of Technology (Crouse et al, 1985).

Most soil properties strongly depend on the confining pressure developed by gravity forces. Under increased gravity loads in a centrifuge, it is possible to test small scale models and obtain similarity for the confining stresses. If for example, a model N times smaller in length scale than the prototype, is tested in a centrifuge with a gravitational field M times greater than the normal prototype gravity, then the strains and stresses at homologous points of the model and prototype will be the same.

Dimensions of the 1:100 scale model are shown in Figure 2.63. The dimensions of the superstructure and abutment walls were scaled to have the equivalent mass and flexural stiffness of the Horsethief Road prototype. The superstructure box section was modelled by a ribbed slab milled out of a solid piece of aluminium plate. Because of the width limitations of the centrifuge specimen box used to contain the model, it was necessary to make the model the full width of the box. Thus the model was essentially restricted to two dimensional behaviour in the vertical and longitudinal horizontal directions. Fine uniform Nevada 120 silica sand was used to model the cohesionless sandy soil of the prototype foundation and backfilling. Dimensions of the sand box and the soil profile are shown

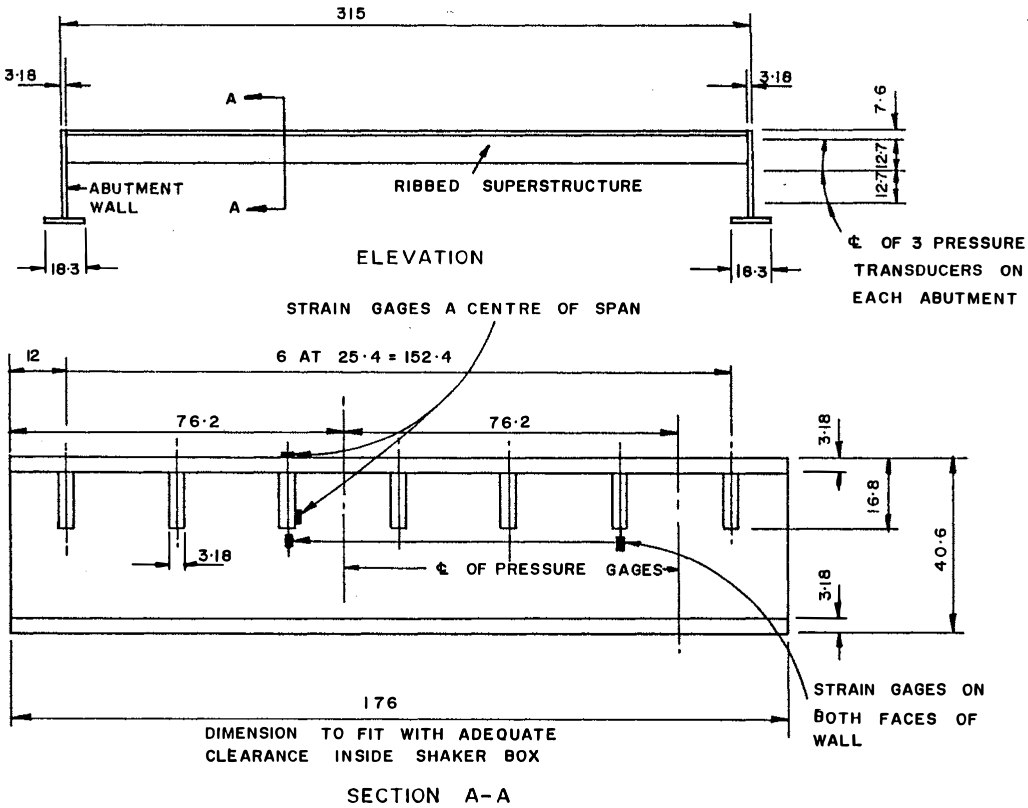

FIG. 2.63 MODEL BRIDGE FOR CENTRIFUGE TESTING

in Figure 2.64. The model foundation and backfilling was placed by hand tamping to produce the maximum density of the dry sand. Shear wave velocities between 210 m/s to 247 m/s were measured for the sand in its dense condition (16.5 kN/m^3) at a confining pressure of 55 kPa to 83 kPa.

The model was extensively instrumented using miniature pressure transducers, accelerometers, strain gauges and displacement transducers. Accelerations were also monitored in the soil under the bridge and on the shaker box.

Earthquake simulated shaking, quick release, forced vibration and cyclic push-pull tests were conducted. Experiments were performed at centrifuge accelerations of 50 g, 87 g and 100 g giving results for three different scaling ratios.

A small air powered counter-rotating mass shaker, mounted on the deck of the model was used in the forced vibration tests. The orientation of the shaker was adjusted to give either longitudinal horizontal or vertical forcing. The soil box used in the testing can be vibrated in a direction tangential to the centrifuge arm by a servo controlled electro-hydraulic piston. In this way the soil surrounding the model can be subjected to shaking simulating an earthquake input to the model. Static or slow loading of the bridge was carried out by fixing the bridge superstructure to a rigid frame and moving the sand box slowly with the hydraulic loading system. In the quick release tests, the model was loaded against the soil in a manner similar to that used in the slow tests. A quick load release was achieved by cutting with an air powered knife the tension string used to load the bridge, (Figure 2.64).

Fourier analysis of the acceleration, strain and pressure records of the model subjected to a 100 g centrifugal acceleration positively identified three natural frequencies at 5.0, 7.2 and 9.8 Hz. The lowest frequency of 5.0 Hz represented the longitudinal flexural mode of the deck. The frequency was higher than the 4.7 Hz measured on the prototype but this difference was probably mainly due to the model mass being slightly less than required for exact similitude. The frequency at 9.8 Hz was associated with a lightly damped mode thought to be the primary transverse deck flexure mode (10.7 Hz in the prototype). The mode at 7.2 Hz was highly damped and was thought to be the primary translational soil-structure interaction mode. It showed up as a strong response in the longitudinal deck acceleration and in the abutment pressures. From the prototype forced vibration testing, this mode was

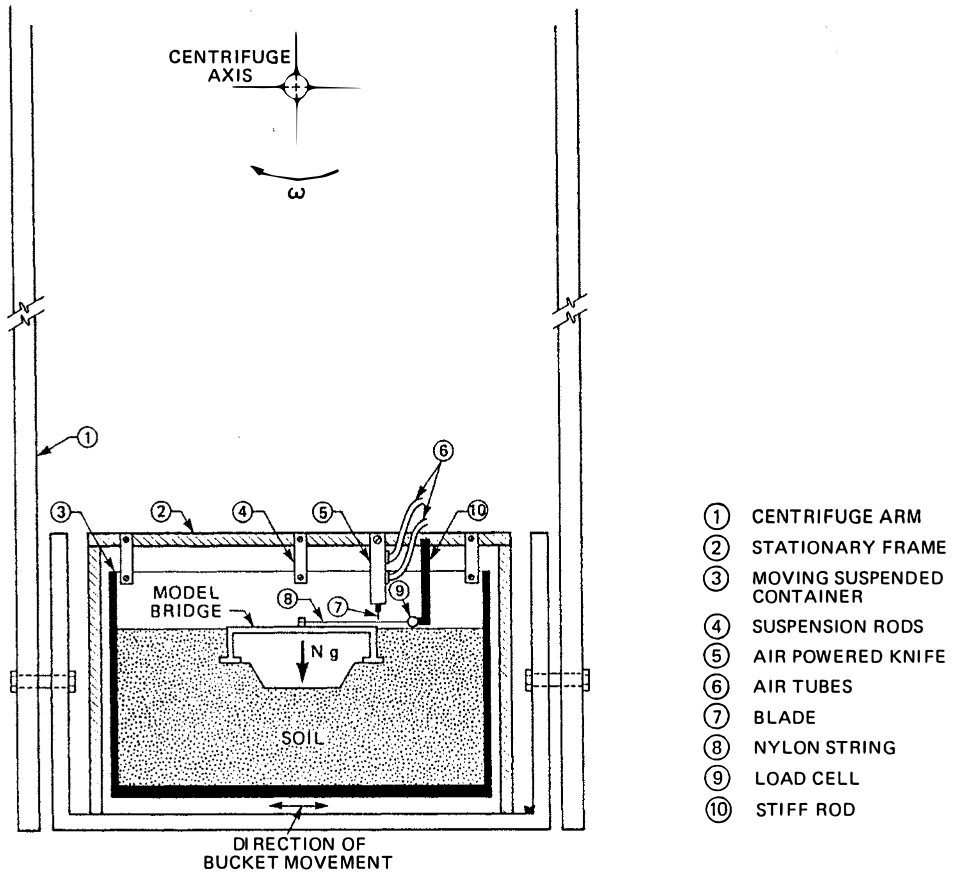

FIG. 2.64 BRIDGE MODEL IN CENTRIFUGE SOIL BOX

thought to have a frequency of about 15 Hz. Because of the relatively high frequency, high damping and interaction with other modes of similar frequency it was not positively identified in the field tests. The finite element model gave a natural frequency of 11.9 Hz for the primary longitudinal mode. The stiffness values used for the soil springs in the finite element model were significantly higher than indicated by the static force results given below for the centrifuge model and this would account for the discrepancy between the numerical and physical model results.

Figure 2.65 shows the time-histories of the base acceleration, deck horizontal displacement, and pressures at three locations on one abutment wall for an earthquake simulation test at 100 g centrifugal acceleration. The maximum pressures on the wall occurred at a time of about 17 s and remain relatively large during the following oscillations of the bridge at the primary longitudinal mode natural frequency (about 7.2 Hz). The pressures on the wall at time 17 s and the static gravity induced profiles are shown in Figure 2.66. For a peak ground acceleration of about 0.12 g, the dynamic pressures on the abutment walls are of similar magnitude to the static gravity induced pressures.

Typical force-displacement results from push-pull static tests are shown in Figure 2.67 for the 50 g, 87.5 g and 100 g centrifugal acceleration tests. The results for the different centrifugal accelerations (gravity load) show how the longitudinal stiffness of the bridge changes with prototype size. Pressures on one abutment wall for the 100 g test are shown in Figure 2.68.

The force displacement measurements showed that the total longitudinal stiffness of the bridge was about 4,500 kN/mm. (This is approximately a factor of 3 less than calculated for the finite element model of the prototype). Estimates of the longitudinal displacement under earthquake loading can be made from this stiffness and the prototype bridge weight of 10.7 MN. Making some allowance for dynamic amplification, it is unlikely that the longitudinal deflection would exceed about 1.5 mm under strong ground shaking.

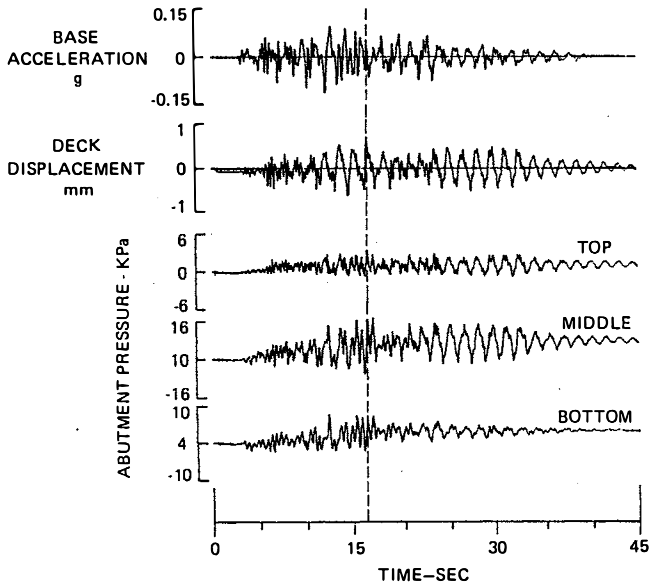

FIG. 2.65 EARTHQUAKE SIMULATION TIME-HISTORIES

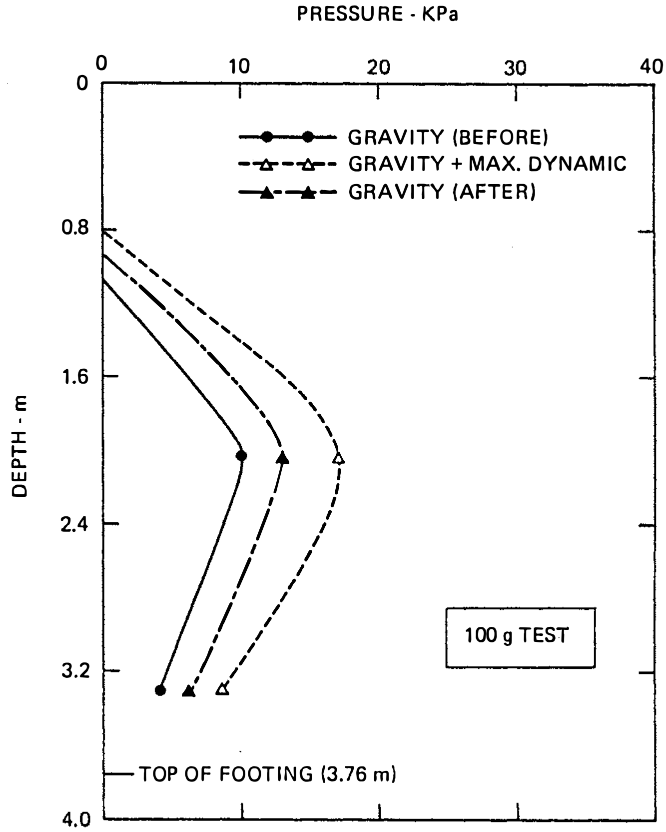

FIG. 2.66 PRESSURES ON BRIDGE ABUTMENT WALL
Dynamic From Simulated EQ Loading

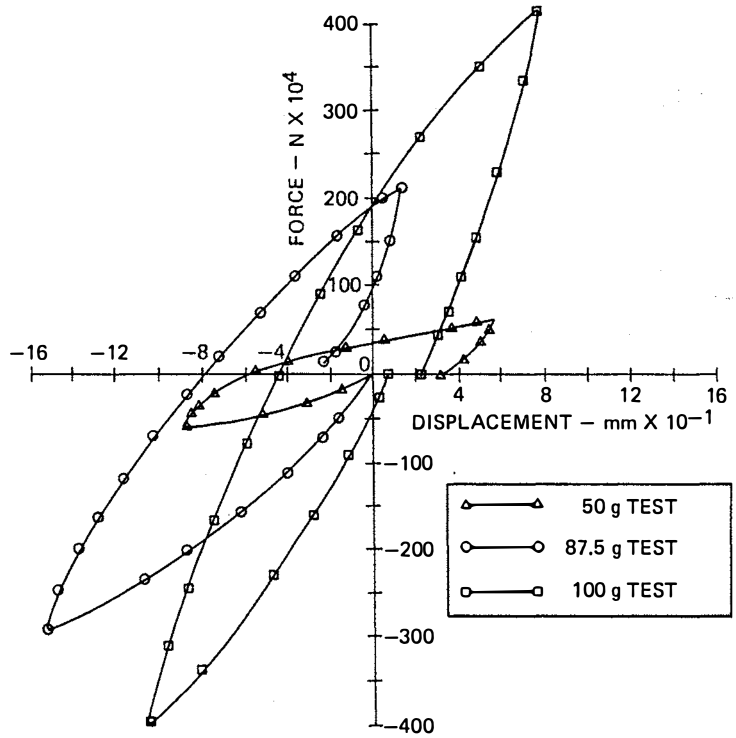

FIG. 2.67 FORCE-DISPLACEMENT FOR STATIC LOADING

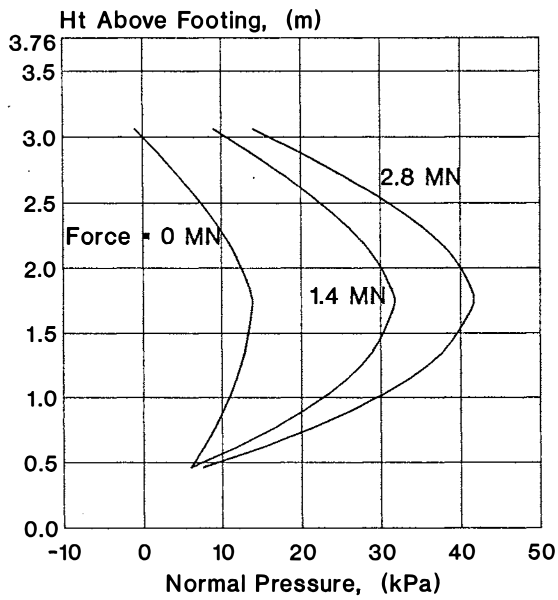

FIG. 2.68 PRESSURES ON ABUTMENT WALL
Static Forcing of Model

2.7 Reinforced Earth Walls

Reinforced earth retaining walls consist of a number of light independent facing panels that are anchored into the soil backfill by reinforcing strips extending horizontally into the soil. The main advantages are the inherent flexibility that makes reinforced earth forgiving of soil and foundation settlements and movements. Reinforced earth walls are also often more economical than conventional retaining methods for high embankments, bridge approaches and abutments.

Previous studies (Richardson et al, 1977) have shown that reinforced earth walls can undergo appreciable outward movement under earthquake loading without loss of integrity, providing a ductile failure mode is achieved by either material yield in the strips or pull-out of the strips. It is important that brittle failure of the strips or their connections to the facing panels is avoided. The expected good performance of reinforced earth walls appears to have been confirmed by reports from recent earthquakes, including the Loma Prieta, California earthquake, where a number of walls were subjected to strong ground shaking without damage (Reinforced Earth Company, 1990).

Although the static behaviour of reinforced earth walls is well understood and design practice well established, there is still a good deal of uncertainty about the mechanics of their behaviour in earthquakes and there is no universally accepted seismic design procedure. Summaries of the currently used seismic design methods have been presented by Nagel (1985) and Fairless (1989). Apparently none of these methods fully recognize the ability of reinforced earth walls to displace outwards without damage. Thus the full potential of reinforced earth as an economical method of soil retaining in seismic areas has not been realized.

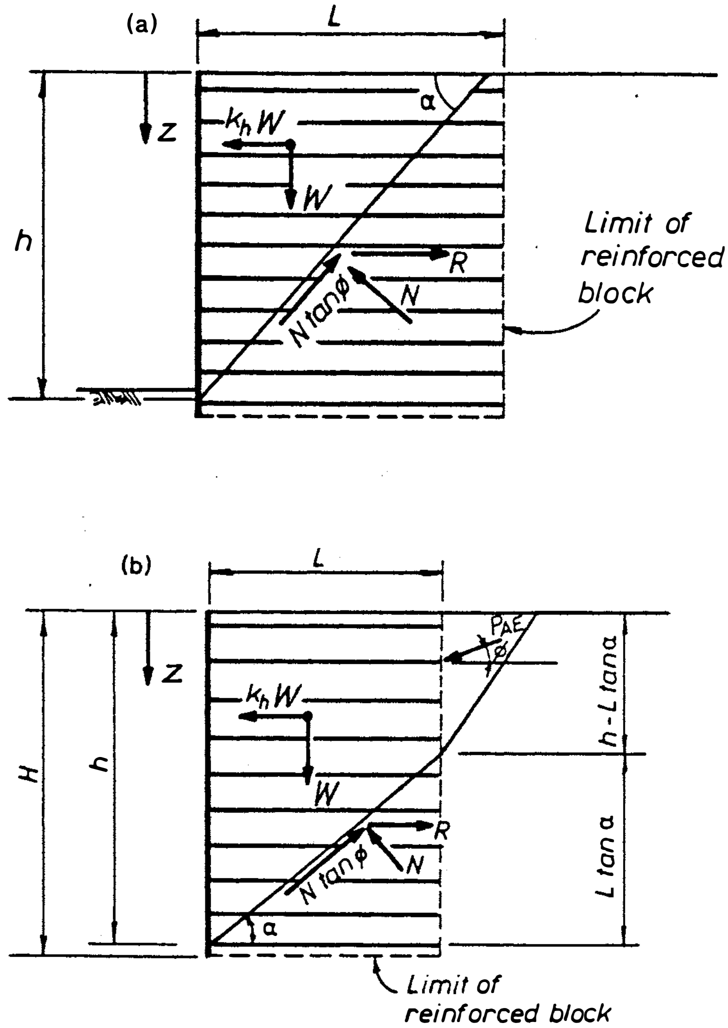

FIG. 2.69 LIMITING EQUILIBRIUM ANALYSIS RE WALLS
(a) Linear Failure Surface Within RE Block
(b) Bilinear Failure Surface

2.7.1 Theoretical Study

Bracegirdle (1980) proposed a seismic design method for reinforced earth walls based on limiting equilibrium theory and acceptable limits to outward movement. This approach is analogous to the Richards-Elms method for the design of gravity walls. The method assumes that a linear or bilinear failure surface will develop from the toe of the wall as shown in Figure 2.69. Equilibrium relations and an upper-bound failure criterion are then applied to find the critical failure surface angles and the critical acceleration at which sliding will commence. The ratio of the critical acceleration to the peak ground acceleration can then be used with the Newmark (1965) sliding block theory to estimate the permanent outward displacement (see Sections 2.3.1 and 3.5.4).

The main difficulty with using the Bracegirdle approach is that one of the required variables is the sum of the reinforcing strip tensions acting across a given failure surface. The strip tensions depend on the localised behaviour of the backfill and cannot be easily predicted. This topic has been the subject of a separate investigation by Tso (1986).

For the general case of a bilinear failure surface through the reinforced earth block and backfill soil as shown in Figure 2.69, the equations of horizontal and vertical force equilibrium can be written as (Fairless, 1989):

$$k_cW = R + N\tan\phi\cos\alpha - N\sin\alpha - P_{AE}\cos\phi \quad (2\text{-}12)$$

$$W + P_{AE}\sin\phi = N\tan\phi\sin\alpha + N\cos\alpha \quad (2\text{-}13)$$

Where:

N = Normal force on the failure plane through the reinforced block.

R = Sum of the strip tensions on the failure plane.

$R = R'\gamma h^2$

$R' = 2bn_hf^*[(L_s/h - \cot\alpha)\Sigma(z_i/h) + \cot\alpha\ \Sigma(z_i/h)^2]$

W = Weight of sliding wedge of soil within the reinforced mass.

Σ = Summation over the strips that intersect the failure plane.

b = Strip width.

n_h = Number of strips per unit width of wall.

f^* = Strip friction parameter.

L_s = Strip length.

h = Height from failure surface intersection with wall face to top of wall.

P_{AE} = MO force from the active wedge on the back face of the wall.

The normal force, N, can be eliminated from expressions 2-12 and 2-13 to give the following expression for the critical acceleration:

$$k_c = \frac{R'}{r(1 - 0.5\, r\tan\alpha)} + \tan(\phi-\alpha) + K_{AE}\frac{(1 - r\tan\alpha)^2\,(\sin\phi\tan(\phi-\alpha) - \cos\phi)}{2r(1 - 0.5\, r\tan\alpha)} \quad (2\text{-}14)$$

Where:

$r = L_s/h$

K_{AE} = MO earthquake active pressure coefficient.

Expression 2-14 can be solved by trial and error variations of α, or by using zero-finding algorithms, to find the minimum value of k_c.

2.7.2 Model Wall Tests

A summary is given in the following sections of two series of tests directed at checking the validity of the Bracegirdle method. In particular it was considered necessary to establish:

(a) The overall behaviour at failure (tilting or sliding).

(b) Whether sliding occurs at constant acceleration.

(c) Methods of predicting the location of the failure surface.

(d) The face connection and maximum strip forces.

(i) Small Scale Model Tests

Model walls 310 mm high by 810 mm wide were tested by Nagel (1985) in a glass sided tank shown schematically in Figure 2.70. The tank was mounted on rollers and set in motion by releasing a compressed spring to produce harmonic motion in a manner similar to that used previously by Lai (1979) and Aitken (1982) for gravity walls failing by sliding. Shock absorbers were used to damp out the oscillations. The use of this technique reduced the difficulty of obtaining smooth input accelerations that are difficult to obtain on some electro-hydraulic shaking tables and allowed the development of the failure plane to be clearly observed.

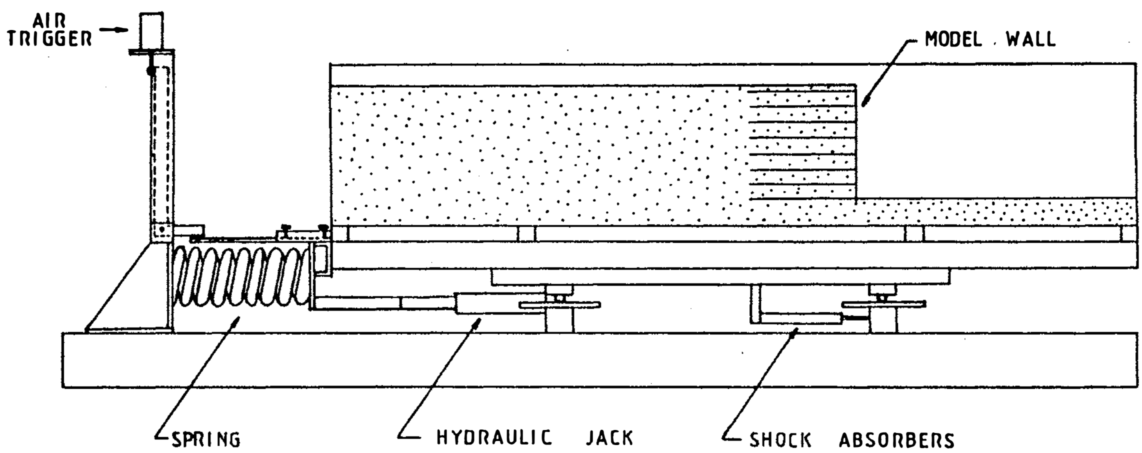

FIG. 2.70 SPRING LOADED TEST TANK FOR RE MODEL (Nagel, 1985)

The walls were constructed with eight 40 mm deep facing panels of 0.45 mm thick aluminium. The facing panels spanned the full 810 mm width of the wall (Figure 2.71). The panels were not connected but PVC tape was used as a seal to prevent leakage of the backfill sand. After preliminary pull out testing, 6 mm wide satin ribbon was chosen for the reinforcing ties to give frictional properties similar to prototype steel strips.

The ties were passed through the facing panels and connected with strain gauge load cells to provide a means of measuring the face loads and strip tensions close to the panels. Displacement transducers and accelerometers were located at the base of the wall, at mid-height and at the top of the wall. Photographic records of displacements were also taken by a camera rigidly attached to the side of the box. To aid visual inspection and photographic work, vertical lines of white sand were inserted between the box glass sides and the sand.

A relatively uniform beach sand was used as backfill and was showered into place to produce a uniform layer with an average in place unit weight of 15.5 kN/m^3. Construction of each wall approximately followed full-scale procedure in that only the current top panel was supported during backfilling, allowing lower panels to adjust to the soil and strip forces acting on them. Thin horizontal layers of white sand were introduced so that the failure surface could subsequently be accurately located.

Eight walls were tested with varying reinforcing strip lengths and spacings. Strip pullout resistance was determined by a series or separate pullout tests. The test procedure in each case was to subject the wall to a number of individual acceleration pulses, starting at a low level. Higher pulses were applied until eventually the wall moved with a large relative displacement. This incremental approach enabled the wall behaviour to be analysed in considerable detail.

The first significant result was that as the walls failed, they moved horizontally outwards with very little tilting or distortion. Figures 2.72 and 2.73 show the typical failure geometry for Wall 6 that was the most geometrically distorted case. Most of the displacement resulted from rotation of the bottom panel. The actual relative displacement of the model wall is of the same order as expected in a prototype wall subjected to the same base accelerations. Because of the small height of the model, the geometric distortion is highly exaggerated.

During the application of successive acceleration pulses, the initial movements of the walls seemed to take place with the formation of a broad shear band extending upwards from the toe of the wall roughly in the direction of the final failure surface. After some initial movement, a distinct shear surface could be seen forming near to the toe of the wall. This propagated towards the surface with further shaking. Finally, a further pulse would cause the failure plane to reach the surface and at that instance a large displacement of the wall would occur. Once a failure surface had developed, subsequent movement took place at acceleration levels considerably lower than those needed to cause failure.

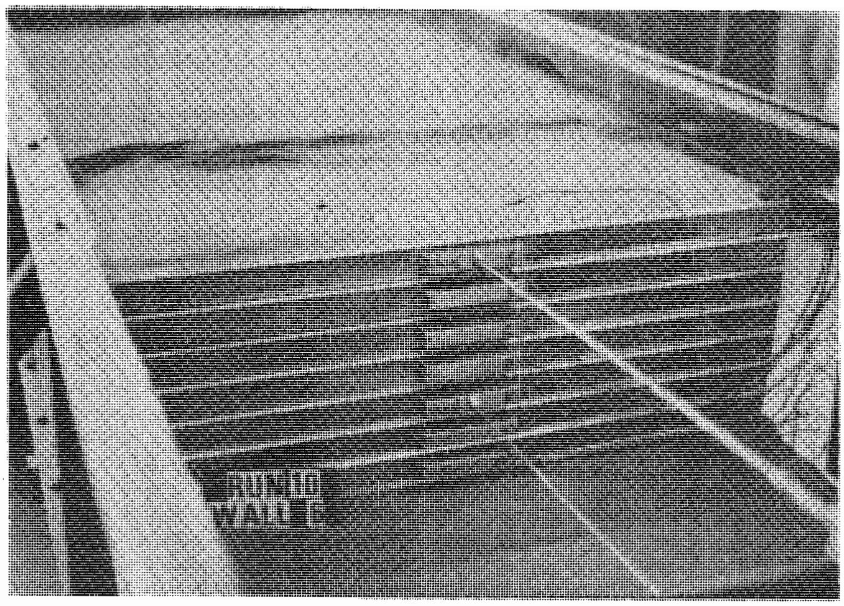

FIG. 2.71 REINFORCED EARTH MODEL WALL
(Nagel, 1985)

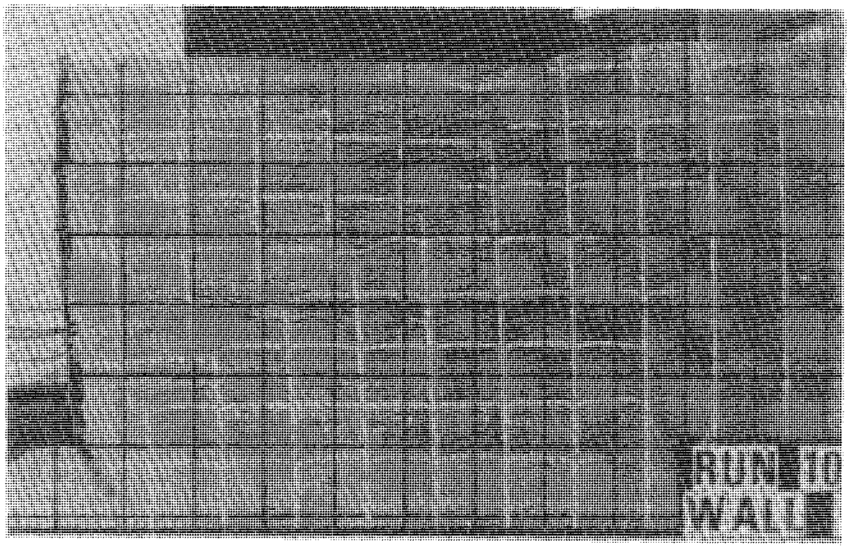

FIG. 2.72 FAILURE WEDGE BEHIND MODEL WALL 6. (REINFORCED EARTH)
(Nagel, 1985)

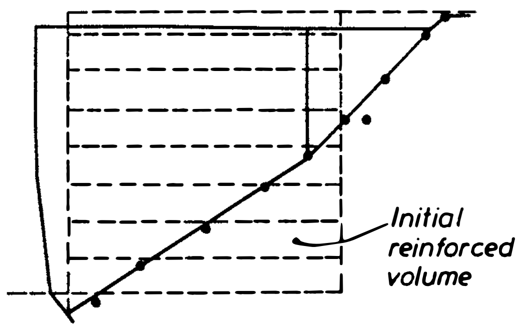

FIG. 2.73 FAILURE GEOMETRY FOR WALL 6
(Nagel, 1985)

Figures 2.74 and 2.75 show the accelerations recorded for Pulses 7 and 11 applied to Wall 8. The accelerations of wall in Pulse 7 are peaked and show little evidence of the plateau behaviour expected for a sliding block. The displacement of the wall acceleration trace relative to the box acceleration shows that a small amount of movement has occurred. On the other hand, the accelerations for pulse 11 show sliding block behaviour very clearly and that sliding occurs at a much lower level of applied acceleration than in the earlier pulses. The difference between the maximum and threshold acceleration to cause failure and the residual or sliding block acceleration can be explained by considering the shearing behaviour of a dense cohesionless material. Such a material has both a peak and a residual large strain angle of internal friction. To obtain a conservative estimate of the outward sliding movement using the Bracegirdle method it is important to use the residual rather than the peak angle of internal friction. The theoretically predicted sliding block critical acceleration for Wall 8 was 0.07 g, which is in good agreement with the observed result.

Failure surface geometries were obtained by carefully removing sand following the end of the test and observing the displacement of the white sand. A typical surface is shown in Figure 2.73 where the bilinear failure surface predicted by Bracegirdle is clearly apparent. Table 2.4 gives a comparison between theoretical and predicted failure surface angles. Agreement is reasonably good.

TABLE 2.4

Reinforced Earth Model Wall: Angle of Failure

Wall No	Expt Angle Deg	Theor Angle Deg
2	47	49
4	46	49
5	38	34
6	33	32
7	40	42
8	51	49

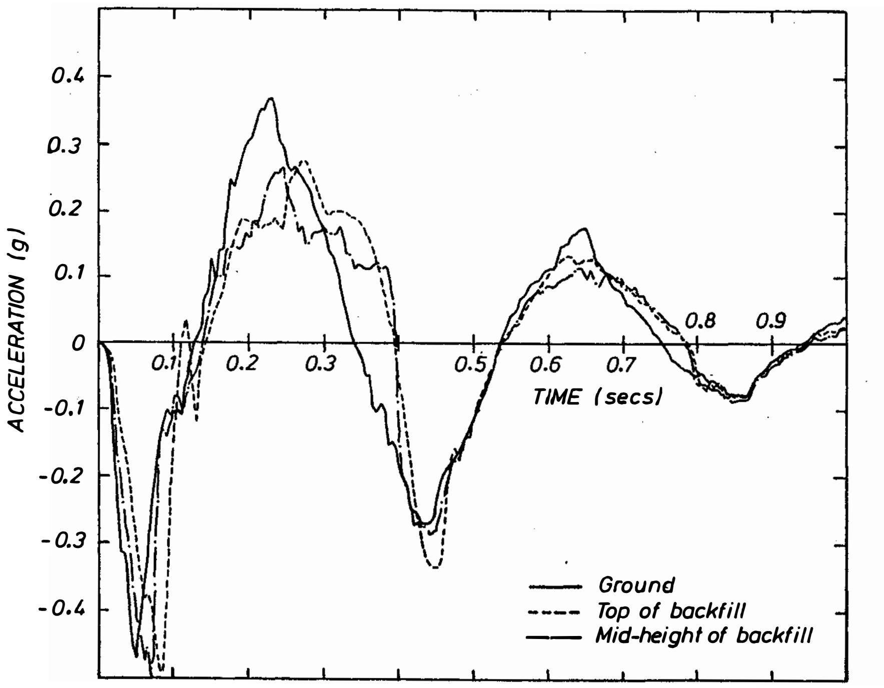

FIG. 2.74 ACCELERATIONS PRIOR TO SIGNIFICANT SLIDING
Wall 6, Pulse 7 (Nagel, 1985)

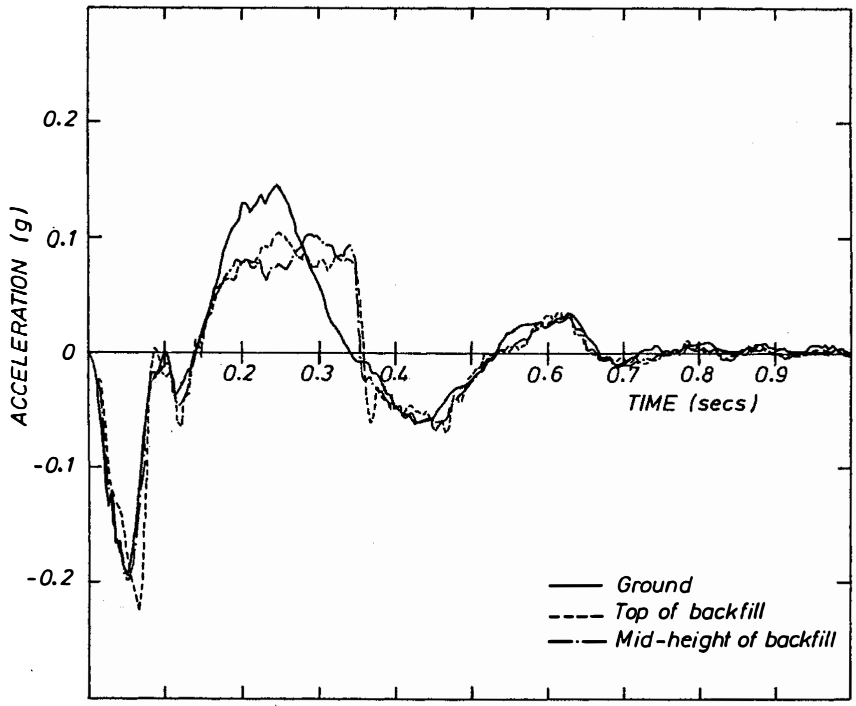

FIG. 2.75 ACCELERATIONS AFTER FAILURE DEVELOPMENT
Wall 6, Pulse 11 (Nagel, 1985)

Figure 2.76 shows the maximum pressures that occurred on the wall facing during the failure of the walls. These values have been computed from the measured tie forces that include gravity loads. By considering the average of all the tests it appears that the total pressure on the facing is roughly triangular in shape with a maximum dimensionless pressure at the base of the wall of p(z)' = 0.4, where the dimensionless pressure is defined by:

$p(z)' = p(z)/\gamma H$

p(z) = Normal pressure on wall at depth z.

Recorded acceleration traces showed that the tops of the walls were subjected to peak accelerations between 0.2 g to 0.4 g. The corresponding Mononobe-Okabe pressure coefficient, K_{AE}, for these accelerations, assuming a soil friction angle of 34°, were calculated to be 0.41 and 0.60. This suggests that the MO pressures might provide a useful upper bound for the design of the facing and ties. But, it would be necessary to compute the MO pressures for peak earthquake accelerations significantly greater than the estimated critical acceleration levels for sliding failure. For example, the theoretical critical accelerations for the walls tested ranged from 0.07 g to 0.27 g but the peak accelerations recorded at the tops of the walls were about a factor of 2 higher than these values. Again this emphasises the need to consider in design both the peak and the maintainable friction angles. The peak shearing resistance controls the design pressures and forces but the maintainable resistance at large strains needs to be used to obtain a conservative estimate of the displacements.

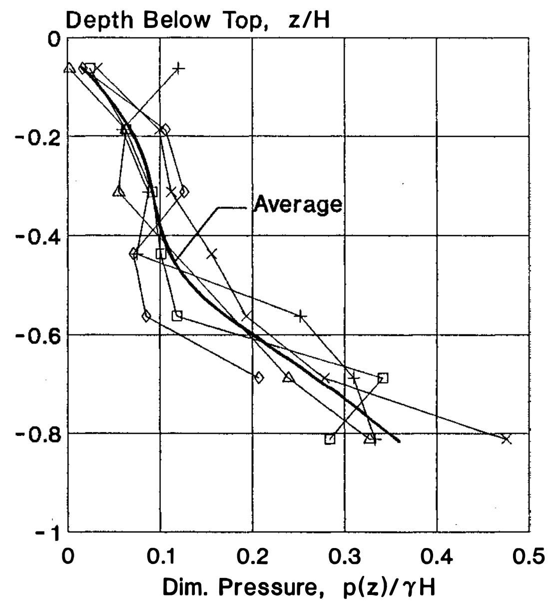

FIG. 2.76 FACING PRESSURES ON TEST WALLS

(ii) Large Scale Model Tests

Fairless (1989) tested six 1.0 m high by 2.0 m wide model walls in a sand tank mounted on an electo-hydraulic shaking table.

The walls were constructed of ten panels formed from 0.45 mm thick aluminium. The facing spanned the full 2.0 m width of the wall and each panel was 100 mm deep. The facing panels were not connected but PVC tape was used as a seal to prevent leakage of the backfill sand. Details of the wall are shown in Figure 2.77.

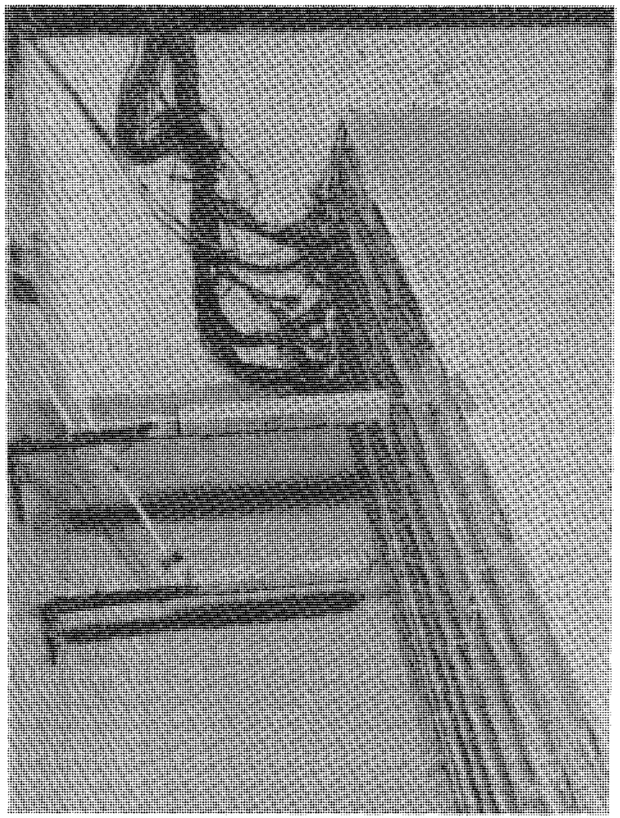

FIG. 2.77 REINFORCED EARTH MODEL WALL (Fairless, 1989)

The reinforcing strips were made from 0.45 mm thick aluminium alloy sheet. Strips were cut to a width of 10 mm using a guillotine. The strips were roughened by gluing sand to them to give interlock with the backfill and simulate the high frictional resistance of the ribbed steel strips used on full scale walls. One strip on each panel level was straingauged with pairs of gauges (top and bottom) spread along the strip length. A vertical spacing of 100 mm was used between the strips in all the models tested. Strip lengths and horizontal spacings were varied and a summary of these dimensions for each test is given in Table 2.5.

TABLE 2.5

Reinforced Earth Model Wall: Strip Spacing

Wall No	Hor Space mm		Length mm	
	Top	Bot	Top	Bot
1	250	250	750	750
2	330	330	1000	1000
3	330	330	750	750
4	250	160	900	500
5	250	160	900	500
6	250	250	750	750

Displacement transducers and accelerometers were located at the top and at mid-height of the wall. The accelerometers were set in the sand backfill at 75 mm from the wall facing. The input motion to the sand box was recorded with an accelerometer mounted on the shaking table.

Mt. Somers sand, an air-dry medium white quartz sand with D_{60} = 0.36 mm and D_{10} = 0.155 mm was used. Backfilling of the walls was carried out by raining the sand from a V-shaped trough towed at a constant speed to produce a relatively uniform placement. Sand density at the completion of each test was measured by placing a Proctor mould in the fill during backfilling and weighing it after testing was complete. Measured unit weights ranged from 15.5 kN/m^3 to 16.1 kN/m^3. Construction of each wall approximately followed full-scale procedure in that only the current top panel was supported during backfilling, allowing lower panels to adjust to the soil and strip forces acting on them. In Tests 4 to 6, thin horizontal layers of grey sand were introduced so that the failure surface could be accurately located. (The main volume of backfill sand was white). Also, by careful dismantling, the bends in all strips passing through the failure surface were located.

Detailed investigations were carried out to measure the soil/strip coefficient of friction. Strip pull-out test were performed prior to the wall tests and sliding shear tests were undertaken using a shear box and an aluminium block, sand coated to roughen it in a manner similar to the strips used in the model walls. Coefficients of friction were also determined by back analysis of the total failure loads and the individual measured strip tension forces at failure.

The angle of internal friction of the backfill was determined using multiple-reversal direct shear, ring shear and vacuum triaxial apparatus. A summary of the test results is given in Figure 2.78 which shows that there is a significant decrease in the friction angle with confining pressure. A friction angle of 40° was used for the theoretical limiting equilibrium calculations carried out in the analysis of the test results.

The first four walls tested were subjected to single pulse sinusoidal acceleration inputs. The final two models were subjected to the 1940 El Centro north-south accelerogram.

Observed yield accelerations were found to decrease when the failure surface became fully developed and outcropped at the surface. Back analysis of the experimental results, using the observed tie forces and failure plane angles showed that the reduction in yield acceleration was caused by the soil friction angle decreasing with increasing displacement of the wall. The apparent friction angle was found to decrease from an initial value of about 46°

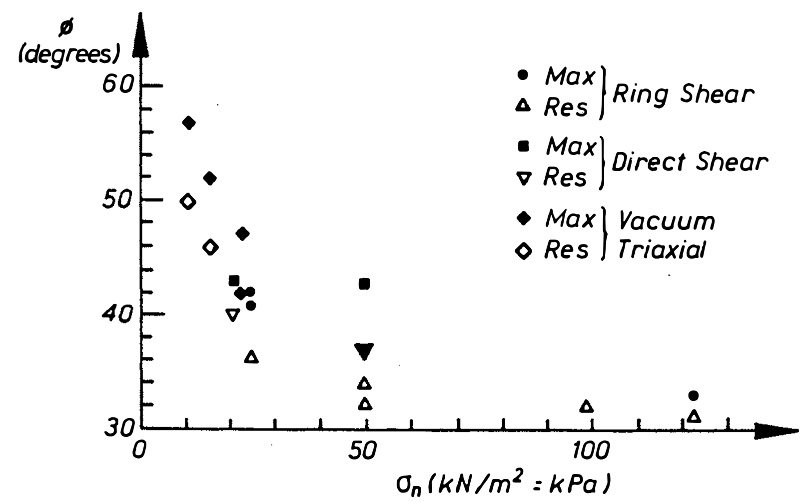

FIG. 2.78 MEASUREMENTS OF SAND FRICTION ANGLE (Fairless, 1989)

to 36° at the time the failure surface became fully developed. This behaviour was similar to that observed by Nagel for the smaller model tests and is apparently related to dense sand having a peak shearing resistance higher than the residual resistance. Before the failure is complete, part of the potential failure plane has a higher strength that reduces as the failure plane propagates from the toe to the surface. Average yield accelerations for test runs prior to the full development of the failure surface, at full development and following the full development are given in Table 2.6. Failure geometries, with lines assumed to represent the failure surface, are shown in Figures 2.79.

TABLE 2.6

Reinforced Earth Model Wall: Average Yield Accelerations

Wall No	Ave Peak Yield Acclns. g		
	Prior to Full Failure	Fully Developed Failure	After Failure
1	0.32	0.25	0.24
2	0.32	0.24	0.20
3	0.22	0.13	0.08
4	0.34	0.23	0.20
5	0.31	0.19	0.20
6	0.34	0.27	0.22

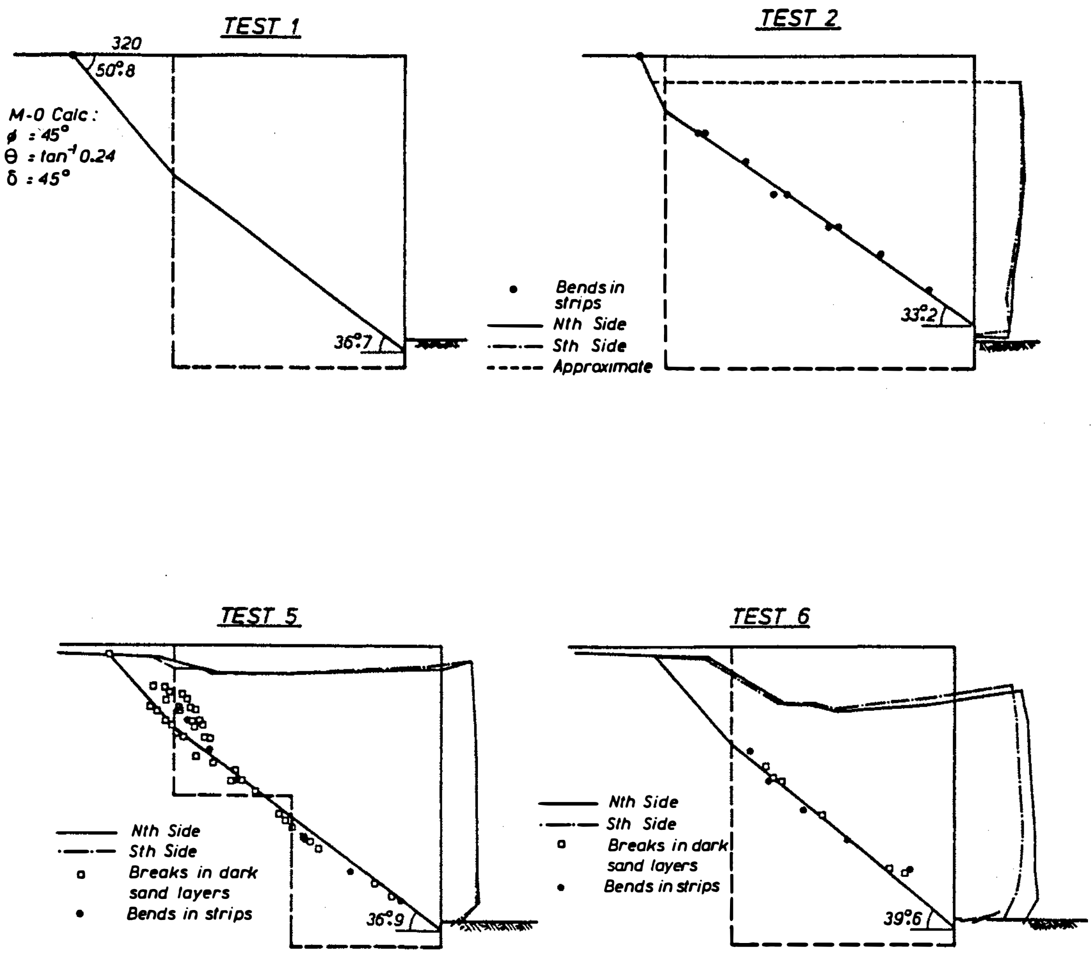

FIG. 2.79 FAILURE GEOMETRIES RE MODEL WALLS (Fairless, 1989)

Table 2.7 shows a comparison of observed and calculated values for the critical acceleration coefficient, k_c, and the failure surface angle, α. The calculated values are based on assumed strip/soil friction of f^* of 1.4 and a backfill friction angle $\phi = 38°$. The value of f^* used is close to the peak friction angle measured in the sliding shear tests and appeared to be consistent with back analysis work using the measured strip tensions. The ϕ value assumed is somewhat lower than the 40° indicated by the residual values from the soil tests and it is though that dilation of the sand may cause an apparent increase in the confining stress at low confining values. If the assumed values for the friction parameters are accepted as reasonably correct, then it is clear from the results given in Table 2.7 that good agreement exists between the observed and calculated results.

TABLE 2.7

**Reinforced Earth Model Wall:
Calculated and Observed Yield Acceleration Coefficients and Failure Surface Angle**

Wall No	k_c		α	
	Calc	Obsd	Calc	Obsd
1	0.26	0.24	35.5	36.7
2	0.34	0.21	32.7	33.2
3	0.18	0.09	43.0	43.0
4	0.21	0.21	36.7	41.8
5	0.21	0.20	36.7	36.7
6	0.26	0.22	35.5	39.5

Plots of forces that developed in the Wall 6 ties are shown in Figure 2.80. This wall was subjected to the simulated earthquake loading and significant outward movement commenced at Run 3. The results show that the post-failure forces may be up to 6 times the construction forces shown as R0 in the plots. The strip forces at failure (when the failure plane meets the soil surface) were typically 4 times the construction forces. Permanent displacements of up to 15% of the wall height were required before the forces in the lower strips appeared to reach their maximum values. The position of the maximum force in the lowest 4 strips generally moves towards the face and these strips appear to be the most important in resisting the earthquake forces. In the higher strips, the maximum force does not necessarily occur at the facing but the forces close to the facing are often near to the maximum values.

The distribution of the maximum total tie forces next to the face of the wall for Tests 3 and 6 are shown in Figures 2.81 and 2.82. Earth pressures for active, K_A, at rest, K_0, and Mononobe-Okabe, K_{AE}, have also plotted by assuming that the pressures are transferred to the strips from the tributary facing areas around each strip. Pressures were calculated assuming the soil friction angle to be 40°. The MO pressures are based on the acceleration coefficients for failure given in Table 2.7. The forces in the lower strips are at least a factor of 2 greater than forces obtained from the MO pressures on the facing.

Back analysis of the tie observed forces was carried to find the variation of f^* with wall displacement and over the height of the wall. It was found that f^* tended to increase as the failure surface was developing. After failure, f^* tended to increase in the lower half of some walls but there was no very consistent behaviour. f^* generally had a minimum value near the middle of the wall, with a significant increase in the two strips above the bottom strip. There was a trend for f^* to increase from the minimum value at the mid-height moving towards the top of the wall. It was found that the direct shear test peak friction coefficient gave a good estimate of the observed strip friction.

Time histories of wall acceleration and displacement for Wall 6 are shown in Figure 2.83. The time histories showed that there is often quite large amplification of the outward accelerations (wall tending to move against the backfill) but little amplification of the inward accelerations. At inward accelerations exceeding the yield level, the wall displaces limiting the response acceleration at the top of the wall to near the yield acceleration.

Analysis of the displacement results recorded when the failure planes had become fully developed showed that the failure displacement was between 3.8% to 7.6% of the height of the wall. These displacement levels are presumably a function of the soil properties, and whether they can be considered to hold for full scale walls needs further investigation.

The permanent displacements recorded in Tests 5 and 6 (earthquake accelerogram inputs) are given in Table 2.8. These displacements are compared in Figure 2.84 with various theoretical predictions.

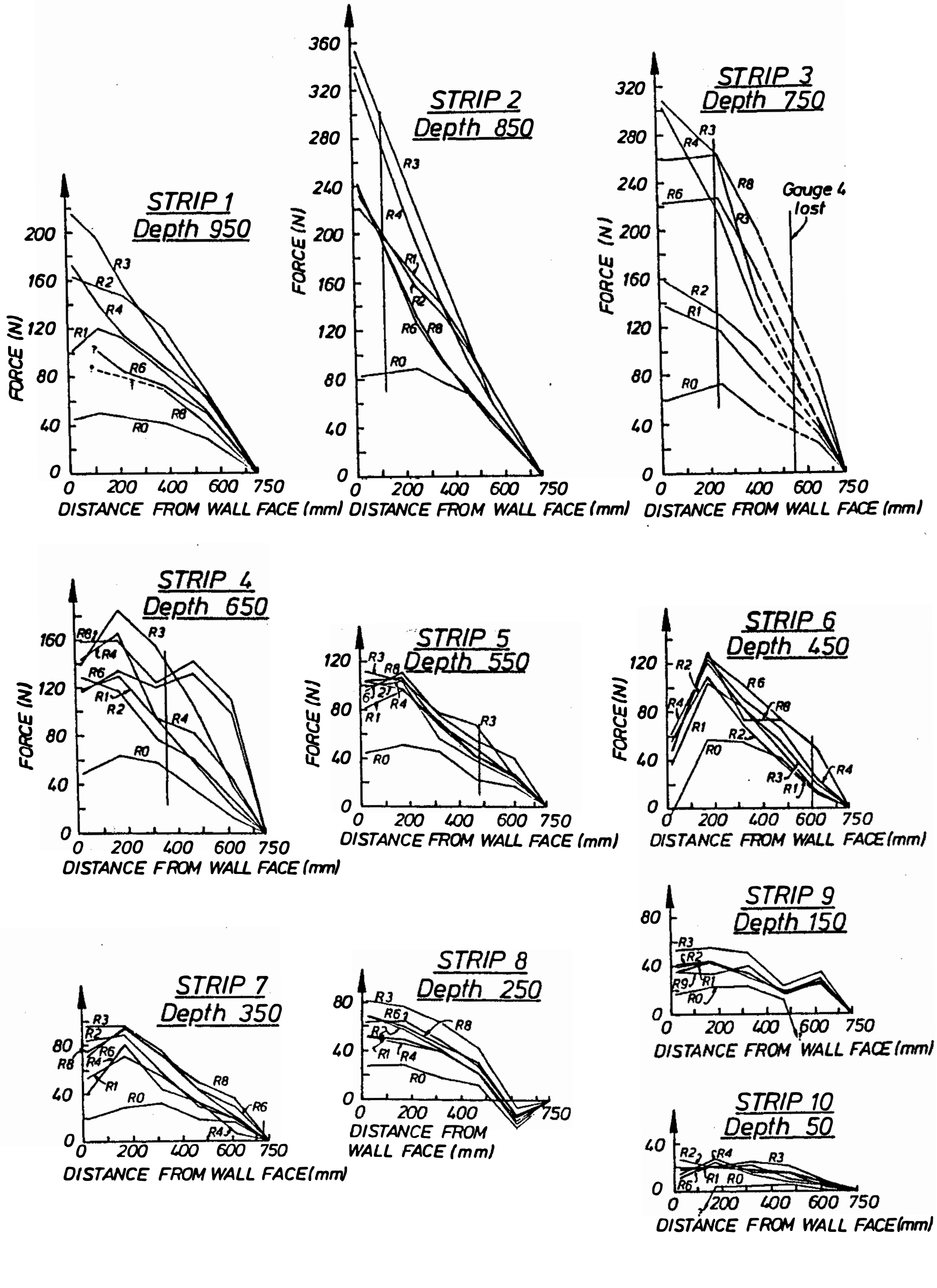

FIG. 2.80 TIE FORCES IN RE MODEL WALL 6
(Fairless. 1989)

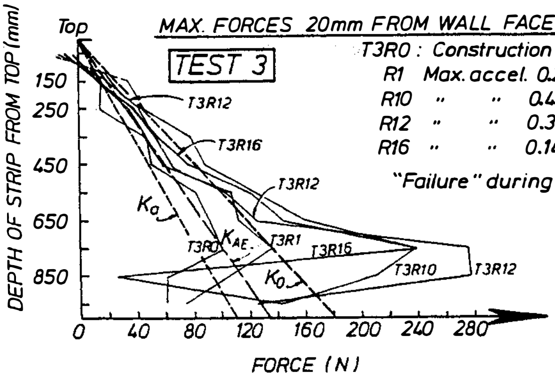

FIG. 2.81 TIE FORCES NEAR WALL FACE, WALL 3
(Fairless, 1989)

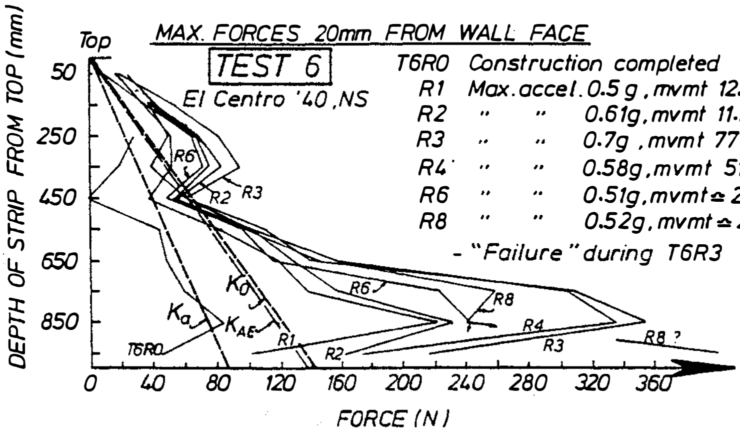

FIG. 2.82 TIE FORCES NEAR WALL FACE, WALL 6
(Fairless, 1989)

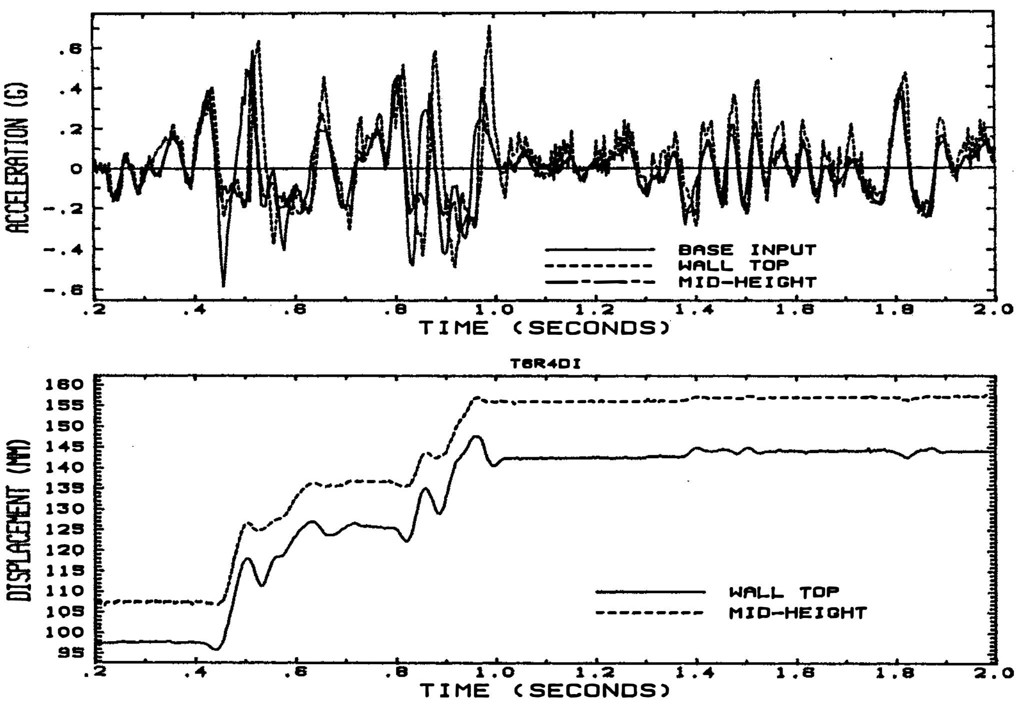

FIG. 2.83 TIME HISTORIES OF ACCN AND DISP, WALL 6
(Fairless, 1989)

TABLE 2.8

Reinforced Earth Model Wall: Observed Displacements

Wall No 5				Wall No 6			
Run	Peak Accn g	Yield Accn g	Disp mm	Run	Peak Accn g	Yield Accn g	Disp mm
2	0.41	0.28	5.4	1	0.50	0.33	12.8
4	0.51	0.32	2.2	2	0.61	0.38	11.2
5	0.64		6.1	3	0.70	0.28	77
6	0.92	0.19	28.5	4	0.58	0.20	51
7	0.68	0.22	21.4	5	0.48		≈20
8	0.64	0.22	17.5	6	0.51	0.23	≈20
9	0.64	0.17	24.5	8	0.52	0.22	≈20

To help interpretation of the experimental results, Fairless carried out a numerical study using the limiting equilibrium equations to determine the importance of various wall and soil parameters. The soil backfill friction angle was the most important parameter with the critical acceleration being almost directly proportional to this parameter. The strip friction coefficient, f^*, has an influence on both the failure surface angle and the critical acceleration. The number of strips per metre length of wall, n_h, has a significant influence on the failure surface angle but does not have a very large effect on the critical acceleration. Some of the numerical results from this part of the project are of considerable value for design applications and are presented in Section 3.7.3.

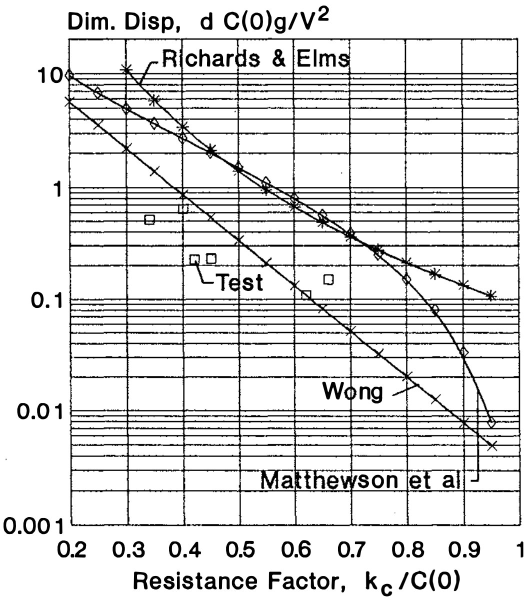

FIG. 2.84 DISPLACEMENTS RE MODEL TEST Wall 6 Test

2.8 Tied-Back Walls

A tied-back wall usually has a relatively flexible facing anchored by ties that extend horizontally (or inclined at a shallow angle) to an anchor of some type located behind the potential failure surface. The anchoring may be provided by passive resistance blocks, soil or rock anchors or another structure. The earthquake behaviour of tied-back walls is more complex than a gravity type wall because stability usually depends on both the anchors and toe restraint.

In tied-back sheet piling walls, it is usual to anchor the toe by embedding it some distance below the base of the wall to develop passive pressure resistance. Other forms of tied-back walls may rely on a number of ties to provide the lateral stability with little resistance being provided by passive pressures.

A reinforced earth retaining wall is a special case of tied-back wall with the anchoring provided by frictional resistance on the strips rather than by a passive resistance block or other type of anchor. For flexible tied-back walls and for cases where outward movement can be accepted, the limiting equilibrium method of analysis described for reinforced earth is applicable.

The pressures on tied back walls are dependent on the type of anchor and flexibility of the wall. If tie-backs are restrained by some form of rigid deadman anchor and the ties are required to remain elastic during earthquake loading, a limiting equilibrium approach may not be appropriate and pressures may need to be obtained by the application of elastic theory using the peak ground acceleration.

2.8.1 Theoretical Study

A simple tied-back wall retaining a cohesionless horizontal backfill is shown in Figure 2.85. It is assumed here that the wall will move sufficiently under earthquake loading for a fully plastic stress state to develop in the backfill. By considering equilibrium of the failure wedge forces in a manner analogous to that described for reinforced earth walls, it can be shown that the critical acceleration to cause sliding failure is given by:

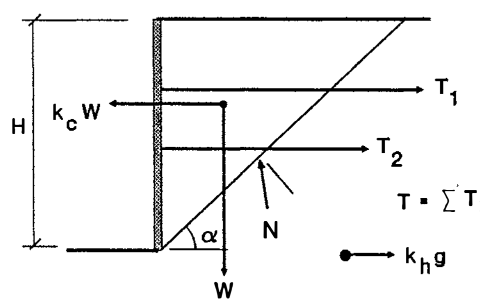

FIG. 2.85 ANALYSIS OF TIED-BACK WALL

$$k_c = T/W + \tan(\phi - \alpha) \qquad (2\text{-}12)$$

Where:

$W = 0.5\ \gamma\ H^2/\tan\alpha$, the weight of sliding wedge.

T = Total tie force.

Rearranging expression 2-12 gives:

$$T' = \frac{k_c + \tan(\alpha - \phi)}{\tan\alpha} \qquad (2\text{-}13)$$

Where:

$T' = T/(0.5\ \gamma H^2)$

Plots of T/W and T' versus the critical acceleration, calculated for friction angles of 30° and 35° are shown in Figures 2.86 and 2.87. The angle of inclination of the failure plane is also plotted. For design applications, the failure plane inclination is required so that ties can be made of sufficient length to locate the anchor beyond the failure zone of the sliding wedge.

By analogy with the MO theory it can be shown that for a tied-back wall with horizontal ties, T' is equal to the MO active earthquake coefficient, K_{AE}, for a smooth wall. In many tied-wall applications, earthquake forces on the ties can therefore be estimated by using published graphical solutions to the MO equations (see Section 3.5.3).

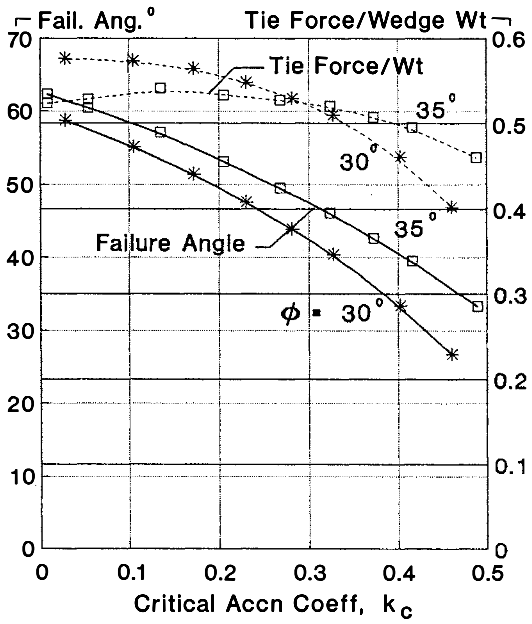

FIG. 2.86 TIED-BACK WALL
Tie Forces Under EQ Load

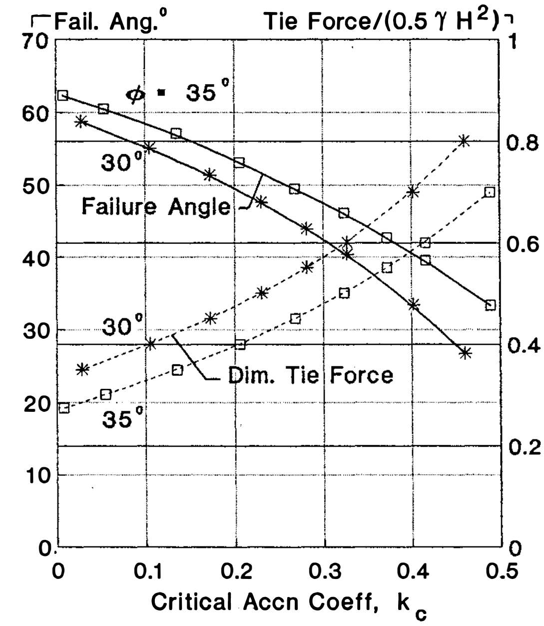

FIG. 2.87 TIED-WALL
Tie Forces Under EQ Load

Expressions 2-12 and 2-13 may also be applied to tied-back walls that have a constant resisting force at the wall toe. Here, T is equal to the sum of the toe resistance and the tie force.

In sheet pile type tie-back walls, the toe resistance will usually be provided by soil passive resistance. The forces acting on a typical sheet pile tie-back wall under earthquake loading are shown in Figure 2.88. A ground acceleration, $k_h g$, directed towards the backfill produces inertia forces on both the active pressure wedge behind the wall and the passive wedge in front of the wall. The inertia force on the passive wedge is directed away from the wall, in the opposite direction to the passive pressure force on the wall, resulting in a reduction of the passive resistance. The change in the passive pressure coefficient with acceleration can be derived using the MO method in a similar manner to the active pressure case, but with a modification to the direction of the inertia force. This analysis shows that the inclination of the passive failure wedge decreases with increasing acceleration, with a corresponding reduction in the passive resistance against the wall. The effects of horizontal acceleration on both the active and passive pressure cases are illustrated in Figure 2.89 (Richards and Elms, 1987).

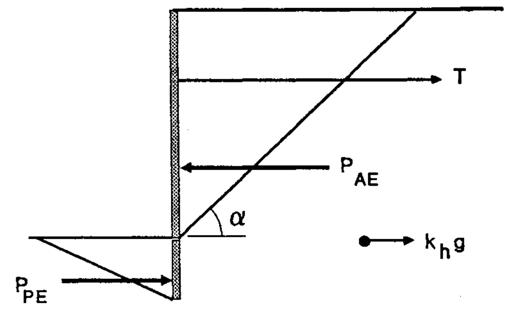

FIG. 2.88 FORCES ON TIED-BACK WALL

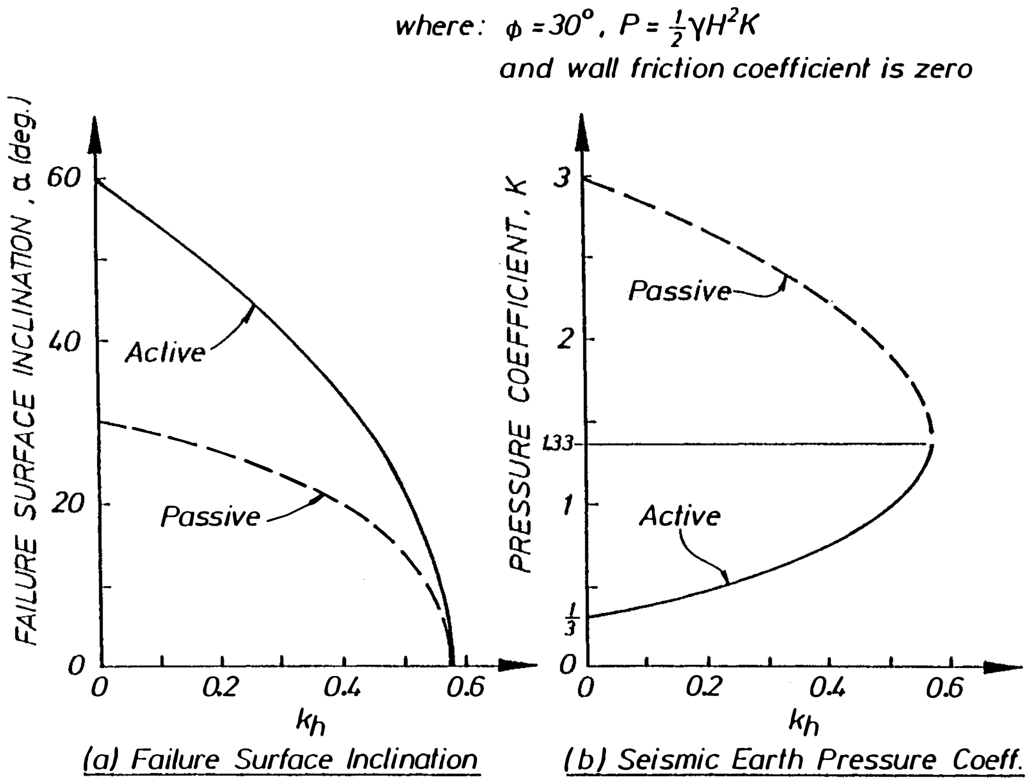

FIG. 2.89 MO ACTIVE AND PASSIVE PRESSURE COEFFS.
(Richards and Elms, 1987)

Richards and Elms (1987) have outlined the procedures for a seismic limit analysis of a tied-back sheet pile type of wall. Their analytical model is illustrated in Figure 2.90. Both the active pressure on the wall and the passive resistance at the toe and anchor can be estimated from the MO method. Because of the reduction in inclination of the failure planes under dynamic loads, there may be interaction between the dynamic failure wedge of the anchor and the dynamic active wedge behind the wall. The ties can be made longer to reduce this effect, or alternatively, a more conservative approach may be required for the anchor design than used for static loads.

By considering equilibrium of the limiting values of the three forces on the wall, it is possible to estimate the critical acceleration at which outward movement would commence. If this acceleration is less than the design level peak ground acceleration, the magnitude of the outward movement of the centre of mass of the sliding wedges can be estimated using the Newmark sliding block theory. A detailed discussion of the possible failure modes and movements is given by Richards and Elms (1987). The most likely action is for the wall to displace outwards by rotating about the toe, but this behaviour is dependent on the type and flexibility of the anchor. Although less likely, a passive failure may occur at the toe, causing the wall to rotate about the top. A more general case would be when movement occurs in both the anchor system and at the toe wedge resulting in both translational and rotational displacement.

2.8.2 Model Wall Tests

In the first stage of a study on tied-back walls, Richards and Elms (1987) carried out model studies to investigate a wall rotating about its top by passive wedge failure at the toe.

Details of the wall model are shown in Figure 2.91. The model wall was mounted in the spring driven test box used in other model wall studies at the University of Canterbury and described previously in Section 2.3.2. To simplify the model, sand was only placed in front of the wall toe and the active pressure was simulated by two small air pressure jacks. These provided an approximately constant trust and could be set and measured independently enabling the seismic behaviour of the passive wedge to be studied alone.

Three walls were tested with variations in the height of the active jacking thrust and the height of the top pin about which the wall rotated. Instrumentation was set-up to measure reaction forces, accelerations and displacements of the wall.

The backfill was New Brighton beach sand of fairly uniform grain size that was rained into position from a height of approximately 500 mm. The initial placement resulted in a medium dense state with a friction angle of about 34° but after the initial acceleration pulses the sand densified to give a friction angle of about 38°.

Figure 2.92 shows typical traces recorded during the testing of one of the walls. Cut-off acceleration peaks in the wall response with corresponding outward displacements are evident and the behaviour is similar to the sliding failure of gravity walls (Figure 2.24). Figure 2.93 shows a typical fully developed passive wedge failure plane. The observed failure planes were almost straight lines.

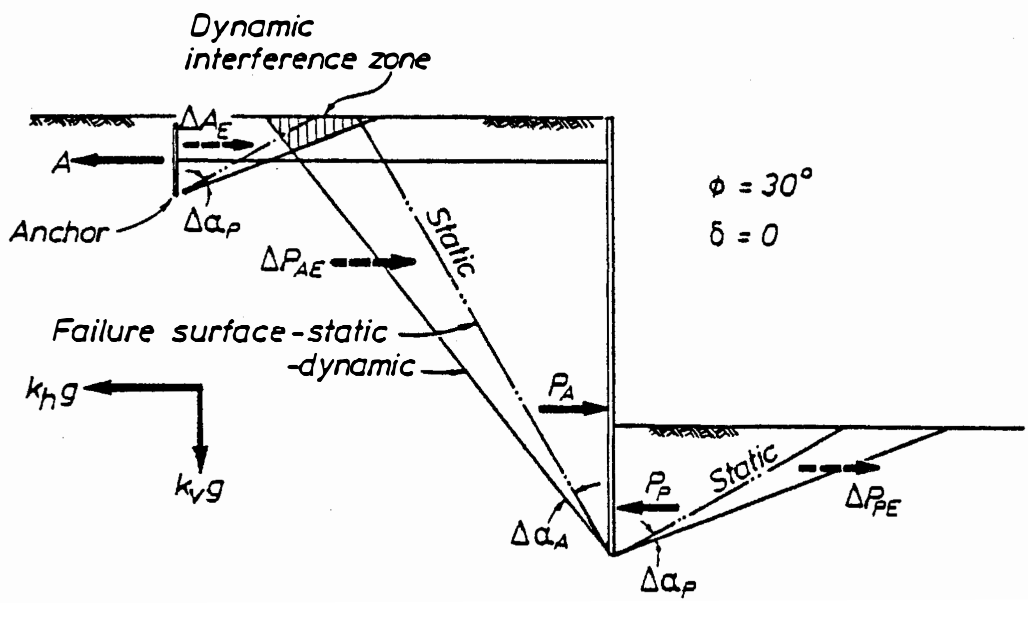

FIG. 2.90 TIED-BACK SHEET PILE WALL ANALYSIS (Richards and Elms, 1987)

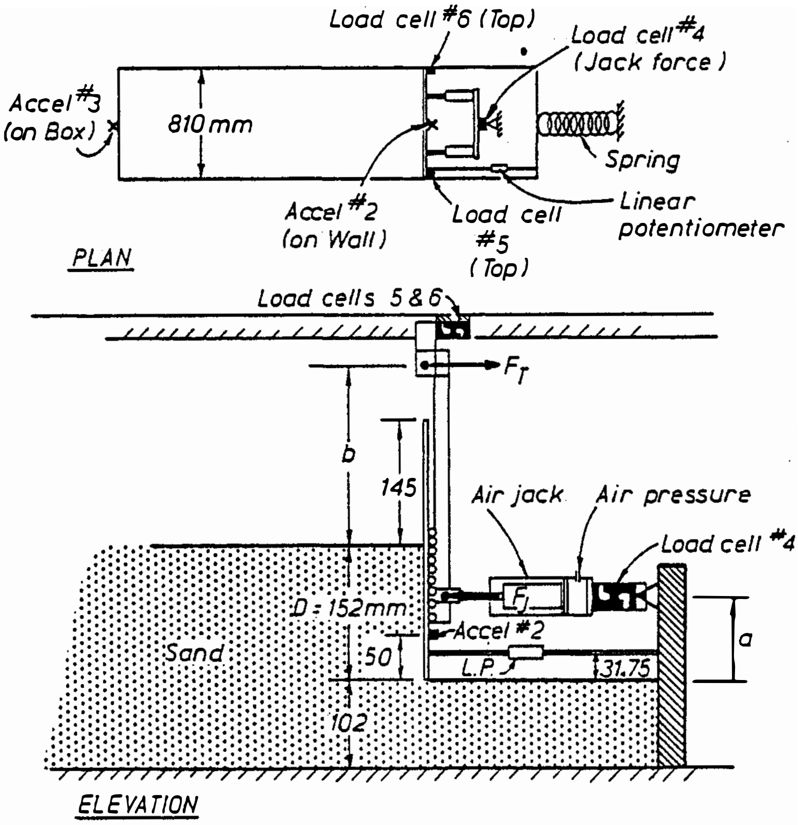

Wall No.	Wt (N)	a (mm)	b (mm)
1	430	76	152
2	660	76	213
3	680	134	213

FIG. 2.91 TIED-BACK MODEL WALL
(Richards and Elms, 1987)

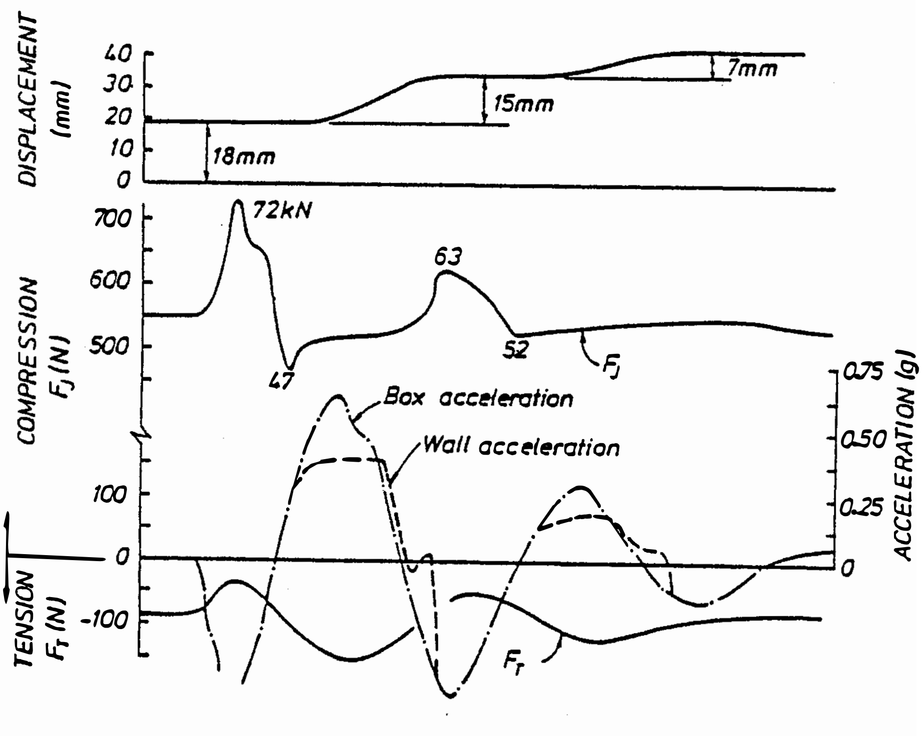

FIG. 2.92 ACCN, DISP AND FORCE TRACES TIED-BACK MODEL WALL, (Richards and Elms, 1987)

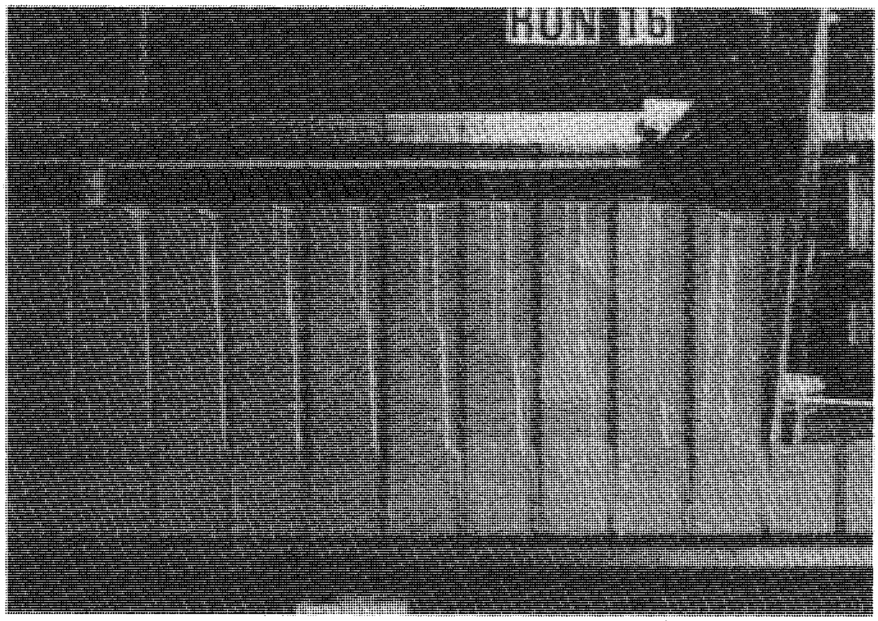

FIG. 2.93 PASSIVE FAILURE WEDGE IN FRONT OF MODEL TIED-BACK WALL. (Richards and Elms, 1987)

Analysis of the results showed good agreement between the measured forces on the wall and the MO prediction of the passive earthquake pressure coefficient, K_{PE}.

It was found that the sand densified during the initial pulses to a greater extent than occurs for the active case where the wall can move away from the sand. This densification increased the angle of internal friction resulting in an increase in the resistance to passive failure. Under acceleration pulses of sufficient magnitude to initiate passive failure of the sand in the densified state, the classic sliding wedge was formed and the sand in the failure zone gradually loosened to the residual friction angle value.

The position of the centre of pressure of the passive force was found to move downwards from the third point as shaking continued until the passive failure wedge was fully developed. For design analysis, it was concluded that the centre of pressure could be assumed to be at 1/6 of the wedge height from the bottom of the wall.

3

DESIGN RECOMMENDATIONS

3.1 Introduction

The basic philosophy recommended for the earthquake design of retaining walls and abutments has been presented in detail in Sections 1.2 to 1.6. A summary of these recommendations is given below.

The pressures that develop on a wall during earthquake loading are very sensitive to the elastic flexibility of the structural components of the wall and the ability of the wall to move outward because of either permanent deformations in the foundation soils or inelastic behaviour within the wall structure. It is therefore recommended that seismic design procedures consider the reduction in pressures arising from wall flexibility and permanent deformation.

For rigid walls, the backfill soil may remain essentially elastic under combined earthquake and gravity loads and the theory of elasticity or elastic finite element solutions can be applied to provide design pressures. More generally, there will be sufficient deformation for nonlinear soil effects to be important and for wall pressures to be significantly lower than for a fully rigid wall. These intermediate cases are more difficult to analyse than the limiting cases of rigid wall behaviour and fully plastic soil conditions. Approximations from theory of elasticity solutions may often be satisfactory for wall design purposes, or alternatively, upper and lower bounds from the limiting cases of rigid wall and fully plastic stress conditions may provide sufficient information for less important structures.

Where the wall displacements are sufficiently large to produce a fully plastic stress state in the soil by either outward movement (active state), or by movement towards the backfill (passive state), it is recommended that the forces on the wall are calculated by the Mononobe - Okabe (MO) method. This procedure is based on the analysis of the limiting equilibrium of a failure wedge bounded by the backface of the wall, the backfill surface and a straight line failure plane. (Figure 1.7)

For walls that are relatively rigid, the initial earthquake accelerations may induce pressures, corresponding to elastic soil behaviour, that are significantly greater than the MO pressures. If the wall has insufficient strength to resist these pressures, yielding and outward movement of the wall may occur with a fully plastic stress condition developing in the soil. With progressive yielding, the pressures on the wall will decrease to the MO values. The outward yielding may result from either permanent displacements in the soil foundation or from yielding in the structural wall elements. The failure mode will depend on the wall type and the relative capacities available in each potential failure mechanism.

If structural damage is to be avoided, it is necessary to design for either the maximum peak earthquake-induced pressures consistent with the type of soil behaviour expected, or to detail the wall to displace outwards, where this is possible, by movement on failure surfaces in the soil. Where soil failure modes are possible, it is recommended that the approximate magnitude of the outward movement be obtained from the Newmark sliding block analogy. The outward movement is related to the critical ground acceleration level required to initiate movement and it is therefore possible to find the design pressures and forces on the wall from the limits considered acceptable for outward movement.

Because of the dynamic displacement response of buildings and bridges during earthquakes, basement and abutment walls that are monolithic or rigidly connected to the main structure, are subjected to displacements relative to the soil mass. For these types of walls, dynamic soil pressures arise from both the displacement response of the structure and earthquake elastic waves (or inertia loads) in the soil, (Figure 1.6). Both these pressure components should be calculated separately and combined in an approximate way to give the total earthquake force on the wall.

3.2 Design Seismic Coefficients

For free standing walls it may be assumed that the wall/soil system has a short fundamental period of vibration and that the inertia loads can be approximated by using the zero period ordinate on the design response spectrum (or peak ground acceleration). (Any resonance effects in the backfill are neglected, although this is not necessarily a conservative assumption). Where walls form integral parts of other structures, such as bridges and buildings, the appropriate design coefficient for estimating the wall displacements should be obtained from the periods of vibration of the structure and the design response spectrum.

Seismic coefficients based on the response spectra given in DZ 4203: 1989 are recommended for wall design. The horizontal earthquake coefficient, C(t), at period, t, is given in DZ 4203 as:

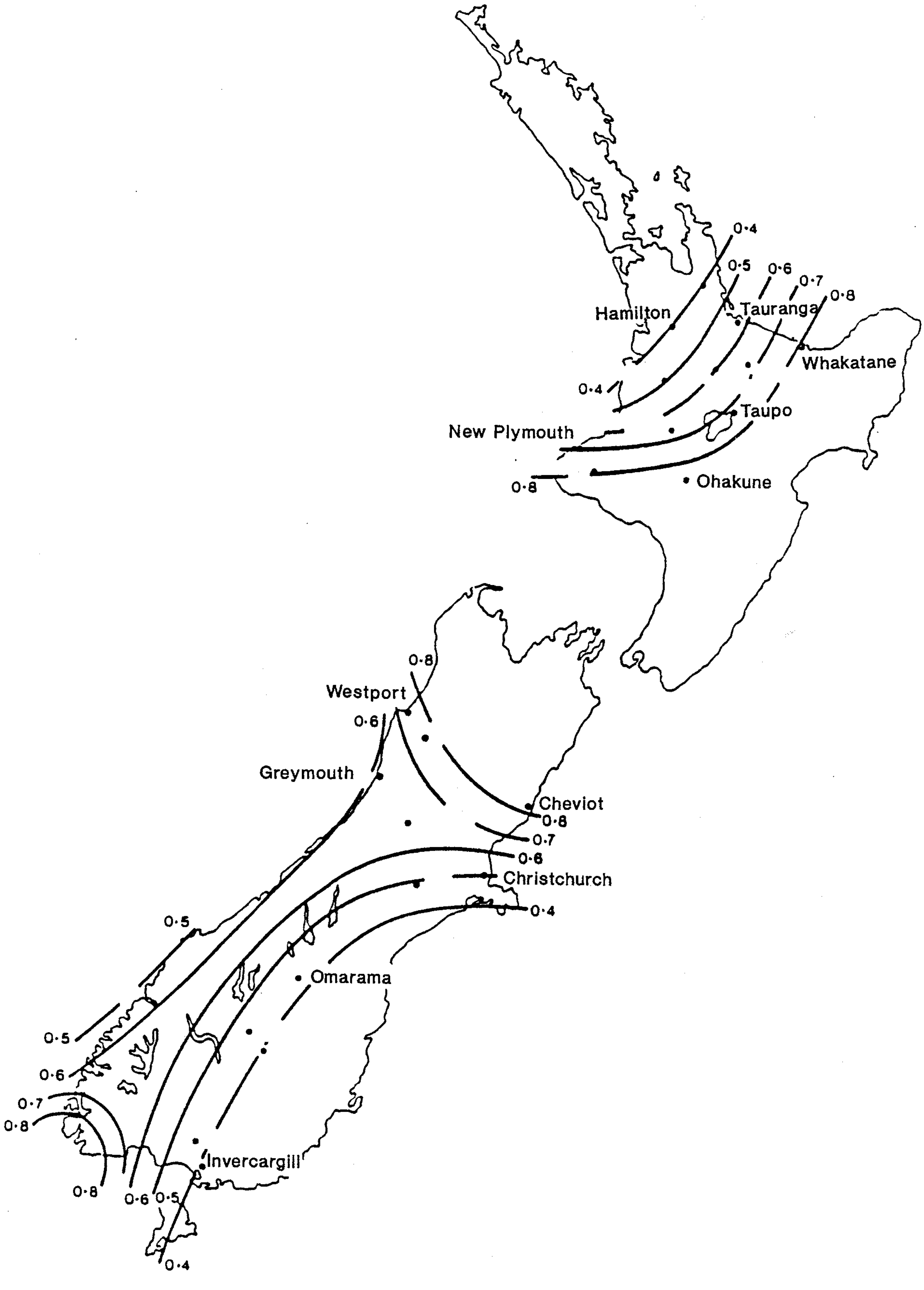

FIG. 3.1 SEISMIC ZONE FACTOR (DZ 4203, 1989)

$C(t) = C_o R Z$

Where C_o is the response function for a 150 year return period earthquake and has a value of 0.4 for zero period (see Figure 1.8). Thus $C(0) = 0.4 R Z$.

Z is a zone factor given in Figure 3.1

R is a risk factor that may vary from 1.3 to 0.8 as defined below.

R = 1.0 for:

> Major retaining walls supporting important structures, developed property or services and where failure would have serious consequences such as cutting vital communication services and loss of life. Walls forming part of the earthquake resisting structure of bridges, major buildings or other important structures.

R = 0.8 for:

> Walls other than as described for R = 1.0 with heights greater than 4 m for level backfills, or 3 m with significant backfill slope.

A risk factor greater than 1.0 may be used for walls that form part of the earthquake resisting structure of buildings classified in DZ 4203 Categories I to III.

The risk factor for highway bridge abutments should be the same as used for the design of the bridge. For important bridges, risk factors greater than 1.0 may be appropriate.

Walls not included in the above descriptions need not be specifically designed for earthquake loading.

The DZ 4203 seismic design coefficients are based on a 150 return period event. A reduction of the risk factor to 0.8 effectively reduces the design return period to about 100 years.

3.3 Load Combinations

Under normal circumstances, when live loads, such as traffic, are of a transient nature, only the combination of earthquake pressures with static gravity pressures need be considered. The static gravity pressure should include water pressures and surcharge loading.

3.4 Factors of Safety

Where the design approach is to prevent outward movements that may develop because of failure in the soil or yielding of the structure, the following factors of safety for the load combination of gravity plus earthquake pressures should be used:

Factor of safety against sliding:

$FS_s = 1.2$

Factor of safety against overturning: (or gross rotational failure)

$FS_o = 1.5$

Where outward movements are to be permitted, an outward sliding mechanism is usually preferred to a rotational failure. It would then be appropriate to prevent a rotational failure by using a factor of safety of at least 1.2 against overturning or gross rotational failure.

The combined gravity and earthquake induced forces to be considered in a wall stability analysis are shown in Figure 3.2. Resisting forces from base friction should be calculated using the usual assumptions made for the soil strength parameters under gravity forces acting alone. Inertia forces acting on the wall and any soil masses in contact with the wall, but not included in the sliding wedge mass, should be considered in the analysis. The resistance of the passive wedge should be based on the MO solution for passive failure. (See Section 3.5.4)

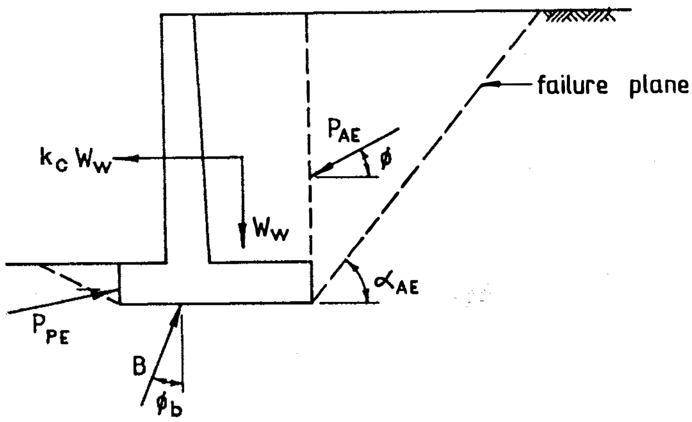

FIG. 3.2 WALL STABILITY ANALYSIS

The bearing pressures under the toe of the wall should be less than the appropriate allowable pressures for earthquake loading on the particular soil. Soil bearing strength is likely to be more critical than wall overturning.

3.5 Dynamic Forces and Pressure Distributions

Simplified pressure distributions resulting from both soil inertia loads and dynamic wall displacements are given in this section for a number of wall categories defined in terms of wall stiffness and relative displacement. The selection of the appropriate pressures for particular types of wall construction and foundation conditions is discussed in Section 3.6.

3.5.1 Rigid Wall

The pressure distributions on a smooth perfectly rigid wall from horizontal inertia loads in the soil were shown in Figure 2.2. An approximate linear pressure distribution suitable for design purposes is given in Figure 3.3 (Matthewson et al, 1980). The increment of earthquake force is given approximately by:

$$\Delta P_E = C(0)\gamma H^2 \qquad (3\text{-}1)$$

The point of application of the earthquake force increment is at approximately 0.6 H above the base.

The earthquake induced pressures and forces are dependent on the soil Poisson's ratio but are not very sensitive over the normal range of values for typical soils (see Figure 2.3). The pressures are also insensitive to the wall roughness. For design purposes, the earthquake pressure distribution and force on a rigid wall can be assumed to be independent of the backface condition and soil elastic constants. The pressure distribution given in Figure 3.3 may therefore be used for soils with both cohesion and frictional properties.

For the case of a rigid wall with sloping backfill, the earthquake forces may be obtained from the finite element solutions for an elastic soil shown in Figure 3.6. For comparison, the MO solution for a soil with a friction angle, $\phi = 35°$ is also plotted. The increase in force produced by the sloping backfill is of comparable magnitude for both the rigid wall and MO assumptions. The ratio of the force increase between horizontal and sloping backfills can therefore be used for all walls, including walls intermediate between rigid and those sufficiently flexible to meet the MO assumptions.

In the rigid wall analysis, the height of the centre of pressure was found to increase by about 10% for the backfill slope increasing from horizontal to 20°. For design purposes, the shape of the pressure distribution for sloping backfills may be assumed to be the same as for the horizontal case.

For backfill slopes greater than 25° more detailed analyses should be undertaken. Slope stability may also be critical on steep backfills.

3.5.2 Stiff Wall

A stiff wall is defined here as a wall that moves outward at the top between 0 to 0.2% of the height, H, under combined gravity and earthquake pressures. An approximation for the increment of earthquake pressure on a wall that displaces 0.2% at the top is shown in Figure 3.4. The increment of earthquake force for 0.2% top displacement may be taken as:

$$\Delta P_E = 0.75\ C(0)\gamma H^2 \qquad (3\text{-}2)$$

The point of application of the earthquake force may be taken as 0.5 H from the base.

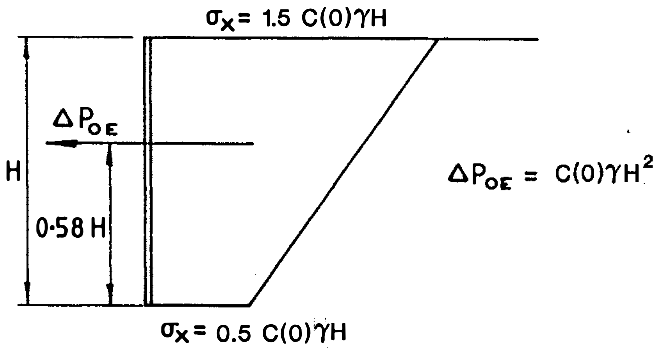

FIG. 3.3 EQ PRESSURE INCREMENT ON RIGID WALL

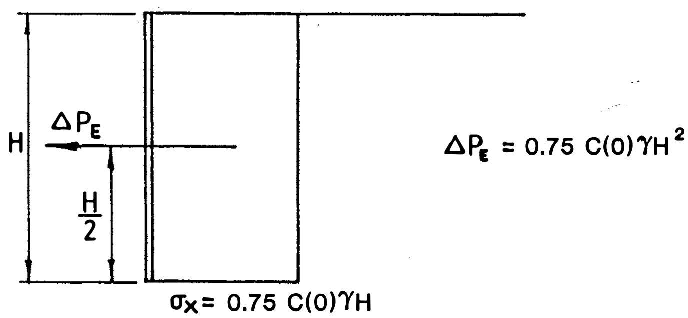

FIG. 3.4 EQ PRESSURE INCREMENT ON STIFF WALL

Pressures and forces on walls that displace less than 0.2% at the top may be obtained by linear interpolation between the stiff and rigid wall pressures and forces.

The earthquake pressures on a stiff wall are more sensitive to the soil properties than for the rigid wall case. If soil stiffness properties are known, then a more detailed analysis can be carried out by evaluating the force ratio parameter P_r and using Figures 2.12, 2.13, 2.15 and 2.17 to obtain pressure distributions and earthquake forces.

The effect of sloping backfill can be obtained by increasing the earthquake component of wall force by the ratio between the horizontal and sloping backfill forces for the rigid wall solution given in Figure 3.6.

3.5.3 Flexible Wall

Where the outward movement of the top of the wall under gravity and earthquake pressures exceeds 0.5% of H, an active pressure state may be assumed and the pressures obtained from the Coulomb sliding wedge theory or the MO equations.

The MO equations cover both passive and active stress states and include effects from both vertical and horizontal earthquake accelerations. Vertical accelerations produce relatively small increases in the horizontal pressures and may be neglected for design purposes.

The MO earthquake pressure increment is shown in Figure 3.5 together with a simplified MO equation for K_{AE}, the active earthquake pressure coefficient. The simplified equation is for the case of a horizontal backfill, smooth wall and no vertical acceleration. The pressure coefficient includes the effect from both gravity and horizontal earthquake loads.

The coefficient of earthquake earth pressure increment, $\Delta K_{AE} = K_{AE} - K_A$, evaluated by the MO equations for a vertical wall with rough contact can be obtained from Figures 3.7 to 3.12. The coefficients are given for two cases of wall friction; $\delta = \phi$ and $\delta = 2\phi/3$. When the shape of the wall forces the wall slip plane to be on a soil interface or virtual plane in the soil behind the wall, it is usual to assume that $\delta = \phi$. When a slip surface can develop on the back face of the wall it may be assumed that the wall friction angle is $\delta = 2\phi/3$. Figures 3.7 and 3.8 give the coefficients for horizontal backfills and Figures 3.9 to 3.12 for backfills with slope angle, ω, from the horizontal.

The earthquake pressure increment curves become infinitely steep when the seismic coefficient values reach the limit that causes general failure in the backfill or slope behind the wall. For a cohesionless soil this occurs when:

$$C(0) \geq \tan(\phi - \omega) \tag{3-3}$$

Conditions that lead to general soil failure are likely to cause excessive damage to structures and should be avoided.

The earthquake increment pressure distributions can be obtained from the plotted coefficients by the following expressions:

$$\Delta p(z) = [\Delta K_{AE}/C(0)] \cdot C(0)\gamma z \tag{3-4}$$

Where:

$\Delta p(z)$ = The earthquake pressure increment at depth z below the top of the wall.

ΔK_{AE} = $K_{AE} - K_A$

K_{AE} = MO active pressure coefficient. (Total gravity plus earthquake component).

K_A = Active pressure coefficient.

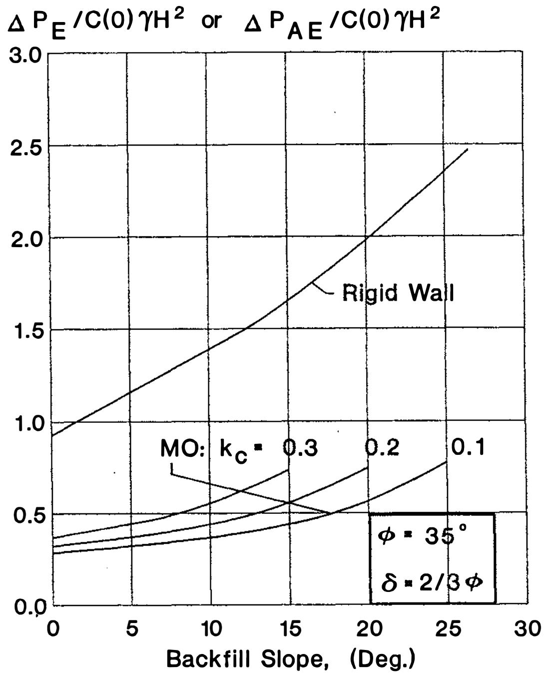

FIG. 3.6 WALL FORCE: SLOPING BACKFILL
Dim. EQ Force Component

The earthquake increment of wall force is given by:

$$\Delta P_{AE} = 0.5\ \Delta K_{AE}\ \gamma H^2 \tag{3-5}$$

A useful approximate expression for estimating the earthquake force increment for a cohesionless backfill soil with a horizontal backfill surface and friction angle between 30° to 35° is:

$$\Delta P_{AE} = 0.5\ C(0)\gamma H^2 \tag{3-6}$$

Expression 3-6 is a good approximation when C(0) is between 0.2 to 0.3.

Where the soil is cohesive or the ground surface is irregular, the trial wedge method, shown in Figure 3.13, can be used to estimate the earthquake force increment. There is no available information on the correct shape of the pressure distribution for these more complex cases. However, for a flexible wall it is reasonable to assume that the earthquake increment acts at H/3 above the base. That is, the assumption

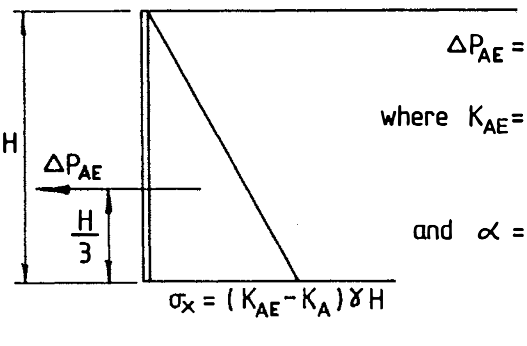

$$\Delta P_{AE} = \frac{1}{2}(K_{AE} - K_A)\gamma H^2$$

$$\text{where } K_{AE} = \frac{\cos^2(\phi - \alpha)}{\cos^2\alpha \left[1 + \sqrt{\frac{\sin\phi \cdot \sin(\phi - \alpha)}{\cos\alpha}}\right]^2}$$

$$\text{and } \alpha = \tan^{-1} C(0)$$

FIG. 3.5 EQ PRESSURE INCREMENT ON FLEXIBLE WALL

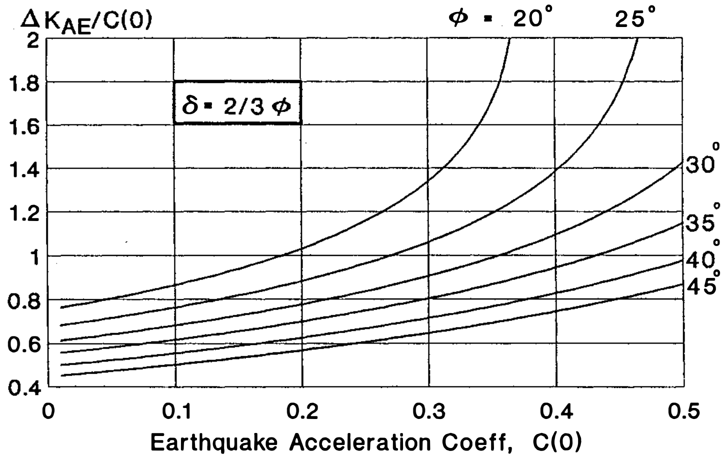

FIG. 3.7 MO PRESSURE COEFFICIENT FOR ACTIVE EQ INCREMENT. HORIZONTAL BACKFILL

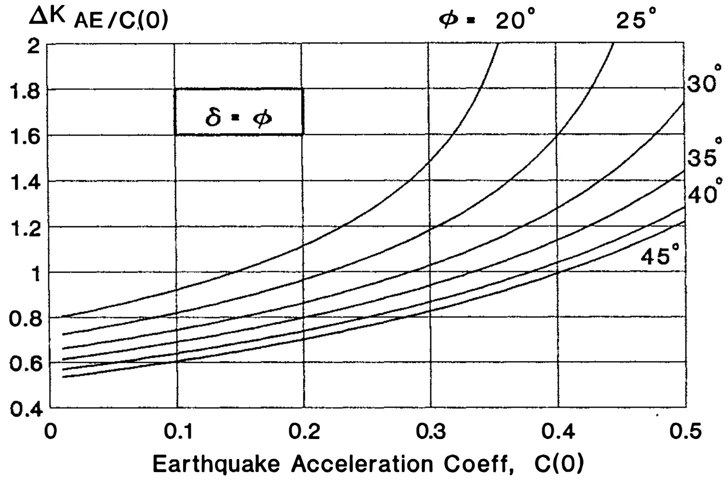

FIG. 3.8 MO PRESSURE COEFFICIENT FOR ACTIVE EQ INCREMENT. HORIZONTAL BACKFILL

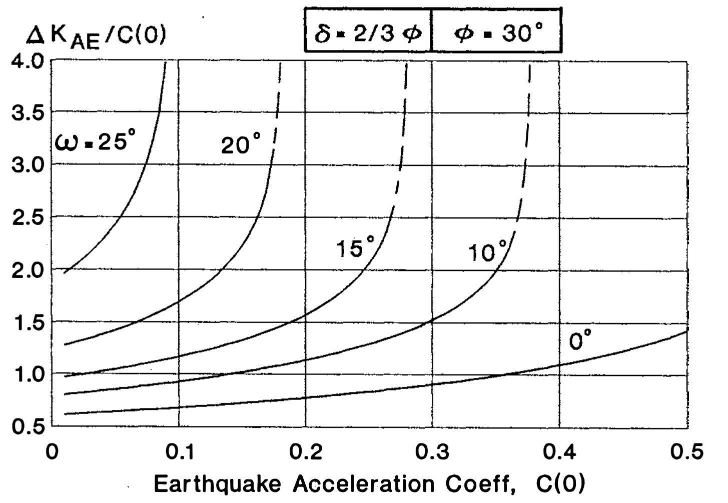

FIG. 3.9 MO PRESSURE COEFFICIENT FOR ACTIVE EQ INCREMENT. SLOPING BACKFILL

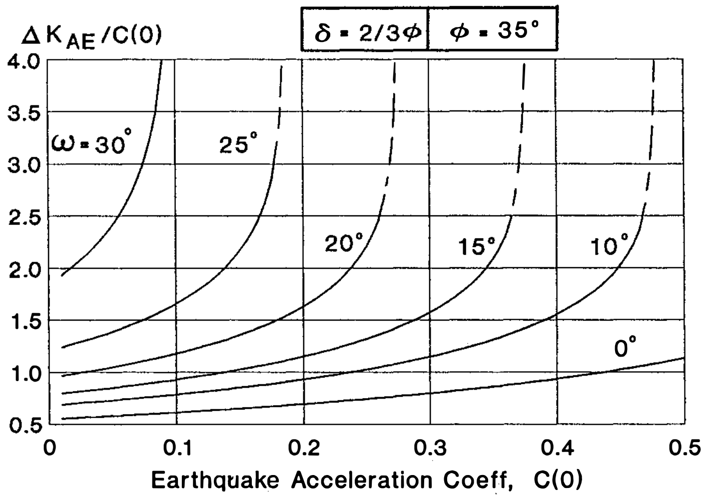

FIG. 3.10 MO PRESSURE COEFFICIENT FOR ACTIVE EQ INCREMENT. SLOPING BACKFILL

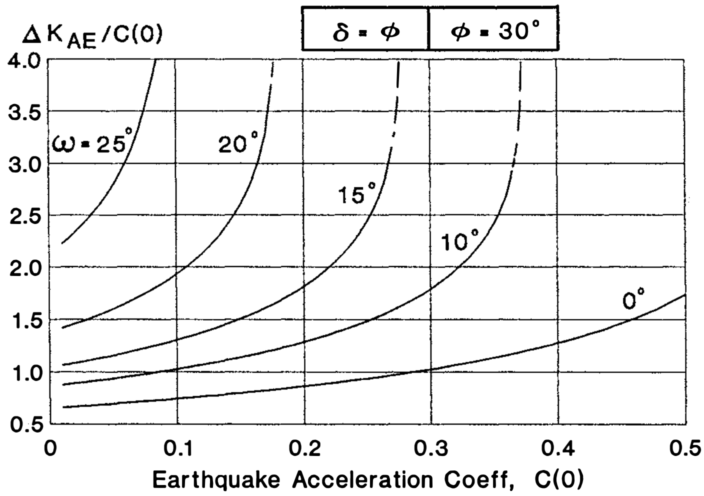

FIG. 3.11 MO PRESSURE COEFFICIENT FOR ACTIVE EQ INCREMENT. SLOPING BACKFILL

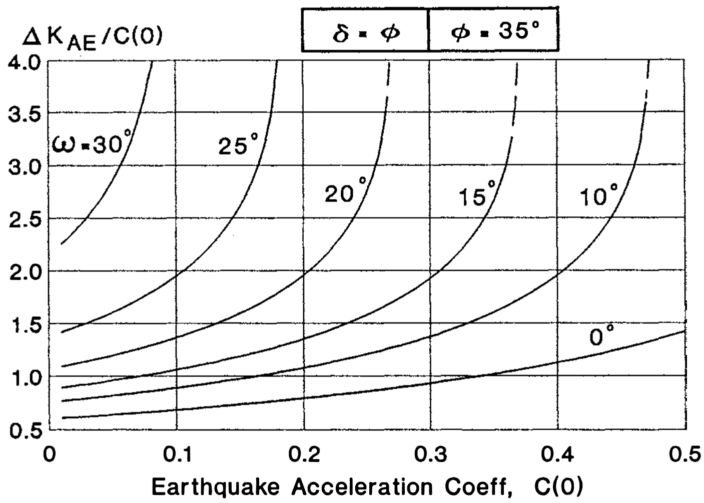

FIG. 3.12 MO PRESSURE COEFFICIENT FOR ACTIVE EQ INCREMENT. SLOPING BACKFILL

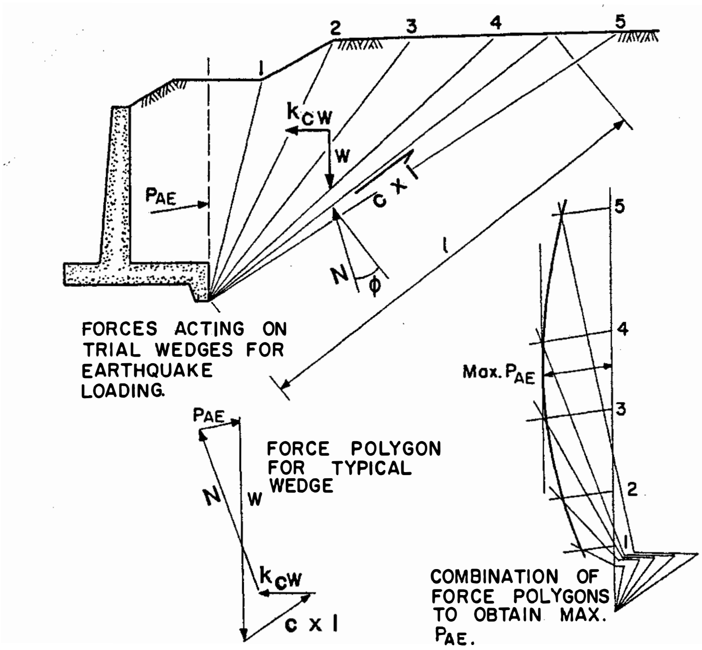

FIG. 3.13 TRIAL WEDGE METHOD FOR EQ LOADS

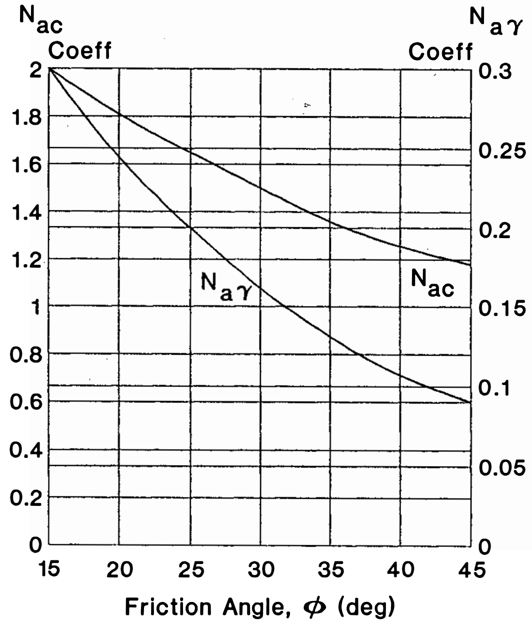

FIG. 3.14 PRESSURE COEFFICIENTS
(Prakash and Saran, 1966)

used for cohesionless soil appears appropriate for all soil types and backfill slopes.

The presence of tension cracks in cohesive soil may be ignored since it is likely that lateral compression at the ground surface from the dynamic inertia forces in the soil will offset the tensile stresses that develop because of outward yielding.

The MO method has been extended to cohesive frictional soils by Prakash and Saran (1966) (Saran and Prakash, 1968). Simplifying their general solution by assuming no surcharge and no tension crack gives:

$$K_{AE} = 2\lambda N_{a\gamma} - \frac{2c}{\gamma H} N_{ac} \qquad (3\text{-}7)$$

Where:

$N_{a\gamma}$, N_{ac} = Dimensionless parameters plotted in Figure 3.14.

λ = Dynamic factor, plotted in Figure 3.15. (λ = 1.0 for static case).

c = Soil cohesion, assumed to have the same value on the failure plane and the back face of the wall.

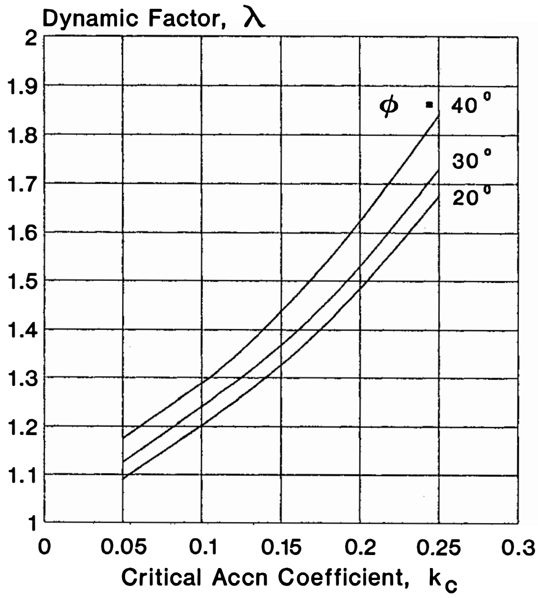

FIG. 3.15 DYNAMIC FACTOR, λ
(Prakash and Saran, 1966)

The extended method may be used for the analysis of saturated clays by carrying out a total stress analysis assuming, ϕ = 0 and c = c_u, the undrained shear strength.

For walls with stiffnesses intermediate between the stiff and flexible cases, linear interpolation may be used between the pressures and forces for the two limiting cases of rigid and flexible walls.

3.5.4 Displaceable Wall

When it is acceptable for a wall to undergo permanent outward displacement during strong earthquake ground shaking, it may be designed for a critical acceleration $k_c g$ less than the peak ground acceleration, C(0)g, of the design earthquake. The critical acceleration is defined as the acceleration level that initiates wall permanent movement. The outward displacement can be calculated using the Newmark sliding block theory. The forward movement of the centre of mass is given approximately by (Matthewson et al, 1980):

$$d = \frac{3V^2}{C(0)g}\left[\frac{C(0)}{k_c} + \frac{k_c}{C(0)} - 2\right] \qquad (3\text{-}8)$$

Where:

V = Peak ground velocity.
$\approx$ 1.3 C(0) m/s

The ratio of d/C(0) from expression (3-8) is plotted in Figure 3.16 against the ratio of the critical acceleration to the peak acceleration, $k_c/C(0)$. (The plotted relationship is only valid for V $\approx$ 1.3 C(0) m/s)

The critical acceleration should be calculated using the maintainable shearing resistance of the soil at large strains.

The acceptable limit of outward displacement should be taken as the minimum of: one-half the available clearance to other structures, 4% of the height of the wall or 300 mm.

The earthquake pressure increment on displaceable walls may be taken as the MO values given in Section 3.5.3 for flexible walls.

The inertia force acting on the wall should be included in the evaluation of the critical acceleration to cause failure.

This can be done using results given by Elms and Richards (1979) or by considering the limiting equilibrium of the horizontal components of the forces shown in Figure 3.2. For gravity walls, the inertia load from the wall will usually result in a significant reduction in the critical acceleration (see Figure 2.20).

Where stability is considered using a virtual back face, (for example at the heel of a cantilever wall), the weight of the soil between the virtual back face and the wall should be included with the wall weight to estimate the horizontal inertia force.

Significant resistance may be provided by passive pressures at the toe and this force should be considered in the limiting equilibrium analysis to determine the critical acceleration. The MO earthquake increment of passive pressure and the total passive pressure coefficient for gravity and earthquake forces can be obtained from Figures 3.17 and 3.18 respectively. The coefficients were evaluated assuming a cohesionless soil, vertical wall face, zero wall friction and a horizontal soil layer. (The passive pressure coefficient is very sensitive to the wall friction and a conservative estimate is obtained by assuming zero friction).

When the soil inertia force in the passive wedge is assumed to be acting in a direction away from the wall, the pressures are lower than the static passive pressure values. (Negative values are plotted in Figure 3.17 to indicate this reduction).

If it is required to prevent yielding in the wall structure, capacity design principles should be used. In estimating the overstrength of a soil failure mode, the estimated values of soil cohesion, c, and friction coefficient, tanϕ, should be increased by a factor of 1.3.

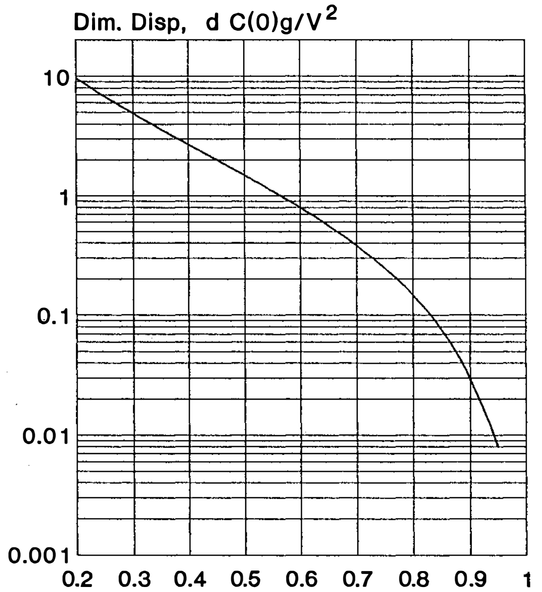

FIG. 3.16 DISPLACEMENTS SLIDING WALL

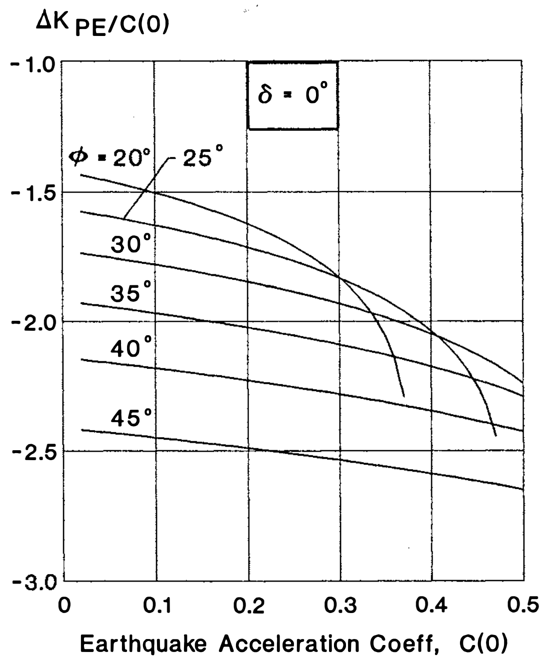

FIG. 3.17 MO PRESSURE COEFFICIENT FOR PASSIVE EQ INCREMENT. HORIZONTAL LAYER

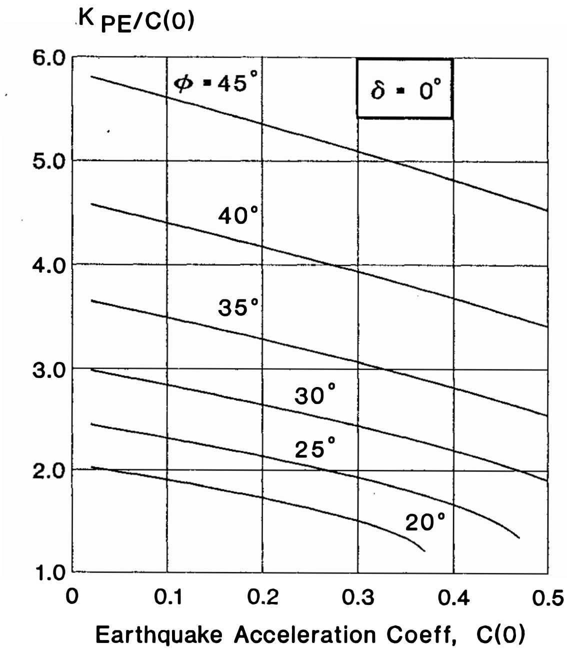

FIG. 3.18 MO COEFFICIENT FOR TOTAL PASSIVE PRESSURE. HORIZONTAL LAYER

3.5.5 Forced Wall

Where the wall is part of a larger structure such as a building or bridge, it may forced to vibrate with amplitudes governed by the inertia loads on the structure. The total earthquake pressure increment can be estimated by combining the component of earth pressure due to inertia forces in the soil (usually based on a rigid wall assumption) with pressures resulting from the wall displacement amplitudes against the soil.

Figure 3.19 shows simplified pressure components produced by rotational (about wall base) and translational forcing of a rigid wall against the backfill. Any flexibility of the wall will influence the pressures but a satisfactory approximation can be obtained for most walls by combining these components for a rigid wall.

An upper limit to the combined static and forced wall pressure at any depth is given by the soil passive pressure distribution.

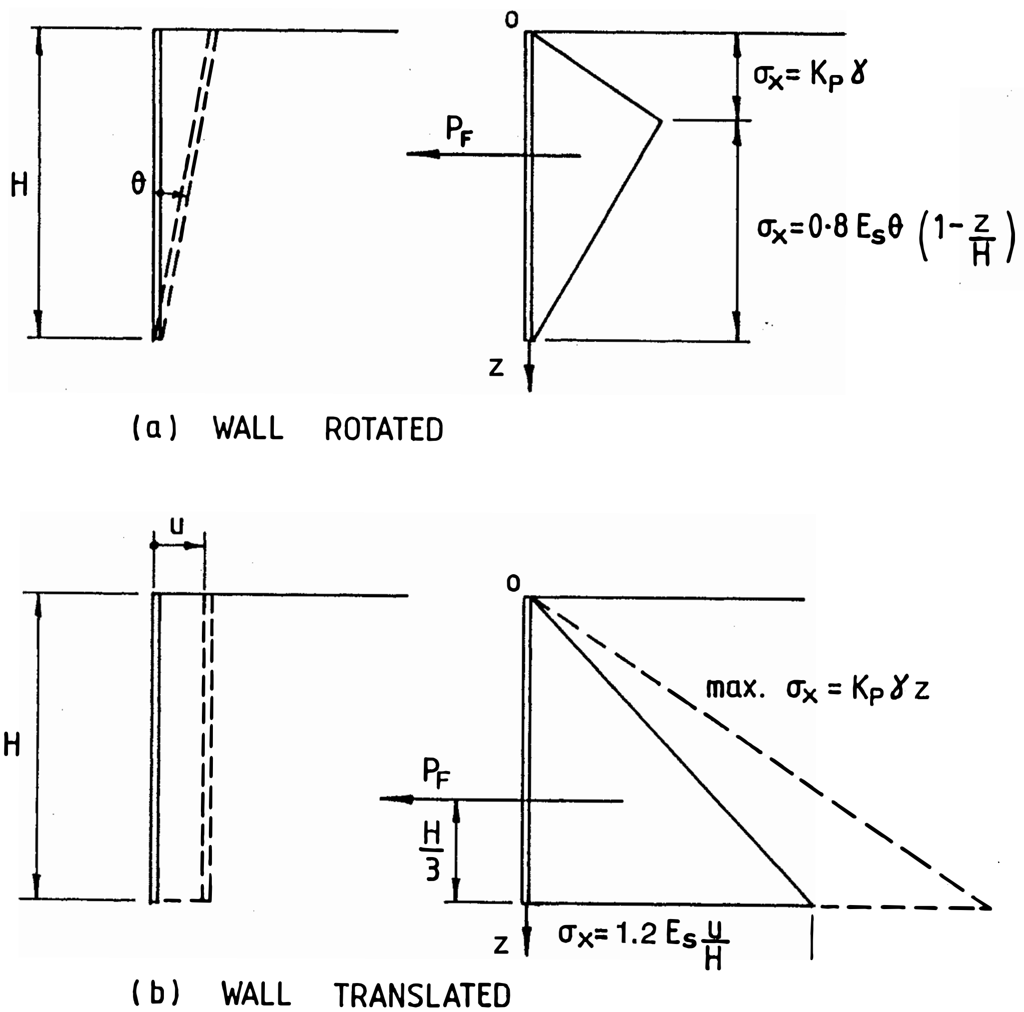

FIG. 3.19 PRESSURES ON FORCED WALL

3.6 Water Pressures

The increase in pore water pressures from earthquake inertia effects should be considered when the backfill soils are below the water table. For some backfill and foundation soils it may also be necessary to consider the effects of soil liquefaction.

A convenient approximate method of including the pore water pressure increase is to consider the effective soil stresses on the wall separately from the water pressures. The coefficient of earthquake pressure increment, ΔK_{AE} can be obtained from the MO solution by assuming the failure plane inclination is unaffected by the presence of the water table.

The effective stress earth pressure increment can then be obtained by using the pressure equations with the soil bulk unit weight above the water table and the submerged unit weight below the water table. The earthquake increment of the pore water pressure can be taken as the static water pressure multiplied by the seismic coefficient. The total seismic increment is then the sum of the effective soil stress increment and the pore water pressure increment as shown in Figure 3.20.

The hydrodynamic pressure from any water in front of the wall (eg, quay walls) may often act in the same direction as the earth pressure increment and should be considered in both stability and wall strength analyses. The critical case for overall stability of the wall will occur when the hydrodynamic water pressure reduces the static water pressure in front of the wall and is in phase with the earthquake earth pressure increment on the wall. It may also be necessary to consider the case when the inertia loads in the water and soil are directed towards the backfill. Although it is unlikely that this direction will be critical, in some circumstances it may be necessary to include this case for the design of the wall structure.

Hydrodynamic pressures can be estimated using the Westergaard (1933) theory. From the solution given by Werner and Sundquist (1949) for a relatively shallow long reservoir, the dynamic water pressure force is given by:

$$P_w = 0.58\ C(0)\gamma_w\ h_w^2 \qquad (3\text{-}9)$$

Where:

γ_w = Unit weight of water.

h_w = Depth of water.

The dynamic water pressure force acts at a height of about $0.4h_w$ above the base.

Further information on the effects of the length of the reservoir and fluid resonance can be obtained from Werner and Sundquist (1949) and Chopra (1967).

3.7 Application to Various Types of Walls

3.7.1 Free Standing Walls Founded on Soil

Most types of free standing walls founded on soil are sufficiently flexible for the MO earthquake pressures to apply. The maximum permissible displacement should usually be adopted as the prime criterion for earthquake design. The failure mode should avoid yielding in the structural elements wherever practicable.

3.7.2 Free Standing Walls Founded on Rock or Piles

If yielding in the structural members of this type of wall is to be avoided, earth pressures and wall inertia forces should be based on the peak ground accelerations and account should be taken of the wall stiffness in estimating the earthquake pressure distribution.

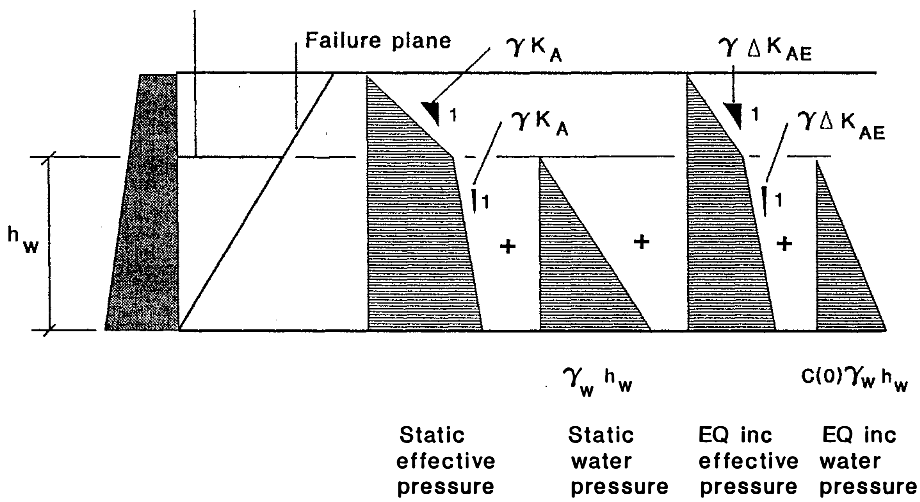

FIG 3.20 EQ PRESSURES FOR PARTIALLY SUBMERGED BACKFILL

Yielding of the structural elements may be permitted when the loss of serviceability, or the cost of removing the backfill and repairing the wall can be justified on economic grounds. Where significant outward displacement occurs because of yielding, the displaceable wall theory may be used.

3.7.3 Reinforced Earth Walls

(i) General Assumptions

The recommended earthquake design method for reinforced walls is based on the limiting equilibrium method. In this approach, the equations of equilibrium for horizontal forces are solved to give the critical acceleration that produces significant outward movement of the wall. The outward movement of the wall can be estimated using the ratio of the critical acceleration to the peak ground acceleration and the sliding block theory in a manner similar to that described for the displaceable wall (Section 3.5.4). Design is based on proportioning the wall to limit the outward movement to an acceptable level.

A minimum L_s/H ratio of 0.7 is recommended for walls designed to resist seismic loading. Walls above 8 m in height, with this minimum ratio, and designed by the usually accepted methods for static gravity loads will often have acceptable earthquake resistance without additional strength provisions. Lower walls will usually require larger L_s/H ratios (of the order of 1.0) because the pullout resistance of the strips reduces with height.

The lower strips in walls with heights exceeding 15 m will have very high pull out resistances and the limiting equilibrium method has not been adequately verified by model tests covering this case. Walls above 15 m in height should be subjected to special studies.

Walls designed for earthquake loading should have a cohesionless backfill with a minimum friction angle, $\phi = 35°$.

(ii) Static design

The static design should be based on the normally accepted procedures for resisting gravity and surcharge loads. A summary of the requirements is as follows:

External Stability

Factor of safety against overturning ≥ 2.0

Factor of safety against sliding ≥ 1.5

Horizontal Pressure Against Panels

$$p(z) = \gamma z K \qquad (3\text{-}10)$$

Where:

z = Depth of overburden.

K is as shown in Figure 3.21

$$K_0 = 1 - \sin\phi \qquad (3\text{-}11)$$

$$K_A = \tan^2(45 - \phi/2) \qquad (3\text{-}12)$$

Strip Design

The tension in the strip is given by:

$$T_m = \frac{p(z)\ A_p}{n} \qquad (3\text{-}13)$$

Where:

n = Number of strips per panel.

A_p = Area of panel.

The maximum tensile stress in the strip is given by:

$$f_t = T_m/A_s \qquad (3\text{-}14)$$

Where:

A_s = Net section area of strip.

f_t should be $\le 0.6\ f_y$, where f_y is the strip yield stress.

The available pullout resistance of the strip is given by:

$$R = 2bf^* L_e \gamma z \qquad (3\text{-}15)$$

Where:

b = Strip width

f^* = Apparent soil-strip friction coefficient as defined in Figure 3.22.

L_e = Effective resistive length of strip as defined in Figure 3.23.

γ = Soil unit weight.

The factor of safety against strip pull-out, FS_p should satisfy:

$$FS_p = R/T_m \ge 1.5 \qquad (3\text{-}16)$$

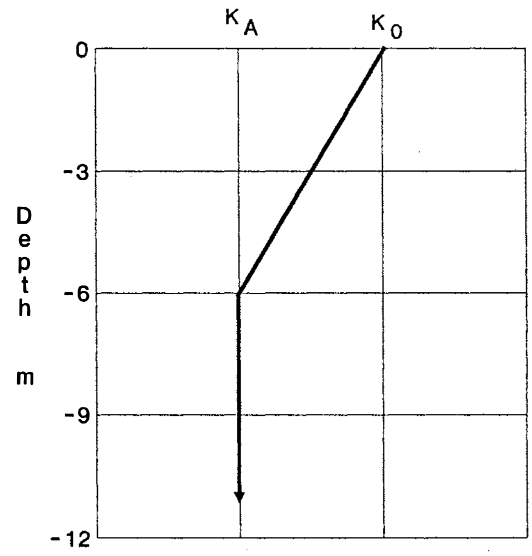

FIG. 3.21 RE WALL: PRESSURE COEFFICIENT

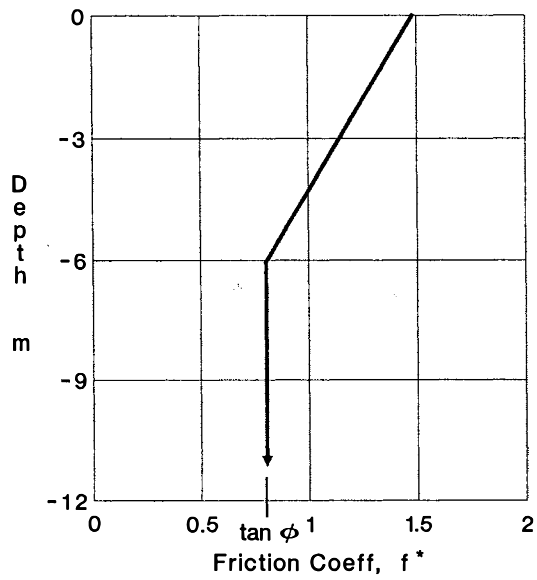

FIG. 3.22 RE WALL: STRIP FRICTION

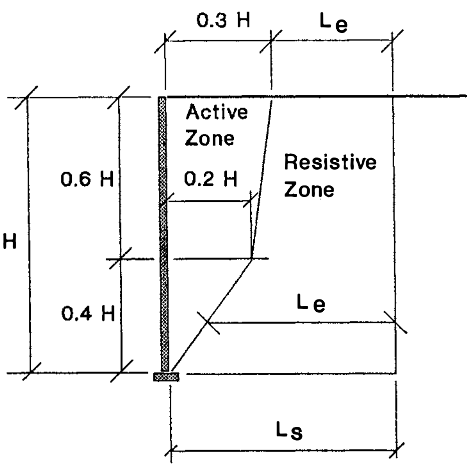

FIG. 3.23 RE WALL: STRIP EFFECTIVE LENGTHS

(iii) Overturning

For walls with L_s/H ratios greater than 0.7 and for earthquake accelerations less than 0.5 g, overturning is not critical.

(iv) Sliding Stability

The sliding stability should be checked using the limiting equilibrium method (Section 2.7.1).

For the simple reinforced block geometry shown in Figure 3.24 the graphical solutions in Figures 3.25 and 3.26 may be used to determine the critical acceleration, k_c, and the failure plane inclination, α. The plots show k_c and a as a function of L_s/h for the dimensionless friction parameter $F^* = 0.075$ and 0.17. This parameter is defined by:

$$F^* = 2bn_hf^* \qquad (3\text{-}17)$$

Where:

n_h = The number of strips per unit width

F^* = 0.075 is approximately the value calculated for standard panels with four 40 mm wide strips. $F^* = 0.17$ is approximately the value for a wall with six 60 mm wide strips per panel.

The graphical solution is based on $\phi = 35°$. It is assumed that the backfill is horizontal, strips remain horizontal across the failure plane and that the strip lengths and f^* are constant over the height. The vertical spacing of the strips has been taken as 750 mm, the standard used by the Reinforced Earth Company.

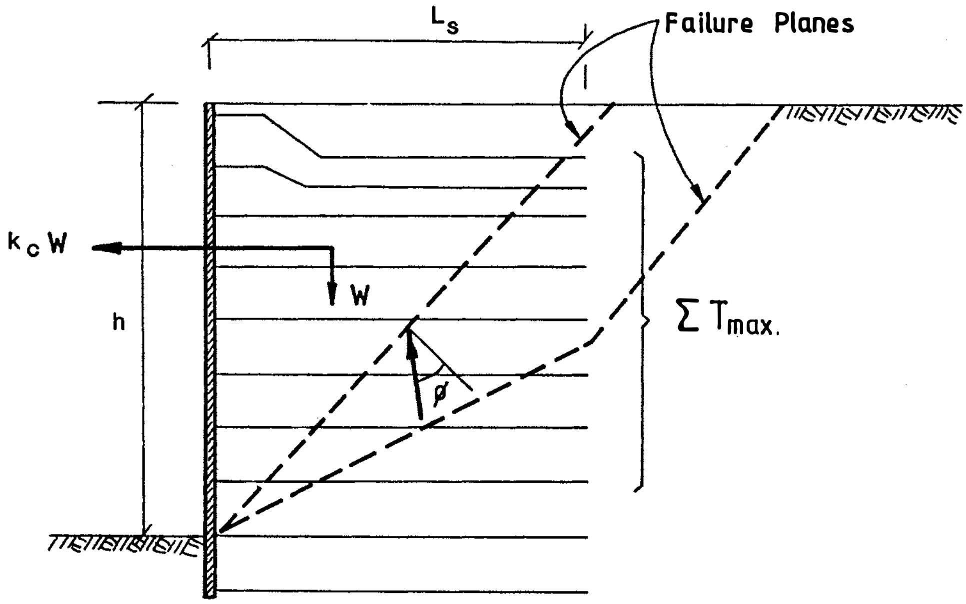

FIG. 3.24 LIMITING EQULIBRIUM ANALYSIS

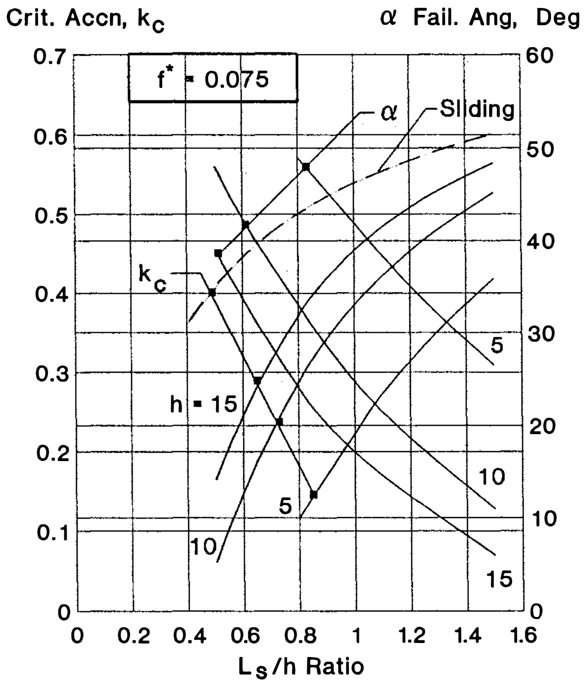

FIG. 3.25 RE WALL: FAILURE ANALYSIS

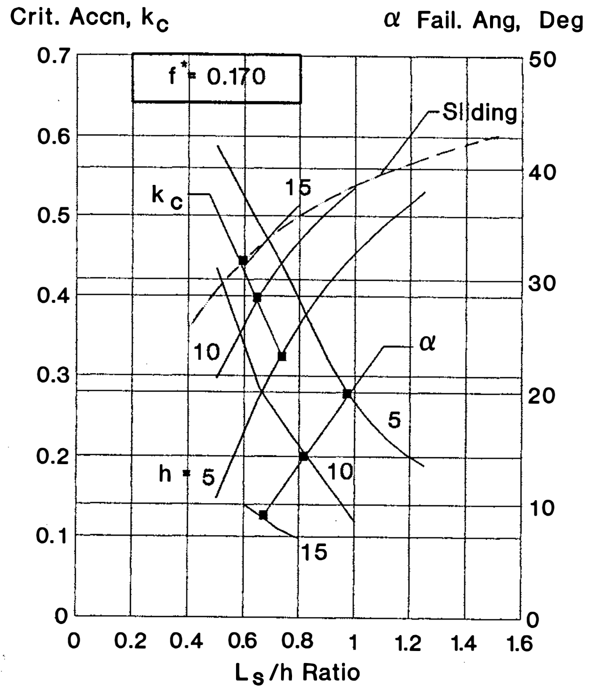

FIG. 3.26 RE WALL: FAILURE ANALYSIS

Curves for the critical acceleration required to produce sliding on an assumed horizontal failure plane through the base reinforced earth block are also shown in Figures 3.25 and 3.26. The forces acting on the block for this assumption are shown in Figure 3.27. The vertical component of the MO force on the back of the wall has been omitted because of the uncertainty of the magnitude of this force. (If the failure wedge behind the wall moves downwards then this vertical component will also be downwards and have a limiting value of $P_{AE}\cos\delta$). The neglect of this force, which is usually assumed to be in a downwards direction, reduces the normal reaction and the critical acceleration value. For high walls and high L_s/h ratios, the critical acceleration for base sliding gives a good approximation to the critical acceleration for the inclined failure plane. However, the base sliding analysis produces an upper bound solution that is significantly in error for low walls and low L_s/h ratios.

(v) Outward Movement

The outward movement of the centre of mass of the sliding wedge can be estimated using Figure 3.16 (Section 3.5.4).

The outward movement should be limited to the lessor of 4% of the clear height of the front face of the wall or 300 mm.

(vi) Base Pressures

Maximum pressures on the base of the reinforced block can be calculated by assuming a rectangular pressure distribution and the earthquake forces shown on the block in Figure 3.27. The maximum value of the dimensionless vertical pressure p_v' is plotted in Figure 3.28 for various values of the peak ground acceleration coefficient C(0). The vertical pressure is related to dimensionless pressure by:

$$p_v = C(0)p_v'\gamma L_s \qquad (3\text{-}18)$$

The vertical earthquake pressures should be less than the allowable bearing pressures specified for the particular soil. Pressures can be reduced by increasing the L_s/H ratio.

(vii) Strip Design

The critical failure plane usually initiates on the wall facing at the intersection with lowest strip above the soil level in front of the wall. But, it is necessary to drape the top strip to a depth of at least 1.0 m to ensure that a local failure does not occur at the top of the wall.

The failure plane angle can be used to obtain the number of strips intersected and the length of the strips in the resistive zone behind the failure plane. The maximum forces in the strips are given by:

$$R = 2bf^*L_f\gamma z \qquad (3\text{-}19)$$

Where:

L_f = length of strip behind the failure plane

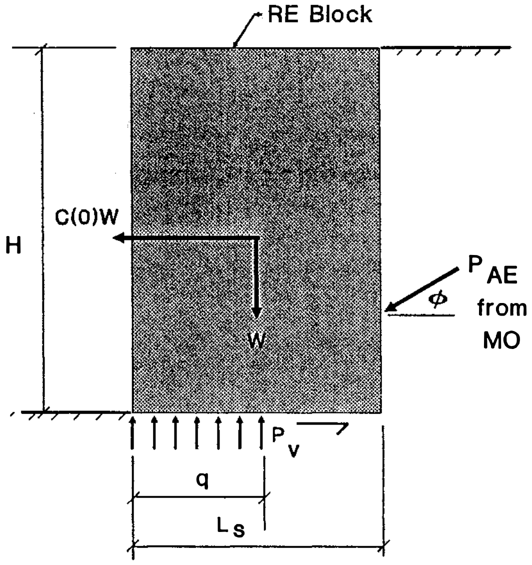

FIG. 3.27 EQ FORCES ON RE BLOCK

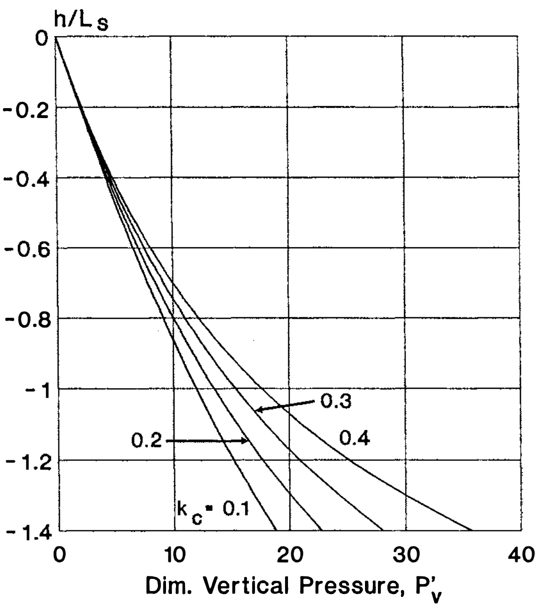

FIG. 3.28 VERTICAL PRESSURES IN RE WALL

The forces in the strips above the intersection of the failure and the back face of the reinforced block can be calculated using the Meyerhof theory. In this approach, the vertical stresses on a horizontal plane through the wall are calculated by applying the forces shown in Figure 3.27, and assuming a rectangular pressure distribution on the section. This is an analogous procedure to that used to calculate the base pressures. The horizontal pressures on the facing can then be obtained from:

$$p(z) = K_A p_v \qquad (3\text{-}20)$$

Values of p_v can be obtained from Figure 3.28 and expression 3-18.

The tension in the strip can be obtained from expression 3-13:

$$T_m = \frac{p(z)\ A_p}{n}$$

Strips just below the failure plane intersection with the back face will have short lengths in the resistive zone resulting in low values of strip tension. These strips should be designed for the greater of the strip tensions from either the Meyerhof pressure or the limiting equilibrium analysis.

The limiting equilibrium analysis shows that the lower strip forces become very high for most designs when the failure plane angle, α, is less than about 30°. Because model testing has been limited to cases where α exceeds 30°, the wall dimensions and properties should be adjusted to avoid values of α less than 20°, or alternatively more detailed analyses undertaken.

To achieve good earthquake performance, it is essential to have a ductile failure by either strip pull out or material yield in the strips. Model studies have shown that the maximum strip forces in the lower part of the wall occur at or close to the facing. It is therefore critical to have the connection between the strip and facing stronger than the ultimate capacity of the strip, based on the ultimate tensile stress and the full section area of the strip.

Although difficult to achieve for higher walls, the strips should be designed to fail by pull-out rather than by material yield. To check this requirement, an overstrength factor of 2 should be applied to f^*. That is:

$$4bf^*L_f\ \gamma z \le f_y\ A_s \qquad (3.21)$$

or

$$2R \le f_y\ A_s \qquad (3.22)$$

In higher walls it may be necessary to accept a material yield failure rather than pull-out. The tensile strength of the strip relative to the pull-out resistance can be improved by reducing the strip widths and increasing their thickness.

Strip lengths below the failure plane may be adjusted to obtain a more uniform distribution of strip forces, providing the total resistive force from the sum of the strip R values is maintained. If this is done, the limiting equilibrium theory will still be applicable since the total force below the failure plane is used in the equilibrium equations.

(viii) Face Pressures

Face pressures may be assumed to be related to the strip tensions by:

$$p(z) = \frac{n\ T_m}{A_p} \qquad (3\text{-}23)$$

As outlined above, the face pressures above the failure plane intersection with the back face can be obtained from the Meyerhof vertical stresses. Below the failure plane intersection point, the face pressures can be obtained from the pull-out or ultimate failure forces calculated for the strips. Just below the failure plane intersection point, the strip forces may not give a good estimate of the face pressure because of the short strip length in the resistive zone. A conservative estimate of face pressures below the failure plane intersection point can be obtained by adding the Meyerhof pressure at the intersection point to the pressures calculated from the strip forces.

3.7.4 Tied-Back Walls

The pressures on tied-back walls are dependent on the type of anchor and flexibility of the wall. Because of the complexity of the interaction between the tie forces and wall facing deformations, major walls should be investigated by structural analysis procedures to estimate the pressure distributions.

If tie-backs are anchored by some form of deadman and the ties are required to remain elastic during earthquake loading, the peak ground acceleration should be used to calculate the pressures and forces. In estimating the earthquake increment of pressure from soil inertia forces, due allowance should be made for the tie and wall flexibility. Where the wall top movement meets the flexible wall criterion given in Section 3.5.3 the MO pressures may be used.

If tie-backs are restrained by a movable anchor, such as a friction slab designed to slide while the other structural components remain elastic, a reduction in the design acceleration may be made based on the displacement criterion given in Section 3.5.4. For walls of minor importance, permanent displacement resulting from yielding of the ties may be acceptable but particular consideration needs to be given to the effectiveness of the tie corrosion protection system after yield extensions.

For all types of anchor systems the mode of failure, when overloaded, should be by yielding of the ties or passive failure of the anchor rather than by failure of the wall face or connections between the ties and the wall face or anchor. The probable variation in the soil parameters and frictional resistance between the wall components and the soil should be considered in determining the critical acceleration for permanent displacement and failure modes.

When investigating the stability of a tied wall, the forces on the face and ties may be estimated using the active wedge failure criterion. The passive failure modes of the toe and the anchor system should be considered (Anderson et al, 1983). Failure by a wedge through the anchor and toe, as shown in Figure 3.29, or by a slip circle, may also be possible under earthquake loading. In these failure modes, the horizontal earthquake force corresponding to the peak ground acceleration should be applied to the wedge or weight of soil within the circular slip.

A limiting equilibrium active wedge theory for the simple tied-back wall shown in Figure 3.30 was presented in Section 2.8.1. Figure 2.86 shows that the ratio of the tie force over the failure wedge weight, T/W, is relatively constant and approximately equal to 0.53 for a critical acceleration coefficient, k_c between 0.1 and 0.3. This gives the following approximate expressions for tie force (earthquake and gravity loads) and the failure plane inclination angle:

$$T = 0.53\ W \tag{3-24}$$

$$(\phi - \alpha) = \tan^{-1}(0.53 - k_c) \tag{3-25}$$

$$W = 0.5\ \gamma H^2/\tan\alpha \tag{3-26}$$

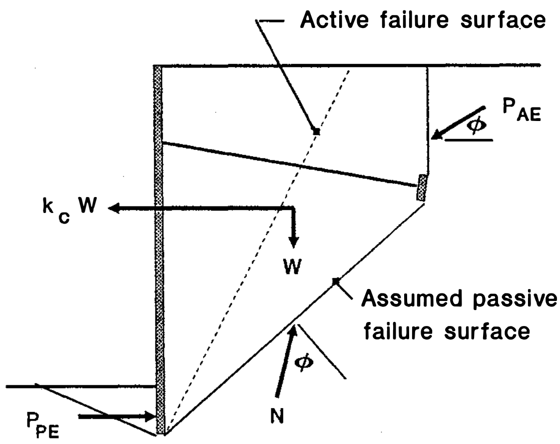

FIG. 3.29 PASSIVE FAILURE OF TIED-BACK WALL

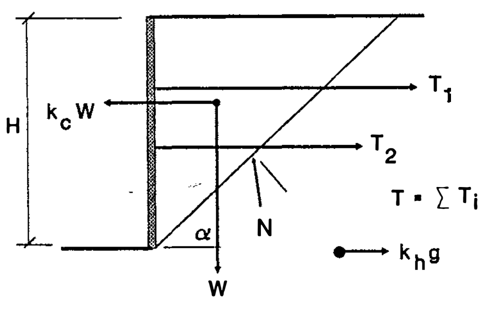

FIG. 3.30 ANALYSIS OF TIED-BACK WALL

3.7.5 Basement Walls

The earthquake pressures that develop on basement walls will generally consist of components from the inertia forces in the soil and pressures resulting from the wall displacement against the soil (Figure 1.6).

The pressures from the soil inertia loads may be conservatively taken as the rigid wall pressures given in Section 3.5.1. The rigid wall pressures may be reduced by the wall flexibility where this is significant.

The component of earthquake pressure from the movement of the wall relative to the soil may be estimated from the forced wall solutions given in Section 3.5.5 (Figure 3.19). Where the structure is founded on rock or very firm soils, the relative movement of the wall against the soil may be small and the resulting pressure component small in relation to the soil inertia increment. When piles are used or the structure is founded on soft soils, the relative movements may lead to pressure components that dominate the total earthquake pressures on the wall. A limiting value of full passive pressure for combined gravity and forced wall components may occur where the basement walls are used to provide lateral resistance against the earthquake base shear forces of the structure supported by the basement.

On flexible foundations, the response of the structure may be affected by the stiffness of the soil surrounding the basement. Here, it may be necessary to investigate the response of the building using Winkler springs to model the soil. Spring stiffnesses may be estimated from the forced wall solutions given in Section 3.5.5.

The two components of earthquake pressure (soil inertia and forced wall) will generally have different vibrational frequencies and may be combined using the square root of the sum of the squares rule (SRSS). If one component is less than 50% of the other, neglecting the smaller component reduces the total obtained by the SRSS method by less than 12%. Thus, it is helpful to make preliminary estimates of the components and only carry out detailed analyses to estimate the smaller component when it is estimated to exceed 50% of the larger component.

3.7.6 Bridge Abutments

Pressures on bridge abutments are influenced by the earthquake forces and displacements transmitted to the abutment by the bridge superstructure. If the bearing between the superstructure and abutment is a sliding type with a low coefficient of friction, the abutment may act essentially as a free standing wall. Another limiting case is a monolithic abutment where the wall is forced with displacements that may be governed by the response of the total bridge system.

It is helpful to consider two categories of abutments. The first type is the case where the soil pressures make no significant change to the dynamic response of the bridge. The second case is when the soil pressures on the abutment have a significant influence on the dynamic response. In this latter case, the abutment will generally be monolithic or integral with the superstructure. Procedures for estimating the abutment pressures for the two cases are given below.

(i) No Significant Interaction

The forces and displacements acting on the abutments in this category are shown in Figure 3.31. Two separate cases are shown. The first case is where the load from the superstructure is limited by a sliding or deformable bearing and the force transmitted to the abutment is known. The second case is where there is a rigid connection to the superstructure and the analysis of the abutment will need to be based on an imposed displacement rather than the force transmitted. The forces and displacements shown in Figure 3.31 are defined as follows:

ΔP_E = Earthquake pressure component from inertia forces in the soil.

P_F = Earthquake pressure component from forcing of the wall against the soil.

P_I = Inertia load acting on the abutment mass.

P_S = Gravity pressure component.

P_L = Load from superstructure.

Δ_u = Displacement of superstructure.

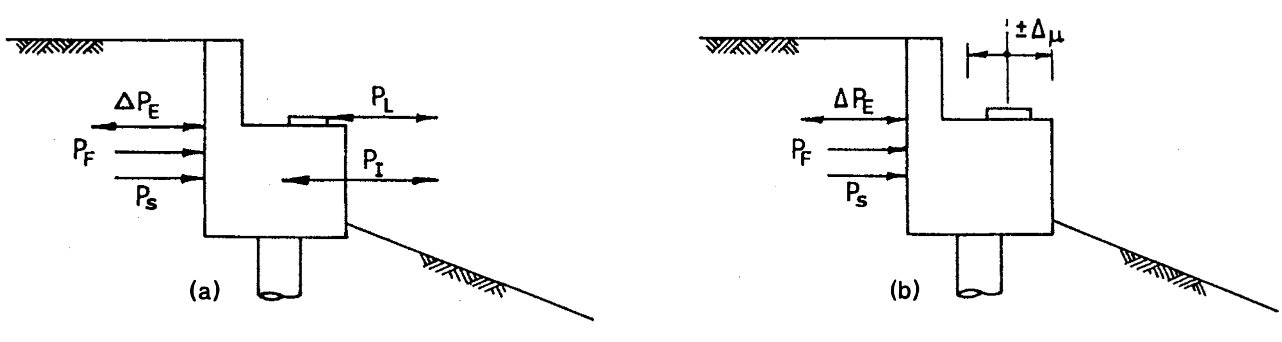

FIG. 3.31 NO SIGNIFICANT INTERACTION WITH SOIL
(a) Load Limiting Connection (b) Rigid Connection

The magnitude and direction to be assumed for some of these forces depends on whether the wall is being displaced against the backfill or away from the backfill. The movement against the backfill is usually the critical case for the abutment wall design and movement away from the backfill is usually critical for the design of the abutment foundations. Particular consideration of the force component directions may be required for the design of clearances, joints, bearings and linkages.

For movement away from the backfill, ΔP_E may be estimated from the pressure solutions given in Sections 3.5.1 to 3.5.3 making due allowance for wall flexibility. When the displacement is against the backfill, ΔP_E may be obtained from the rigid wall pressure distribution.

P_F may be estimated from the forced wall solutions given in Section 3.5.5. For translational deformation, P_F is given by:

$$P_F = 0.6 \; E_s \; a \; \Delta_u \qquad (3\text{-}27)$$

Where:

a = Horizontal width of abutment.

For the rigid connection case, Δ_u is known and P_F can be obtained from expression. For the case where the load from the superstructure is known rather than the displacement, P_F cannot be obtained directly and must be evaluated by analysing the abutment, including both the foundation and wall soil stiffnesses, loaded by $P_L + P_I$. The wall stiffness can be approximated using expression 3-27.

P_F always acts in the direction opposite to the movement of the wall. For abutment movement towards the backfill, P_F effectively increases the static gravity pressure and, the maximum resultant of $P_F + P_S$ is limited by the static passive pressure force. For abutment movement away from the backfill, P_F reduces the static pressure and the minimum resultant of $P_F + P_S$ is the static active pressure force.

ΔP_E and P_I should be assumed to be in phase. P_L or Δu may or may not be in phase with ΔP_E and P_I. Directions of the forces should be chosen to produce the most critical loading case. Because the earthquake pressure components P_E and P_F are caused by vibrational effects with different frequencies, they may be combined for the case of abutment movement against the backfill (critical case for wall design) using the SRSS method. For movement away from the backfill, the critical loading on the abutment foundation probably will occur with P_E and P_F acting in opposite directions. The correct method of summing forces will depend on the relative magnitude of the forces and whether the connection is load limiting or rigid. In view of the complexity for this case, the individual force components should be combined by taking the algebraic sum.

(ii) Significant Interaction

When the bridge response is significantly influenced by the interaction with the abutment soil it is difficult to account for the dynamic effects in a simple analysis procedure. The critical loading on the abutments and lateral load resisting elements can usually be obtained by considering the two cases of in-phase and out-of-phase earthquake soil inertia pressure components shown in Figure 3.32.

When the dynamic components of earth pressure are out of phase at either abutment (Figure 3.32 (a)) it may be assumed that the structure does not move relative to the foundation and is subjected to rigid wall pressures on each abutment wall. That is, the total pressures on the walls are the sum of the at-rest static pressure and a rigid wall earthquake component from the soil inertia loads. This assumption may overestimate the earthquake pressure components on short bridges where it is unlikely that out-of-phase accelerations will occur. Because of the influence of the soil properties and the frequency content of the incoming waves on the phase relationships at either abutment wall, it is difficult to make more precise predictions of the effect of the bridge length on the wall pressures.

When the dynamic components of pressure from the soil inertia loads are in phase at either abutment (Figure 3.32(b)) the bridge will displace relative to the foundation generating forced wall dynamic pressures that are dependent on the overall displacement response of the bridge. The analysis procedures for this case are similar to those discussed in Section 3.6.4 for basement walls.

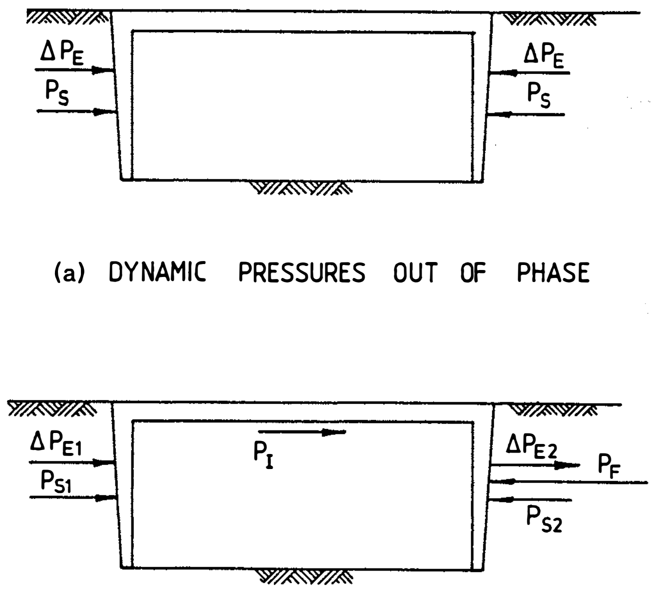

(a) DYNAMIC PRESSURES OUT OF PHASE

(b) DYNAMIC PRESSURES IN PHASE

FIG. 3.32 SIGNIFICANT INTERACTION WITH SOIL

The dynamic pressure components on the abutments due to the relative displacement of the bridge can be estimated by computing the period of vibration taking into account the abutment soil stiffness. The displacement response can then be estimated from the design response spectrum and the overall ductility factor. For relatively rigid structures, a satisfactory estimate of the displacement can be obtained by using the peak ground acceleration to obtain the inertia load on the bridge.

The minimum limiting value of $P_S + P_F$ on the abutment moving away from the soil is the active static pressure. The maximum limiting value of $P_S + P_F$ on the abutment moving towards the soil is the passive pressure.

Peak ground acceleration should be used to calculate the earthquake pressure component from the soil inertia loads. The upper limits for these components are the rigid wall pressures. On the abutment moving away from the soil, the component may be reduced by considering the wall flexibility. A lower limit for this component is the MO earthquake active pressure increment.

4

CONCLUDING COMMENTS

A considerable wealth of experimental data has been obtained by the wide range of wall studies completed in New Zealand. This information has been used to check the validity of theoretical predictions as well as highlighting several effects that could not have been predicted by theoretical studies alone. The change in the threshold acceleration behaviour in the reinforced earth tests and the residual static pressure increase in the rigid wall experiments are particular examples of details that were not considered in the initial theoretical studies.

The results from both the experimental and theoretical studies will form the basis for improvements in design code loadings and the accepted earthquake design procedures for walls and bridges. The test results also will provide data that will be of considerable value in calibrating and developing further refinements in analytical methods.

Although reinforced earth walls and monolithic abutments have not yet been widely used in New Zealand, both these recent developments in wall and abutment structural form have the potential to reduce construction costs. The results of the research have increased the understanding of the earthquake behaviour of these newer developments as well as other structural types more commonly in use. The research will form the basis for more rational and economical design of wall structures to resist earthquakes.

Further testing on larger scale models or full scale walls using a wider range of backfill materials than used in the model tests would be desirable.

A more detailed examination should be carried out of the residual stresses produced by strong shaking with a variation in parameters such as the wall stiffness and soil properties.

To provide a level of earthquake resistance in walls and abutments that is consistent with the more predictable performance of the main lateral load resisting components of buildings and bridges, there is a need to continue research into the dynamic response and soil-structure interaction effects.

5

REFERENCES

(1) AITKEN, G. H., (1982), "Seismic Response of Retaining Walls", Rept No 82-5, Dept of Civil Eng, Univ of Canterbury, March.

(2) AMANO, R., AZUMO, H., and ISHII, Y., (1956) "Aseismic Design of Quay Walls in Japan", Proc. First World Conf on Earthquake Engineering.

(3) ANDERSON, W. F., HANNA, T. H., and ABDEL-MALEK, M. N., (1983) "Overall stability of Anchored Retaining Walls", Proc ASCE, Journal of Geotechnical Engineering, Vol 109, No 11, November.

(4) ATHANASIOU-GRIVAS D., (1978), "Reliability of Retaining Structures During Earthquakes", VI Symp on Earthquake Engineering, Univ of Roorkee, Vol I.

(5) BRACEGIRDLE, A., (1980), "Seismic Stability of Reinforced Earth Retaining Walls", Bull NZ National Society for Earthquake Eng, 13 (4), 347-54.

(6) CHOPRA, A. K., (1967), "Hydrodynamic Pressures on Dams During Earthquakes", Jour of Eng Mechanics Div, ASCE, Vol 93, EM6, pp 205-223.

(7) CLOUGH, G. W., and FRAGASZY, R. F., (1977) "A Study of Earth Loadings on Floodway Retaining Structures in the 1971 San Fernando Earthquake", 6th World Conf on Earthquake Eng, New Deli, Vol 7.

(8) CORMACK, L. G., BLAKELEY, J. P., TOAN, D. V. and GOLDSMITH, P. R., (1980) "Reinforced Earth Retaining Walls with Specific Reference to Earthquake Resistant Design", Project 4787, Structures Committee, R.R.U., National Roads Board, NZ.

(9) CROUSE, C. B., HUSHMAND, B., LIANG, G., MARTIN G. R., and WOOD J. H. (1985) "Dynamic Response of Bridge-Abutment-Backfill Systems", Proc Joint US-NZ Workshop on Seismic Resistance of Highway Bridges, San Diego, May.

(10) DUKE, C. M., AND LEEDS, D. J., (1963) "Response of Soils, Foundations, and Earth Structures to the Chilean Earthquake of 1960", Bulletin of the Seismological Society of America", Vol 53, No 2, February.

(11) DZ 4203: 1989 "General Structural Design and Design Loadings for Buildings", Draft Standard, Standards Association of New Zealand.

(12) EARTHQUAKE ENGINEERING RESEARCH INSTITUTE (1975) "Engineering Aspects of the Lima, Peru, Earthquake of October 3, 1974", Oakland, California.

(13) ELLISON, B. K., (1971) "Earthquake Damage to Roads and Bridges, Madang, T.P.N.G. - November 1970", Bull NZ National Soc for earthquake Eng, Vol 4, No 2, April.

(14) ELMS, D. G., and MARTIN, G. R., (1979) "Factors Involved in The Seismic Design of Bridge Abutments", Workshop on the Research Needs of Seismic Problems Related to Bridges, Applied Technology Council, Palo Alto.

(15) ELMS, D. G., and NAGEL, R. B., (1987) "Dynamic Model Testing of Reinforced Earth Walls", Pacific Conference on Earthquake Engineering, Wairakei.

(16) ELMS, D. G., and RICHARDS, R. (1979) "Seismic Design of Gravity Retaining Walls", Bulletin of NZ National Society for Earthquake Engineering, Vol 12, No 2.

(17) ELMS, D. G., and RICHARDS, R. (1988) "Seismic Behaviour of Overturning Retaining Walls", Australiasian Conference on the Mechanics of Structures and Materials, University of Auckland.

(18) ELMS, D. G., and WOOD, J. H., (1987) "Earthquake Induced Displacements and Pressures on Retaining Walls and Bridge Abutments", Proc NZ Roading Symposium, Wellington.

(19) EVANS, G. L., (1971) "The Behaviour of Bridges Under Earthquakes", Proc NZ Roading Symposium, Victoria University of Wellington, Vol 2, pp 664 - 684.

(20) FAIRLESS, G. J., (1989) "Seismic Performance of Reinforced Earth Walls", Research Report 89-9, Dept of Civil Engineering, University of Canterbury, Christchurch.

(21) FRANKLIN, A. G., AND CHANG, F. K., (1977) "Earthquake Resistance of Rock Fill Dams: Report 5: Permanent Displacements of Earth Embankments by Newmark Sliding Block Analysis", Misc Paper S-71-17, Soils and Pavements Laboratory, U.S. Army Engineers Waterways Experiment Station, Vicksburg, Miss.

(22) FUNG, G. G., LE BEAU, R. J., KLEIN, E. D., BELVEDERE, J., and GOLDSMITH, A. F., (1971) "Field Investigation of Bridge Damage in the San Fernando Earthquake", Preliminary Report, State of Calif Business and Transportation Agency, Dept of Public Works, Div of Highways, Bridge Dept.

(23) GAZETAS, G., (1983) "Analysis of Machine Foundation Vibrations: State-of-the-Art", Soil Dynamics and Earthquake Engineering, 2.

(24) HAYASHI, S. AND KATAYAMA, T., (1970) "Damage to Harbour Structures by the Tokachioki Earthquake", Soils and Found, X (2).

(25) HRADILEK, P.J., (1972) "Behaviour of Underground Box Conduits in the San Fernando Earthquake", US Army Eng Dist, Los Angeles Corps of Eng.

(26) JACOBSEN, P. N., (1980) "Translational Behaviour of Gravity Retaining Walls During Earthquakes", Rept No 80-9, Dept of Civil Eng, Univ of Canterbury, March.

(27) JENNINGS, P. C., (Editor), (1971) "Engineering Features of the San Fernando Earthquake", February 9, 1971, Rept 71-02, Earthquake Eng Research Laboratory, Calif Inst of Technology, Pasadena.

(28) KAWASUMI, H., Editor, (1964) "General Report on the Niigata Earthquake of 1964", Tokyo Electrical Engineering College Press.

(29) KITAJIMA, S., and UWABE, T. (1979) "Analysis on Seismic Damage in Anchored Sheet-Piling Bulkheads", Report of Port and Harbours Research Institute, Vol 18, No 1.

(30) LAI, C. S., (1979) "Behaviour of Retaining Walls under Seismic Loading", Rept 79-9, Dept of Civil Eng, Univ of Canterbury, February.

(31) LAI, C. S., and BERRILL, J. B., (1979) "Shaking Table Tests on a Model Retaining Wall", Bull NZ National Soc for Earthquake Eng, Vol 12, No 2, June.

(32) LEW, H. S., LEYENDECKER, E. V. and DIKKERS, R. D., (1971) "Engineering Aspects of the 1971 San Fernando Earthquake", Building Series 40, Build Res Div, Inst of App Tech, NBS, Washington D.C.

(33) LIAM FINN, W. D., (1963), "Boundary Value Problems of Soil Mechanics", ASCE, Jour of Soil Mechanics and Foundation Div, SM5, September.

(34) LIN, J-S. and WHITMAN, R. V., (1986) "Earthquake-Induced Displacements of Sliding Blocks", ASCE, Journal of Geotechnical Eng Div, Vol 12, No GT 1.

(35) MATTHEWSON M. B., WOOD J. H., and BERRILL J. B., (1980) "Seismic Design of Bridges - Earth Retaining Structures", Bull NZ National Soc of Earthquake Eng, 13, (3), 280-293.

(36) MATUO, M., and OHARA, S., (1960) "Lateral Earth Pressures and Stability of Quay Walls During Earthquakes", Proc Second World Conf on Earthquake Eng, Tokyo.

(37) MEEHAN, J. F., and DEGENKOLB, H. J., et al (1973) "Nicaragua Earthquake of December 23, 1972", Earthquake Engineering Research Institute Report, Oakland, California, May.

(38) MINISTRY OF WORKS AND DEVELOPMENT, NEW ZEALAND, (1973) "Retaining Wall Design Notes", C.D.P. 702 C, July.

(39) MINISTRY OF WORKS AND DEVELOPMENT, NEW ZEALAND, (1980) "Reinforced Earth - Notes on Design and Construction", Supplement to Retaining Wall Design Notes", C.D.P. 702 C, (1973).

(40) MONONOBE, N. and MATSUO, H., (1929) "On the Determination of Earth Pressures During Earthquakes", Proc World Eng Conf 9: 177-185.

(41) NADIM F., and WHITMAN R. V., (1985), "Seismically Induced Movement of Retaining Walls", Norwegian Geotechnical Institute, Publication No 155, Oslo.

(42) NAGEL, R. B., and ELMS, D. G., (1985) "Seismic Behaviour of Reinforced Earth Walls", Rept 85-4, Dept of Civil Eng, Univ of Canterbury.

(43) NAZARIAN, H. N., and HADJIAN, A. H., (1979) "Earthquake-Induced Lateral Soil Pressures on Structures", ASCE, Journal Geotechnical Engineering Div, Vol 105, No GT 9, September.

(44) NEWMARK, N. M., (1965) "Effects of Earthquakes on Dams and Embankments", Geotechnique, XV (2).

(45) PRAKASH S. "Soil Dynamics", McGraw-Hill Book Co.

(46) PRAKASH S., and NANDAKUMARAN P., (1979) "Earth Pressures During Earthquakes", Proc 2nd US National Conference on Earthquake Engineering, Stanford University.

(47) PRAKASH, S. and SARAN, S., (1966) "Static and Dynamic Earth Pressures Behind Retaining Walls". Proc 3rd Symposium on Earthquake Engineering, University of Roorkee, India, Vol 1, pp 277-288.

(48) REINFORCED EARTH COMPANY, (1990) "An Investigation of Reinforced Earth Structures Impacted by the Loma Prieta Earthquake", Report published by Reinforced Earth Company, Western Division, Sacramento, California.

(49) RICHARDS, R. and ELMS, D. G., (1979) "Seismic Behaviour of Gravity Retaining Walls", Proc ASCE, 105 (GT4), 49-64.

(50) RICHARDS, R. and ELMS, D. G., (1987) "Seismic Behaviour of Tied Back Walls - Initial Analysis and Experiments" Rept 87-8, Dept of Civil Eng, Univ of Canterbury, November.

(51) RICHARDSON, G. N., FEGER, D., FONG, A. and LEE, K. L. (1977), "Earthquake Resistant Reinforced Earth Walls", Proc ASCE, Jour Geotechnical Eng Div, Vol 103, No GT 1, January.

(52) ROSS, G. A., SEED, H. B. and MIGLIACCIO, R. (1969), "Bridge Foundation Behaviour in Alaska Earthquake", Proc ASCE, Jour Soil Mechanics and Foundation Eng Div, Vol 95, No SM 4, July.

(53) SARAN S., and PRAKASH S., (1968), "Dimensionless Parameters for Static and Dynamic Earth Pressure for Retaining Walls", Indian Geotech Jour, Vol 7, No 3, pp 295-310, July.

(54) SARAN S., and PRAKASH A., (1970), "Seismic pressure Distribution in Earth Retaining Walls", Proc 3rd European Symp on Earthquake Engineering, Sofia.

(55) SCOTT R. F., (1973), "The Great Alaska Earthquake of 1964: Engineering: Behaviour of Soils during the Earthquake", National Academy of Sciences, Washington.

(56) SEED, H. B. and WHITMAN, R. V., (1970) "Design of Earth Retaining Structures for Dynamic Loads, ASCE Spec Conf, Lateral stresses in the Ground and the Design of Earth Retaining Structures, Cornell University.

(57) SHARMA, N., (1990) "Refinement of the Newmark Sliding Block Model and Application to New Zealand Conditions", Rept 90-3, Dept of Civil Eng, Univ of Canterbury.

(58) SHERIF, M. A., ISHIBASHI, I. and LEE, C. D., (1982) "Earth Pressures Against Rigid retaining Walls", Proc ASCE, 108 (GT5).

(59) STEVENSON, R. B., (1978) "Dynamic Sand Pressures Against a Flexible Retaining Wall", Report No 5-87/8, Central Laboratories, Lower Hutt.

(60) TAJIMI, H., (1970) "Dynamic Earth Pressure on Basement Walls in The Elastic Ground", Proc THird Japan Earthquake Eng Symposium, Tokyo.

(61) THURSTON, S. J., (1986 a) "Load Displacement Response of a Rigid Abutment Wall Translated into Sand Backfill", Rept 5-86/1, Central Laboratories, Ministry of Works and Development, Lower Hutt.

(62) THURSTON, S. J., (1986 b) "Rotation of a Rigid Abutment Wall into Dense Backfill", Rept 5-86/3, Central Laboratories, Ministry of Works and Development, Lower Hutt.

(63) THURSTON, S. J., (1986 c) "Dynamic Sand Pressures Against a Rigid Retaining Wall", Rept 5-86/4, Central Laboratories, Ministry of Works and Development, Lower Hutt.

(64) THURSTON, S. J., (1987) "Translation of a Rigid Abutment Wall into Dense Backfill", Rept 5-87/1, Central Laboratories, Ministry of Works and Development, Lower Hutt.

(65) TSO, Y. H., (1986) "Investigation of Soil-Reinforcement Interaction in Reinforced Earth Structure", ME Thesis, Dept of Civil Eng, Univ of Canterbury.

(66) WERNER P. W., and SUNDQUIST K. J. (1949), "On Hydrodynamic Earthquake Effects", Trans, American Geophysical Union, Vol 30, No 5, October.

(67) WESTERGAARD, H. M., (1933) "Water Pressures on Dams During Earthquakes", Transactions, ASCE, Vol 98, pp 418-433.

(68) WHITMAN, R. V. (1979) "Dynamic Behaviour of Soils and its Application to Civil Engineering Projects", Pan American Conference on Soil Mechanics and Foundation Engineering, Lima, Peru.

(69) WOOD, J. H., (1973) "Earthquake-Induced Soil Pressures on Structures", Rept No. EERL 73-05, Earthquake Eng Research Laboratory, Calif Inst of Technology, Pasadena.

(70) WOOD, J. H., (1985) "Earthquake Pressures on Monolithic Bridge Abutment Walls", Report No M1.85/3, Central Laboratories, Lower Hutt.

(71) WOOD, J. H., and JENNINGS, P. C., (1971) "Damage to Freeway Structures in the San Fernando Earthquake", Bull NZ National Soc for Earthquake Eng, Vol 4, No 3, December.

(72) WOOD, J. H., and YONG, P. M. F., (1987) "Dynamic Soil Pressures on Rigid Retaining walls and Abutments", Pacific Conference on Earthquake Engineering, Wairakei.

(73) WONG, H. L., and LUCO, J. E., (1978) "Tables of Impedance Functions and Input Motions for Rectangular Foundations", Report No. CE 78-15, Dept of Civil Eng, Univ of Southern Calif.

(74) YAP, K. K., (1987) "Dynamic Sand Pressures Against Stiff Retaining Walls", Rept 5-87/2, Central Laboratories, Ministry of Works and Development, Lower Hutt.

(75) YEO, E. H., (1987) "Translation of a Rigid Abutment Wall, Incorporating a Friction Slab, Into a Sand Backfill", Rept 5-87/5, Central Laboratories, Ministry of Works and Development, Lower Hutt.

(76) YONG, P. M. F., (1985) "Dynamic Earth Pressures Against a Rigid Retaining Wall", Rept 5-85/5, Central Laboratories, Ministry of Works and Development, Lower Hutt.

(77) ZARRABI-KASHANI, K., (1979) "Sliding of Gravity Retaining Walls During Earthquakes Considering Vertical Acceleration and Changing Inclination of Failure Surface", M.S. Thesis, Dept of Civil Engineering, Massachusetts Institute of Technology.

WOOD AND ELMS

6

NOTATION

A_p area of reinforced earth wall panel

A_s net section area of soil reinforcing strip

B reaction force on base of wall

b soil reinforcing strip width

c soil cohesion

C(0) horizontal acceleration coefficient for zero period (peak ground acceleration coefficient)

C_{AE} $\Delta K_{AE}/k_c$

C_o acceleration response function for 150 year return period specified in DZ 4203

c_u undrained shear strength of soil

d outward displacement of centre of mass of sliding wall/soil wedge

D_n soil grain size corresponding to n% finer by mass in particle size distribution

E Young's modulus for soil

E_c Young's modulus for concrete

f^* friction coefficient for soil reinforcing strip

F^* $2bn_hf^*$

F_f force on forced wall per unit length of wall

F_r force on rigid wall per unit length of wall

FS factor of safety against sliding under static loads

FS_o factor of safety against overturning under earthquake loading

FS_p factor of safety against reinforcing strip pull-out

FS_s factor of safety against sliding under earthquake loads

F_t total force on wall per unit length of wall

f_t maximum tensile stress in soil reinforcing strip

f_y yield stress for soil reinforcing strip material

g acceleration of gravity

H height of wall

h distance from failure surface intersection with wall face to top of wall

h_w depth of water

K_A coefficient of active pressure

K_{AE} Mononobe-Okabe coefficient of active earthquake pressure

k_c critical horizontal acceleration coefficient

k_h horizontal acceleration coefficient

K_0 coefficient of at rest pressure

k_w translational stiffness of wall spring

k_v vertical acceleration coefficient

L length of wall backfill layer

L_e resistive length for soil reinforcing strip

L_f length of soil reinforcing strip behind failure plane

L_s length of soil reinforcing strips

L_w length of wall

M_f moment on forced wall per unit length of wall

M_r moment on rigid wall per unit length of wall

m building storey mass

N normal force on failure plane in reinforced earth block

n number of reinforcing strips per panel

$N_{a\gamma}$ Prakash-Saran dimensionless parameter for force on wall with cohesive/frictional backfill

N_{ac} Prakash-Saran dimensionless parameter for force on wall with cohesive/frictional backfill

n_h number of reinforcing strips per unit length of wall in each layer of reinforcement

p(z) soil normal pressure on wall at depth y below top of wall

p(z)' dimensionless normal pressure on wall, $p(z)/(C(0)\gamma H)$

P_{AE}	Mononobe-Okabe active earthquake force on wall
P_F	earthquake pressure component from forcing of abutment wall against backfill
P_I	inertia load acting on abutment mass
P_L	load on abutment from superstructure
P_0	force due to at rest earth pressure
P_r	force ratio parameter, $E\theta/(C(0)\gamma H^2)$
P_S	gravity pressure component on abutment wall
P_t	dynamic force component on wall
P_t'	dimensionless dynamic force component on wall, $P_t/(C(0)\gamma H^2)$
p_v	vertical pressure on horizontal plane through reinforced earth wall under earthquake loads
p_v'	dimensionless vertical pressure on base of reinforced earth wall under earthquake loads, $p_v/(C(0)cH)$
P_w	water pressure on front face of wall
q	width of pressure distribution on base of wall
R	risk factor specified in DZ 4203
R	sum of strip tensions across failure plane in reinforced earth block
r	L_s/h
R'	$R/(\gamma H^2)$
s	height of centre of pressure above base of wall
T	total tie force on tie-back wall
t	period of vibration
T'	$T/(\gamma H^2)$
T_m	tension force in soil reinforcing strip
u	displacement in x (horizontal) direction
u_b	base acceleration
u^o	displacement of top of wall
V	earthquake peak ground velocity
v	displacement in y (vertical) direction
W	weight of wall and sliding wedge of soil
W_w	weight of wall
y	height above base of wall
Z	zone factor specified in DZ 4203
z	depth below top of wall
α	angle of inclination of failure surface from horizontal
β	wall backface slope angle
γ	unit weight of soil
γ_w	unit weight of water
ΔK_{AE}	Mononobe-Okabe coefficient of active earthquake pressure increment, $(K_{AE}-K_A)$
$\Delta p(z)$	increment in pressure on wall at depth z below top of wall due to earthquake
ΔP_{AE}	Mononobe-Okabe increment of earthquake force on wall
ΔP_E	increment in pressure force on wall due to earthquake
$\Delta PE'$	$\Delta PE/(C(0)\gamma H^2)$
ΔP_{0E}	increment or decrement in at rest earth pressure due to earthquake
Δ_u	displacement of bridge superstructure
δ	friction angle on back face of wall
θ	wall rotation angle
λ	earthquake dynamic factor for force on wall with a cohesive/frictional backfill
ν	Poisson's ratio
ν_c	Poisson's ratio for concrete
ρ	mass density of soil
σ_x	normal stress in x direction
σ_y	normal stress in y direction
τ_{xy}	shear stress in the x and y directions
ϕ	angle of internal friction of soil
ϕ_b	friction angle for wall base
ϕ_c	soil friction parameter for rotating wall
ω	angle of inclination from horizontal of backfill slope

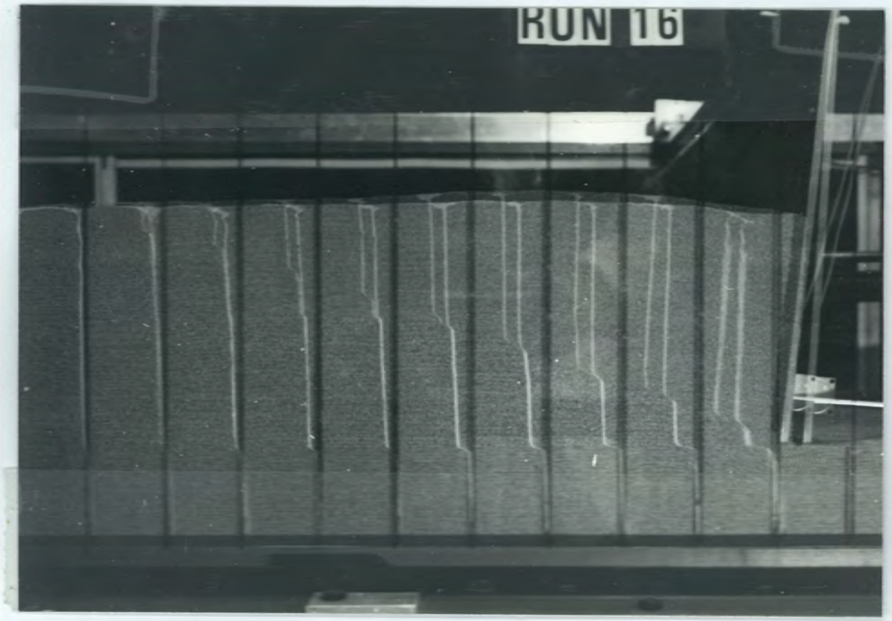
RUN 16

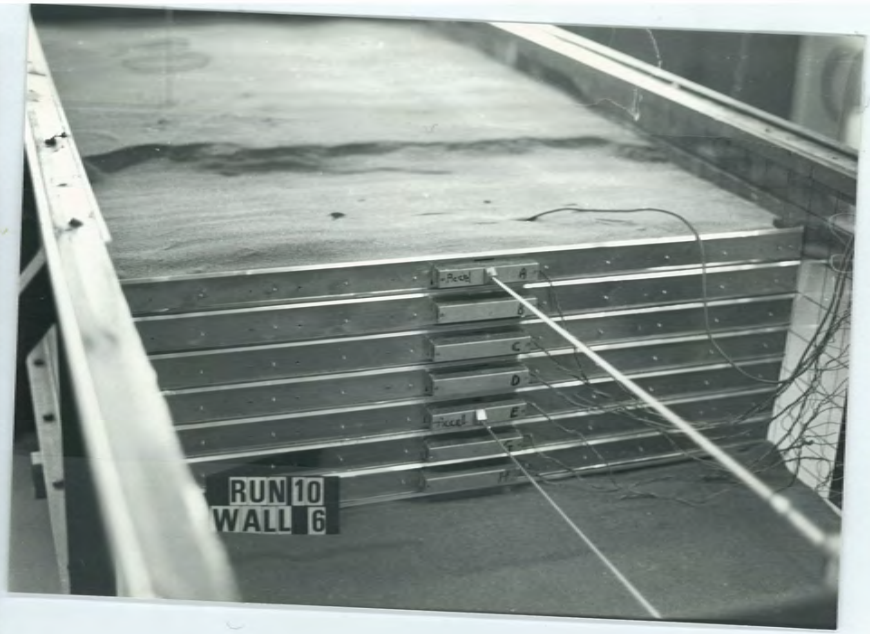
RUN 10
WALL 6

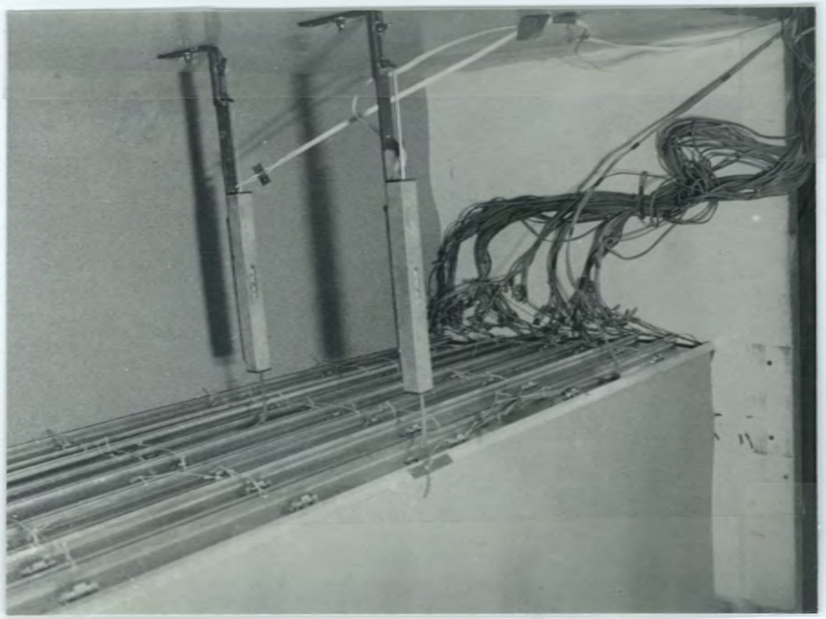

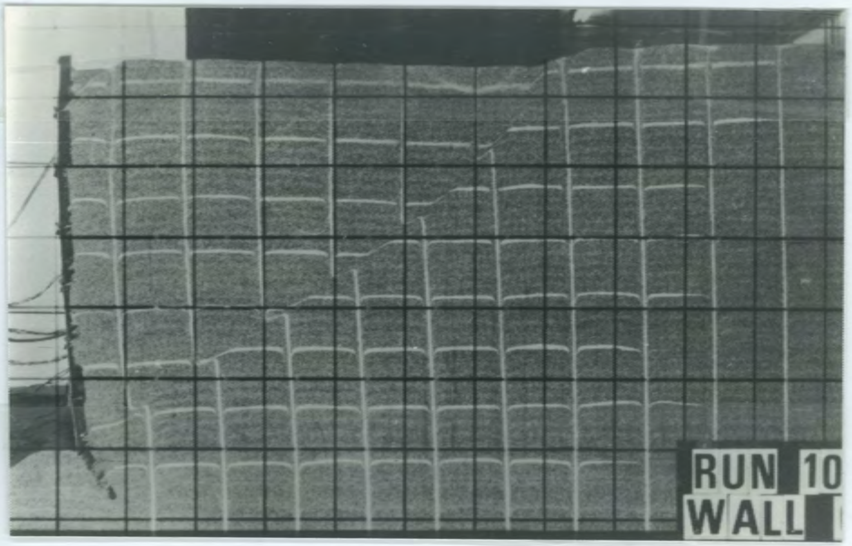
RUN 10
WALL

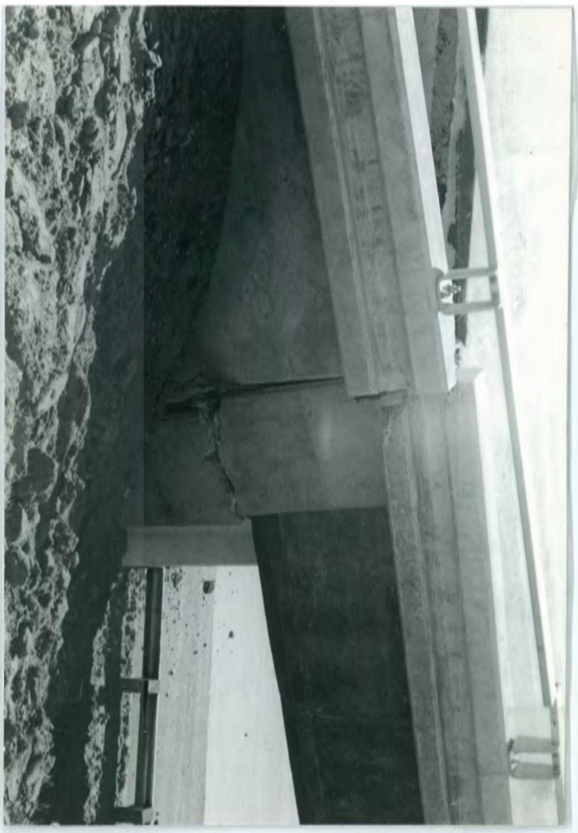


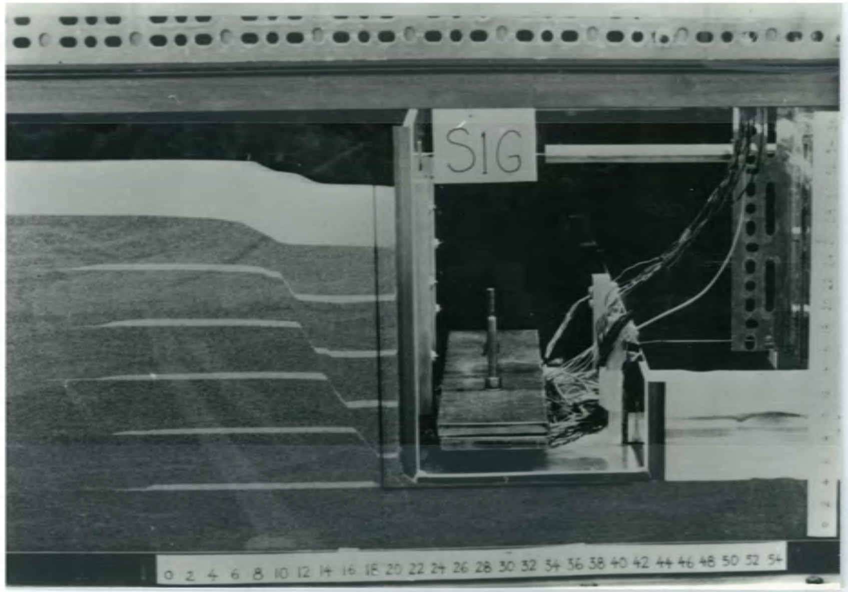
SIG
0 2 4 6 8 10 12 14 16 18 20 22 24 26 28 30 32 34 36 38 40 42 44 46 48 50 52 54

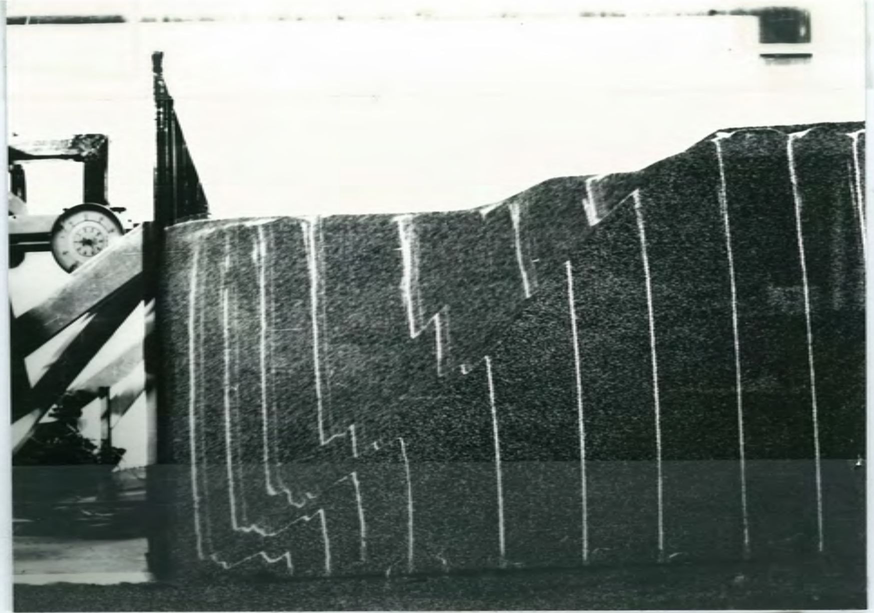


ALCORN